Roquin family proteins control T cell co-stimulation and differentiation

Dissertation

der Fakultät für Biologie

der Ludwig-Maximilian-Universität München

zur Erlangung des Doktorgrades der Naturwissenschaften



vorgelegt von

Katharina Ursula Vogel

aus Bayreuth, Deutschland

angefertigt am Helmholtz Zentrum München

München, den 13.12.2012

Eidesstattliche Erklärung:

Hiermit versichere ich, Katharina Ursula Vogel, an Eides statt, dass die vorgelegte Dissertation mit dem Titel “Roquin family proteins control T cell co-stimulation and differentiation" von mir selbstständig und ohne unerlaubte Hilfe angefertigt ist und ich mich dabei nur der ausdrücklich bezeichneten Quellen und Hilfsmittel bedient habe. Ich erkläre, dass diese Dissertation nicht ganz oder in wesentlichen Teilen einer anderen Prüfungskommission vorgelegt worden ist und dass ich mich anderweitig einer Doktorprüfung ohne Erfolg **nicht** unterzogen habe.

Katharina Vogel München, der 13.12.2012

Erster Gutachter: Prof. Dr. Dirk Eick

Zweiter Gutachter: PD Dr. Bettina Bölter

Tag der Abgabe: 13.12.2012

Tag der mündlichen Prüfung: 11.06.2013

It’s not lupus
(Dr. House)

1 Abstract

This thesis investigates the function of Roquin-1 (Rc3h1) and its paralog Roquin-2 (Rc3h2) in the immune system. Roquin-1 is an essential factor in the prevention of autoimmune diseases by controlling T cell co-stimulation. This was first observed in mice harboring a single point mutation (san mutation) in Roquin-1, which developed a lupus-like disease with increased levels of the inducible co-stimulator Icos on all T cells. Roquin-1 represses Icos mRNA levels by interacting with factors of the mRNA decay machinery to induce mRNA degradation.

The first part of this thesis significantly contributes to the discovery of this mechanism by demonstrating direct Roquin-1 protein interaction with human ICOS mRNA. Furthermore, *in vitro* shift assays reveal a newly defined *cis*-element in the 3'untranslated region (UTR) of ICOS mRNA, which is required for preferential Roquin-1-binding. This *cis*-element comprises a two-finger-like secondary RNA structure that might be crucial for Roquin-1 protein recognition. The paralog of Roquin-1, Roquin-2, with so far unknown function, is equally able to bind to the *cis*-element in the ICOS 3'UTR, indicating some degree of redundancy.

The second part of the presented work focuses on potential redundancy of Roquin-1 and Roquin-2 in mice to solve a current paradox: The san mutation in Roquin-1 leads to severe autoimmune disease, but the complete absence of the protein does not. Investigating the complete deletion of the paralog Roquin-2 reveals postnatal death, but no unique role can be found for Roquin-2 upon conditional deletion in T cells. However, combined ablation of Roquin-1/2 in T cells reproduces most of the phenotypes observed in san/san mice. This implies that Roquin-2 can compensate for loss of Roquin-1-function, but is inhibited by the Roquin-1^{san} protein. We suggest the disrupted splenic architecture in *Rc3h1/2*-deficient mice as one reason, why these mice do not develop anti-nuclear antibodies, a hallmark of lupus-disease. Mechanistic analyses reveal that both Roquin-1 and Roquin-2 proteins can independently repress Icos mRNA and further identify Ox40 mRNA as a novel molecular target of both proteins. In addition, combined acute ablation of Roquin-1/2 proteins augments Ox40 co-stimulation through the alternative NF-κB pathway and increases Irf4 transcription factor levels. This results in enhanced follicular T helper (Tfh) cell and Th17 differentiation, implying that Roquin-1/2 proteins control these differentiation programs. Adoptive transfer experiments further corroborate this finding. Finally, the contribution of Icos or IFN-γ to the observed phenotypes in *Rc3h1/2*-deficient mice is investigated in triple knockout situations, revealing a potential overlap of Icos and Ox40 functions in Tfh cell differentiation.

In summary, this thesis demonstrates the redundant functions of Roquin-1 and Roquin-2, which provide a crucial safeguard mechanism in the prevention of autoimmunity.

2 Zusammenfassung

Diese Dissertation untersucht die Funktion von Roquin-1 (Rc3h1) und seinem Paralog Roquin-2 (Rc3h2) im Immunsystem. Durch die Kontrolle von T-Zell Co-Stimulierung verhindert Roquin-1 die Entstehung von Autoimmunerkrankungen. Diese wichtige Funktion wurde in der san/san Maus entdeckt, die eine Punktmutation in Roquin-1 aufweist. Das dadurch entstehende Lupus-ähnliche Krankheitsbild ist unter anderem durch die Überexpression von dem induzierbaren Co-Stimulator Icos auf T-Zellen gekennzeichnet. Roquin reprimiert Icos mRNA durch Interaktion mit Proteinen, die den Abbau von mRNA einleiten.

Der erste Teil dieser Dissertation trägt wesentlich zu der Entschlüsselung dieses Mechanismus bei, indem sie aufzeigt, dass Roquin-1 direkt mit der humanen ICOS mRNA interagiert. Hierbei bindet Roquin-1 bevorzugt an ein neu entdecktes *cis*-Element in dem 3'untranslatierten Bereich (UTR) der ICOS mRNA. Dieses *cis*-Element weist eine zwei-Finger artige Sekundärstruktur der RNA auf, die eine wichtige Rolle bei der Erkennung durch Roquin-1 Proteine spielen könnte. Das Paralog von Roquin-1, Roquin-2, dessen Funktion bis jetzt nicht bekannt ist, bindet genauso gut an das *cis*-Element im ICOS 3'UTR, wodurch eine gewisse Redundanz angedeutet wird.

Im zweiten Teil dieser Arbeit sollen daher redundante Funktionen von Roquin-1 und Roquin-2 untersucht werden um eine wichtige Frage zu klären: Warum führt die san Mutation, nicht jedoch das völlige Fehlen von Roquin-1, zu einer schweren Autoimmunerkrankung? Fehlt das Paralog Roquin-2 in der Maus, stirbt diese. Das Fehlen von Roquin-2 nur in T-Zellen legt keine einzigartige Funktion von Roquin-2 offen. Das Fehlen beider Proteine in T-Zellen, ruft jedoch die meisten san/san Phänotypen hervor. Dies bedeutet, dass Roquin-2 den Funktionsverlust von Roquin-1 ausgleichen kann, nicht jedoch wenn das mutierte Roquin-1^{san} Protein Roquin-2 daran hindert. Die zerstörte Milz-Struktur in *Rc3h1/2*-defizienten Mäusen ist eine mögliche Ursache, weshalb im Gegensatz zur san/san Maus keine anti-nuklearen Antikörper entstehen. Funktionell zeigt diese Arbeit, dass Roquin-1 und Roquin-2 unabhängig voneinander Icos reprimieren können und Ox40 mRNA eine weitere Ziel-RNA beider Paraloge ist. Der Verlust von Roquin-1/2 steigert Ox40 Co-Stimulation durch den alternativen NF-κB Signalweg und erhöht die Expression des Transkriptionsfaktors Irf4. Dadurch erhöht sich die Differenzierung in follikuläre Helfer-T-Zellen (Tfh) und Th17 Zellen, die offenbar von Roquin-1/2 Proteinen kontrolliert wird. Dies wird auch durch Transfer-Experimente bestätigt. Zuletzt wird der Effekt von Icos oder IFN-γ auf den Funktionsverlust von Roquin-1/2 Proteinen in Dreifach-Knock-out Studien untersucht. Dabei zeigt sich eine mögliche Redundanz von Icos und Ox40 in der Tfh Differenzierung.

Diese Arbeit zeigt somit die Redundanz von Roquin-1 und Roquin-2 Proteinen auf, welche einen wichtigen Schutzmechanismus zur Vermeidung von Autoimmunität darstellt.

3 Directory

1 Abstract 7

2 Zusammenfassung 9

3 Directory 11

4 Abbreviations and nomenclature 15

5 Introduction 21

5.1 Boon and Bane of the immune system 21

5.1.1 Generation and selection of T lymphocytes 21

5.1.2 T cell co-stimulation and signaling 22

5.1.3 Common co-receptor signaling pathways 26

5.1.4 Differentiation of T helper cells 29

5.1.5 Autoimmunity caused by inappropriate or defective co-stimulation and T cell differentiation 32

5.2 Post-transcriptional gene regulation 33

5.2.1 *Trans*-acting factors and *cis*-elements regulate mRNA stability 33

5.2.2 P bodies and stress granules regulate mRNA processing 36

5.3 Objective of the research work 38

6 Material 41

6.1 Mice 41

6.2 Cell lines and cell culture 41

6.3 Antibodies and cytokines 42

6.4 Vectors and oligonucleotides 44

6.4.1 Entry vector constructs 44

6.4.2 Viral expression constructs 45

6.4.3 Additional constructs 45

6.4.4 Oligonucleotides synthesized by the company METABION 46

6.5 Chemicals, enzymes and kits 47

6.6 Buffer and solutions 49

6.7 Instruments 49

7 Methods 51

7.1 Molecular standard procedures 51

7.1.1 Bacterial culture 51

7.1.2 PCR for cloning and genotyping 51

7.1.3 Preparation and purification of DNA 52

7.1.4 DNA extraction from agarose gels 52

7.1.5 TOPO® cloning and site-specific recombination 52

7.1.6 Site-directed mutagenesis with QuikChange® II XL 52

7.1.7 Ligation of DNA fragments 53

7.1.8 Extraction of RNA 53

7.1.9 Reverse transcription of RNA 54

7.2 Cell culture 54

7.3 Preparation and stimulation of primary T cells 54

7.4 Generation of mouse embryonic fibroblasts 55

7.5 Virus production and transduction 55

7.5.1 Adenovirus 55

7.5.2 Retrovirus 56

7.6 *In vitro* deletion of loxP-flanked *Rc3h1/2* alleles ... 56
7.7 Confocal microscopy ... 56
7.8 Protein purification ... 56
7.9 *In vitro* RNA transcription ... 57
7.10 Electrophoretic mobility shift assay (EMSA) ... 57
7.11 SHAPE assay ... 57
7.12 Flow cytometry and intracellular staining ... 58
7.12.1 Surface staining ... 58
7.12.2 Intracellular staining ... 58
7.13 Co-immunoprecipitation and immunoblotting ... 59
7.14 Nuclear fractionation ... 60
7.15 Histology ... 60
7.16 Quantitative real-time PCR ... 60
7.17 Statistical analysis ... 60

8 Results ... 61
8.1 Characterization of protein–RNA interactions in post-transcriptional gene regulation ... 61
8.1.1 Roquin-1 is able to directly bind to RNA and has an intrinsic preference for the 3'UTR of ICOS mRNA ... 61
8.1.2 Roquin-1 binds to a specific *cis*-element in the 3'UTR of ICOS ... 68
8.1.3 The RNA sequence in the ICOS *cis*-element adopts a finger-like structure ... 70
8.1.4 Roquin-2 binds equally well to the 3'UTR of Icos mRNA ... 74
8.1.5 An array-approach to identify new targets of Roquin-1 ... 75
8.1.6 Roquin-1 binding to new mRNA targets ... 77
8.2 Function of Roquin-1 and Roquin-2 *in vivo* ... 78
8.2.1 Expression levels of Roquin-1 and Roquin-2 in mouse tissues ... 79
8.2.2 In $CD4^+$ T cells Roquin-1 localizes to P bodies ... 80
8.2.3 Evaluation of the complete Roquin-2 knockout ... 81
8.2.4 Conditional Roquin-2 knockout in T cells ... 85
8.2.5 Conditional Roquin-2 knockout in the hematopoietic system ... 87
8.2.6 Conditional knockout of Roquin-1 and Roquin-2 in T cells resembles phenotypes of the *Rc3h1*$^{san/san}$ mouse ... 89
8.2.7 Roquin-1 and Roquin-2 both repress ICOS mRNA ... 92
8.2.8 *Rc3h1/2*-deficient mice show increased follicular helper T and germinal center B cells, but no auto-antibodies ... 94
8.2.9 The spleen architecture in *Rc3h1/2*-deficient mice is massively disrupted ... 96
8.2.10 Roquin-1 and Roquin-2 control the transition point between Th1 and Tfh cell differentiation ... 98
8.2.11 Roquin-1/2 reciprocally influence Th17 and Treg differentiation ... 103
8.2.12 The NF-κB pathway is activated in *Rc3h1/2*-deficient cells ... 106
8.2.13 Ox40 activates the NF-κB pathway and is a novel target of Roquin-1 and -2 ... 107
8.2.14 Loss of Roquin-1/2 drives Tfh cell differentiation independently of Icos ... 110
8.2.15 Reducing IFN-γ levels in *Rc3h1/2*-deficient mice rescues splenic architecture but not effector-like phenotype ... 114

9 Discussion ... 119
9.1 The RNA-binding of Roquin-1 and Roquin-2 ... 119
9.1.1 Roquin-1 recognizes a *cis*-element in the 3'UTR of ICOS mRNA ... 119
9.1.2 Characterizing the *cis*-element in the ICOS 3'UTR further ... 121
9.1.3 The ROQ domain is a new RNA-binding domain ... 122
9.2 Roquin-1 and Roquin-2 serve redundant functions ... 123
9.2.1 Redundancy and lateral inhibition of Roquin-1 and Roquin-2 ... 123
9.2.2 Evolutionary role of *Rc3h1* gene duplication ... 125

9.3 Role of Roquin-1 and Roquin-2 in autoimmune disease 126
9.3.1 Do Roquin-1 and Roquin-2 intrinsically control Tfh cell differentiation? 126
9.3.2 How can increased co-stimulation drive Tfh cell commitment? 127
9.3.3 Which factors cause the splenic disorder in *Rc3h1/2*-deficient mice? 129
9.3.4 Can loss of Icos reverse the Roquin-1/2-knockout phenotype? 130
9.3.5 What is the role of IFN-γ in *Rc3h1/2*-deficient mice? 131
9.4 Conclusion 132
10 References 133
11 Publications 143
12 Contributions and acknowledgements 145

4 Abbreviations and nomenclature

Human RCK, EDC4, ICOS, OX40 and CTLA4 are written in capitals.

Mouse Rck, Edc4, Icos, Ox40 and Ctla4 are written in lowercase.

-/-	knockout
%	percent
°C	degree Celsius
+/+	wild-type
α	alpha
A	adenine
A549	human lung adenocarcinoma epithelial cell
AGO	argonaute protein
Ala	alanine
ANAs	anti-nuclear antibodies
APC	antigen-presenting cell
APS	ammonium persulphate
ARE	AU-rich element
Arg	arginine
Asn	asparagine
ATP	adenosine triphosphate
AUF	ARE RNA-binding protein
β	beta
BAFF	B cell-activating factor
BATF	basic leucine zipper transcription factor
BCR	B cell receptor
Bim	Bcl2-like 11 (BCL2L11)
Blimp1	B lymphocyte-induced maturation protein 1
bp	base pairs
BSA	bovine serum albumin
C	cytosine
Ca^{2+}	calcium
CAR	coxsackie adenovirus receptor
CCR7	CC-motif chemokine receptor 7
CD	cluster of differentiation
cDNA	complementary DNA
CDS	coding sequence
cIAP	cellular inhibitor of apoptosis protein
CTLA4	cytotoxic T-lymphocyte antigen 4
CXCR	CXC-motif chemokine receptor
δ	delta
DAG	diacylglycerol
DAPI	4,6-diamidino-2-phenylindol-dihydrochloride
DCP	decapping protein
dG	Gibbs free energy
DDX6	DEAD box helicase 6 (Rck)

DLBCL	diffuse large B cell lymphoma
DMSO	dimethyl sulfoxide
DN	double negative
DNA	deoxyribonucleic acid
dNTP	deoxynucleotide triphosphate
DP	double positive
dpc	days post coitum
ds	double-stranded
DTT	dithiothreitol
ε	epsilon
E. coli	*Escherichia coli*
EAE	experimental autoimmune encephalomyelitis
EDC	enhancer of decapping
EDTA	ethylenediaminetetraacetic acid
eGFP	enhanced green fluorescent protein
eIF	eukaryotic translation initiation factor
EMSA	electrophoretic mobility shift assay
EPRS	glutamyl-prolyl tRNA synthetase
EtOH	ethanol
FACS	fluorescence-activated cell sorting
FCS	fetal calf serum
FITC	Fluorescein isothiocyanate
FL	full-length
fl/fl	floxed allels
Foxp3	forkhead box P3
γ	gamma
G	glycine
g	relative centrifugal force
g	gramm
GAIT	IFN-γ-activated inhibitor of translation
GAPDH	glyceraldehyde 3 phosphate dehydrogenase
Gata3	GATA binding protein 3
GC	germinal center
GM-CSF	granulocyte-macrophage colony-stimulating factor
GRB	growth factor receptor-bound protein
GSK	glycogen synthase kinase
h	hour
HBS	Hank's Balanced Salt solution
HEDLS	human enhancer of decapping large subunit
HEK	human embryonic kidney cells
HIV	human immunodeficiency virus
HLA	human leucocyte antigen
HNRNPQ1	heteronuclear ribonucleoprotein Q1
HRP	horseradish peroxidase
i.v.	intravenously
ICOS	inducible T cell co-stimulator (CD278)
ICOSL	ICOS ligand
IFN	interferon
Ig	immunoglobulin
IKK	IκB kinase
IL	interleukin

IP_3	inositol-1,4,5-trisphosphate
IPTG	Isopropyl b-D-1-thiogalactopyranoside
IRES	internal ribosome entry site
Irf4	interferon regulatory factor 4
ITAM	immunoreceptor tyrosine-based activation motif
IκB	inhibitor of κB
κ	kappa
kb	kilo base pairs
kDa	kilo Dalton
LAT	linker for activation of T cells
LB	lysogeny broth (Luria-Bertani) medium
LCK	lymphocyte-specific protein tyrosine kinase
LMW	low molecular weight standard
LPS	lipopolysaccharide
LR	lambda recombination
Lsm	Like Sm proteins
LTαβ	lymphotoxin alpha, beta
Lys	lysine
μ	micro
M	molar
MEF	mouse embryonic fibroblast
Met	methionine
Mg^{2+}	magnesium
MHC	major histocompatibility complex
min	minute
miR	microRNA
miRNA	microRNA
ml	milliliter
mM	millimolar
Mnab	membrane-associated nucleic acid binding protein (Roquin-2)
MOI	multiplicity of infection
mRNA	messenger RNA
mRNP	messenger ribonucleoprotein
NEMO	NF-κB essential modulator
Neo	neomycin
NFAT	nuclear factor of activated T cell
NIK	NF-κB inducing kinase
NK cell	natural killer cell
NKT cell	natural killer T cell
NLS	nuclear localization signal
nm	nanometer
NMIA	N-methylisatoic anhydride
NMR	nuclear magnetic resonance
nts	nucleotides
OVA	ovalbumin
P body	processing body
PABP	poly(A)-binding protein
PAGE	polyacrylamide gel electrophoresis
PAMP	pathogen-associated molecular pattern
PBS	phosphate buffered saline
PCR	polymerase chain reaction

PD-1	programmed cell death protein 1
PDK	phosphoinositide-dependent kinase
pH	*potentia hydrogenii*
PI3K	phosphatidylinositol 3-kinase
PIP_2	phosphoinositol-4,5-bisphosphate
PIP_3	phosphoinositol-3,4,5-triphosphate
PKB / AKT	protein kinase B
PLC	phospholipase C
PTEN	phosphatase and tensin homologue deleted on chromosome 10
PTK	protein tyrosine kinase
PVDF	polyvinylidene fluoride
qPCR	quantitative PCR
R	arginine
RA	retinoic acid
RAG	recombinase activating gene
RANKL	receptor activator of NF-κB ligand
Rc3h1	ring finger and CCCH-type zinc finger domains 1 (Roquin-1)
Rc3h2	ring finger and CCCH-type zinc finger domains 2 (Roquin-2)
Rck	DEAD box helicase 6 (DDX6)
RIP1	receptor interacting protein 1
RISC	RNA-induced silencing complex
RNA	ribonucleic acid
RNase	ribonuclease
RORγt	RAR-related orphan receptor gamma T
RPL13A	ribosomal protein L13A
RRM	RNA recognition motif
RT	room temperature
s	second
san	*sanroque* allele (Roquin-1 mutation M199R)
SD	standard deviation
SDS	sodium dodecyl sulfate
SH	SRC homology
SHAPE	selective 2'-hydroxyl acylation analyzed by primer extension
SLE	systemic lupus erythematosus
SLP	SRC homology 2 (SH2)-domain-containing leukocyte protein
SP	single positive
SRBC	sheep red blood cells
SRC	sarcoma
Stat	signal transducer and activator of transcription
T	thymidine
T-bet	T-cell-specific T-box transcription factor
TAK1	Transforming growth factor beta activated kinase-1
TCR	T cell receptor
TEC	tyrosine-protein kinase
TEMED	N,N,N',N'-tetramethylethylendiamine
Tfh	follicular helper T cells
TGF	transforming growth factor
Th cell	T helper cell
TIA	T cell internal antigen
TKO	triple knockout
TNF	tumor necrosis factor

TNFR	tumor necrosis factor receptor
TNFRSF	tumor necrosis factor receptor superfamily
TRADD	TNFR1-associated DEATH domain protein
TRAF	TNF receptor associated factor
Treg cell	regulatory T cell
tRNA	transfer RNA
TTP	tristetraprolin
TUTase 4	terminal uridylyltransferase 4 (ZCCHC11)
Tyr	tyrosine
U	units
U	uracil
UTR	untranslated region
UV	ultraviolet
V	volt
v/v	volume per volume
vs.	versus
w/v	weight per volume
WT	wild-type
Xaa	unspecific amino acid
XRN	exoribonuclease
ζ	zeta
ZAP	zeta-chain-associated protein

5 Introduction

5.1 Boon and Bane of the immune system

The immune system protects an organism from invading pathogens. One of the most ancient means of defense is the innate immune system, which ensures rapid, unspecific responses to pathogens without establishing long-lasting immunity. The innate immune system is found in all animals and plants [1] and is seen as an evolutionary early immune response based on the recognition of specific pathogen-associated molecular patterns (PAMPs) such as bacterial LPS (lipopolysaccharide), double-stranded RNA viruses or glycolipids [1,2]. Detection of such structures by the innate immune system can activate the complement system or attract anti-microbial peptides, which attack the invaders. However, the fast co-evolution of pathogenic microorganisms necessitated the development of a second defense mechanism capable of fast adaptation and memory. This was established in jawed vertebrates, when a transposon carrying the precursors for the recombinase activating genes *RAG-1* and *RAG-2* created a new line of defense, called the adaptive immune system [2]. RAG-1 and RAG-2 proteins are essential for V-D-J gene rearrangement of T and B cell receptors (TCR and BCR, respectively) [3,4]. V-D-J rearrangement is a mechanism to create an enormous repertoire of heavy and light chains of the TCR or BCR [5]. During an immune response there is additional diversification of the variable (V) region of these receptors by somatic hypermutation, which introduces mutations into the V region to increase the receptor affinity. Together with further mechanisms, the human immune system comprises at least an estimated 10^8 lymphocyte receptors with unique specificity to detect invading pathogens [1]. However, the enormous diversity of the adaptive immune system is seen as double-edged sword as in this random process of modifying the receptor repertoire, each newly generated receptor could potentially react against the body's own cells (self-reactivity). Therefore, a number of tolerance mechanisms co-evolved to protect the body against self-reactive cells.

5.1.1 Generation and selection of T lymphocytes

The T and B lymphocytes are the centerpiece of the adaptive immune system. The bone marrow is the place of origin of both B and T cells. While B cells further mature in the bone marrow, T cell precursors migrate to the thymus for maturation and selection. The thymus

therefore has a pivotal role in shaping the peripheral T cell repertoire with unique T cell receptors recognizing foreign antigens [6].

During T cell development, two T cell lineages with different TCRs (α:β or γ:δ) are formed, and α:β T cells differentiate further into $CD4^+$ or $CD8^+$ T cells. Progenitor T cells start to rearrange their T cell receptor genes upon entering the thymus. If gene rearrangement creates a functional β-chain first, γ and δ gene rearrangement is stopped and vice versa [1,7]. The predominant T cell lineage in the thymus exhibits α:β TCRs. Development of α:β T cells starts with a CD4/CD8 double-negative (DN) state, which can be divided into the four precursor stages DN1, DN2, DN3 and DN4. Rearrangement of the β-chain starts at the DN2 stage and stalls in the DN3 stage, where the first pre-T cell receptor is expressed. In the DN4 stage, CD3, an essential component of the mature TCR complex, is expressed. Subsequently, the surface molecules CD4 and CD8 are expressed in a double-positive (DP) stage, which is accompanied by α-chain rearrangement and a process called positive selection [1,7]. In this process, α-chain gene rearrangement is continued until the TCR recognizes a self-peptide:self-MHC complex (major histocompatibility complex). Self-MHC restriction is a crucial step in the process of positive selection. It is ensured by a germline-encoded specificity of both chains of the TCR to the MHC and the requirement for CD4 and CD8 co-receptor binding [1,8]. T cells recognizing MHC class I molecules become cytotoxic $CD8^+$ T cells, while cells recognizing MHC class II complexes become $CD4^+$ T cells. The latter develop either into helper T cells or thymic regulatory T (Treg) cells. To limit maturation of potential self-recognizing T lymphocytes, cells will undergo apoptosis if they bind too strongly to their MHC. An intermediate-affinity to self-peptide:self-MHC complexes selects for thymic Treg cells [9]. During the process of positive selection only 10–30% of all thymocytes are selected. These cells further undergo negative selection during the double-positive and single-positive stage. Negative selection ensures that T cells recognizing self-peptides presented by stromal cells in the cortex as well as in the medulla of the thymus die by apoptosis. Only 2% of all thymocytes survive these selection processes and migrate into the periphery [1].

5.1.2 T cell co-stimulation and signaling

The strict selection processes to eliminate potentially self-reactive T cells during T cell development are not the only safety mechanisms in the adaptive immune system. Further receptor editing or deprivation of nutrients and growth factors can eliminate self-reactive T

cells [6]. Another fundamental control mechanism is the need of co-stimulation for T cell activation in the periphery, known as the "two-signal hypothesis" [10]. T cells encountering an antigen without receiving a second signal via a co-stimulatory receptor will become anergic (Figure 1).

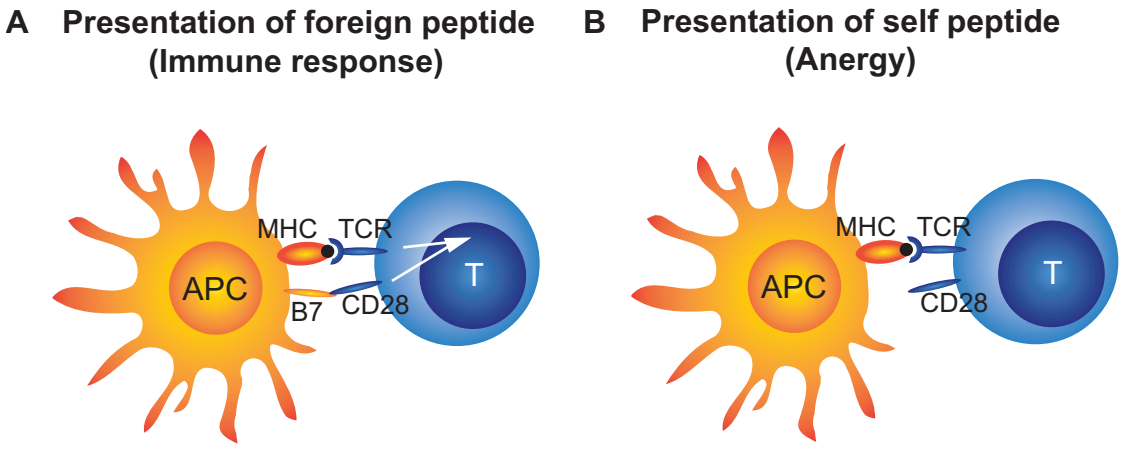

Figure 1: Two signals are required for effective T cell activation. (A) Antigen-presenting cells (APC) activated by contact with pathogens present foreign peptides bound to their MHC. Furthermore they up-regulate the expression of co-stimulatory ligands such as B7. T cells are activated by B7–CD28 co-stimulation in combination with recognition of peptide-MHC complexes. (B) APCs presenting self-peptides on their MHC do not provide co-stimulatory signals. Without a second signal, the interaction is not sufficient to fully activate the T cell, which becomes anergic. (Modified from [11].)

Anergy is a state of T cell unresponsiveness and ensures that self-reactive T cells cannot be activated but still survive. The avoidance of anergy is achieved by at least two mechanisms [12]. Signaling via the essential co-stimulatory receptor CD28 can inhibit the production of anergic factors [13]. However, the co-stimulus alone is not sufficient to avoid an anergic state. In addition, the stimulated cell has to progress through the cell cycle to develop its effector functions [14].

Upon encounter of a pathogenic microorganism, antigen-presenting cells (APCs) will take up the invading microorganism or antigens derived from them and present the antigen peptides on their MHC. Furthermore, they will up-regulate the ligands B7 and ICOSL (inducible co-stimulator ligand) for T cell co-stimulation [11,15]. CD28 is crucial for early signaling events after antigen-encounter [16-18]. It binds to the B7 ligands B7.1 (CD80) and B7.2 (CD86) on APCs. In the process of antigen recognition, an immunological synapse forms, to bring co-receptors and their ligands in close proximity [19]. Upon activation of the T cell by TCR and receptor stimuli, a complex cascade of TCR signaling events switches on effector functions in

the T cells. The ζ-chain dimer in the TCR complex contains immunoreceptor tyrosine-based activation motifs (ITAMs) in its cytoplasmic tail, which are phosphorylated upon activation and lead to the recruitment of the protein tyrosine kinase (PTK) ZAP70 (ζ-chain-associated protein of 70 kDa). ZAP70 is activated by the co-receptor-associated Src kinase LCK and in turn activates LAT (linker for activation of T cells) and SLP76 (SRC homology 2 (SH2)-domain-containing leukocyte protein of 76 kDa). These proteins act as scaffold and recruit PLCγ (phospholipase Cγ1), which is subsequently phosphorylated by kinases of the TEC family. Active PLCγ catalyzes the cleavage of phosphoinositol-4,5-bisphosphate (PIP_2) to inositol-1,4,5-trisphosphate (IP_3) and diacylglycerol (DAG). While DAG stays associated with the membrane, IP_3 causes the depletion of Ca^{2+} stores in the endoplasmic reticulum. This store-depletion induces an opening of store-operated calcium channels in the membrane that then allows extracellular Ca^{2+} to enter the cytoplasm. This influx of Ca^{2+} eventually activates NFATs (nuclear factors of activated T cells), which are essential for the induction of genes involved in establishing effector functions [1,20].

One of the most important co-stimulatory receptors in early T cell activation is CD28. It induces the expression of the growth-factor IL-2 and anti-apoptotic factors, thereby preventing anergy and apoptosis [20]. Furthermore, CD28 ligation reduces the number of TCRs sufficient for activation by lowering the activation threshold for signaling [21]. The essential role of CD28 in co-stimulation is demonstrated in mice deficient for CD28. These mice exhibit reduced levels of immunoglobulins and are impaired in class switching [22]. Likewise, mice deficient for B7 receptors fail to elicit immunoglobulin class switching and germinal center formation after immunization [23]. However, these studies also point out the existence of alternative co-stimulatory mechanisms [22].

CD28 belongs to the immunoglobulin superfamily with a variable immunoglobulin-like domain for ligand recognition. The inducible co-stimulator ICOS and Cytotoxic T-Lymphocyte Antigen 4 (CTLA4) are two additional co-stimulators, which are structurally related to CD28 [24,25]. They all share the common intracellular signaling motif Tyr-Xaa-Xaa-Met. This motif functions as a binding site for the SH2 domains of p85, an adaptor protein for the catalytic subunit of phosphatidylinositol 3-kinase (PI3K). PI3K signaling is one of the central pathways for T cell activation and the production of an active immune response.

CD28, ICOS and CTLA4 have developed diversified functions, despite their structural relationship. The cytosolic portion of CD28 binds to GRB2 (growth factor receptor-bound protein 2) via an asparagine (Asn) residue at the +2 position (Tyr-Xaa-Asn-Met), which is not present in the cytosolic tails of ICOS or CTLA4 [25]. On the extracellular level, both CD28 and

CTLA4 bind to the B7.1 and B7.2 receptors on APCs. CTLA4 has a higher binding affinity to these receptors, as it interacts as a dimer with two different B7 dimers, while CD28 can only bind one dimer [25]. CTLA4 is an essential negative regulator of the immune response. It is induced on T cells after activation and captures its ligands on APCs by a mechanism called *trans*-endocytosis. The ligands are internalized into the CTLA4-expressing cells and subsequently degraded. This leads to a stop of T cell proliferation, as CD28 is no longer able to signal [26]. Mice deficient for Ctla4 die soon after birth, because of overshooting T cell proliferation, which finally causes organ destruction by lymphocyte infiltration [27]. This highlights the importance of negative co-stimulation and regulation in immune responses.

ICOS is another activator of the immune system. It is induced after T cell activation and is dependent on CD28 co-stimulation [17,28]. Its ligand (ICOSL) is constitutively expressed on B cells and macrophages and can be induced on non-lymphoid tissues by inflammatory stimuli [15]. Unlike CD28, ICOS cannot induce IL-2 expression, but is responsible for stimulating the production of a number of other cytokines such as IFN-γ, TNFα, IL-4, IL-5 and IL-10 [17,28,29]. ICOS influences both IL-4 and IL-21 expression by regulating the transcription factor c-Maf [30-32]. Furthermore, ICOS is essential for class switching and affinity maturation of immunoglobulins. Mice deficient for Icos exhibit diminished T cell effector functions and impaired germinal center formation, which cannot be formed in a secondary immune reaction [33-35]. Additionally, the development of follicular T helper (Tfh) cells is severely impaired in the absence of ICOS co-stimulation [36,37]. Both deficiency and overexpression of ICOS are linked to autoimmune diseases. *Icos*-deficient mice are more susceptible to experimental autoimmune encephalomyelitis (EAE) than wild-type mice [38]. Conversely, increased ICOS levels are linked to systemic lupus erythematosus (SLE), as an overactive immune system fails to suppress self-reactive T cell responses [39].

Other co-stimulators such as tumor necrosis factor (TNF) receptor family members 4-1BB (tumor necrosis factor receptor superfamily 9 or TNFRSF9) or OX40 (tumor necrosis factor receptor superfamily 4 or TNFRSF4) also play key roles in T cell survival and cell division. OX40 and 4-1BB are important for memory formation and maintenance [40-43]. Transgenic expression of OX40L on T cells leads to autoimmune-like diseases with massive accumulation of effector memory $CD4^+$ T cells [44]. A single dose of an antibody, which stimulates OX40 signaling was able to break established tolerance in $CD4^+$ T cells and restored T cell effector function [45]. This further underlines the potential damage of excessive or defective co-stimulation. Therefore, therapeutic targeting of co-stimulatory receptors might be beneficial in a number of human autoimmune diseases.

5.1.3 Common co-receptor signaling pathways

There are numerous signaling pathways that determine lymphocyte development and differentiation, thereby responding to a complex network of intracellular and intercellular signals. This section focuses on the fundamental mechanisms of NF-κB and PI3K signaling (Figure 2), both involved in the regulation of cell growth, proliferation, survival and differentiation [46,47].

The co-receptors CD28, ICOS and CTLA4 can all signal via PI3K recruitment [25]. Receptors binding to PI3K stimulate the generation of phosphatidylinositol-3,4,5-triphosphate (PIP_3), leading to the subsequent activation of PDK1 (phosphoinositide-dependent kinase 1) and PKB (protein kinase B, also known as AKT) [46]. PKB phosphorylates GSK3 (glycogen synthase kinase 3) and loss of inhibition by GSK3 as well as dephosphorylation of NFAT by Ca^{2+} signaling events allow the translocation of NFAT into the nucleus and the induction of transcription [25]. PTEN (phosphatase and tensin homolog deleted on chromosome 10) is opposing PI3K signaling by controlling basal PIP_3 levels [48]. In the absence of PTEN, TCR engagement without co-stimulation is sufficient for proliferation and induction of IL-2, leading to lymphomas and autoimmunity [49-51]. Buckler et al. therefore suggest that CD28 co-stimulation is required to overcome negative regulation by PTEN, which sets a threshold for full TCR activation [49] (Figure 2, left).

CD28 family members can also induce the NF-κB (nuclear factor-κB) pathway [52-54]. NF-κB signaling is also responsible for the production of IL-2 and anti-apoptotic factors as well as for the induction of other transcription factors such as Irf4 [55]. Rel/NF-κB family members include RelA, c-Rel, RelB, NF-κB1 (p50 and its precursor form p105) and NF-κB2 (p52 and its precursor p100). They share a common Rel homology domain (RHD) in their amino-terminal region, which is essential for their dimerization and binding to DNA [56]. RelA, RelB and c-Rel further contain a carboxy-terminal TAD domain (transcription activation domain). Without activation, these NF-κB factors are retained in the cytoplasm by IκBs (inhibitors of NF-κB), comprising several members such as IκBα, IκBβ or IκBε. These inhibitors bind to NF-κB dimers by multiple ankyrin repeats and mask their nuclear localization signal (NLS) [57,58]. Both the canonical and alternative NF-κB pathway can be activated by a number of stimuli such as cytokines or the receptors of the TNF family OX40 and CD40L. There are, however, also specific sets of receptors activating only one of these pathways [59]. For example RANKL (receptor activator of NF-κB ligand) and LTαβ predominantly activate the alternative pathway [47], while LPS, IL-1β and TNFα activate the canonical pathway. Upon TNFα signaling via the receptor TNFR1, the adapter protein TRADD (TNFR1-associated

DEATH domain protein) recruits the ubiquitin ligases TRAF2 and TRAF5 (TNF receptor associated factor) as well as the protein kinase RIP1 (receptor interacting protein 1). However, RIP1 probably functions more as another adapter protein for the recruitment of the trimeric IKK (IκB kinase) complex. TRAF2 ubiquitinates RIP1 and further recruits IKKα, IKKβ and IKKγ (also named NEMO for NF-κB essential modulator). The binding of the IKK complex to ubiquitinated RIP1 stabilizes the interaction with the TRAF receptor complex. Furthermore, RIP1 ubiquitination as well as conformational changes in the IKK complex structure lead to the recruitment of TAK1 (transforming growth factor β activated kinase-1) to TRAF2. TAK1 phosphorylates IKKβ and the subsequent phosphorylation of IκBα leads to ubiquitination and proteasomal degradation of the inhibitor [60]. This liberates the NF-κB heterodimer p50 and RelA (also named p65), which translocates into the nucleus for activation of transcription (Figure 2, middle).

Activation of the alternative NF-κB pathway establishes the formation of an ubiquitin ligase complex consisting of TRAF2, TRAF3, cIAP1 and cIAP2 (cIAP1/2, cellular inhibitor of apoptosis protein). The formation of this complex leads to self-ubiquitination of TRAF2 and TRAF2-dependent polyubiquitination of cIAP1/2. Modified cIAP1/2 ubiquitinates TRAF3, which leads to the proteasomal degradation of the latter. Low levels of TRAF3 stabilize NF-κB inducing kinase (NIK) as it cannot be recruited to the TRAF2/cIAP1/2 complex anymore, which would ensure constant degradation of NIK in the absence of activation. However, stabilization of NIK, accompanied by *trans*-autophosphorylation, results in the phosphorylation and activation of the IKKα dimers. IKKα phosphorylates p100, which is partially degraded to p52, and releases the p52/RelB complex to translocate into the nucleus for inducing gene transcription [47,56,61] (Figure 2, right).

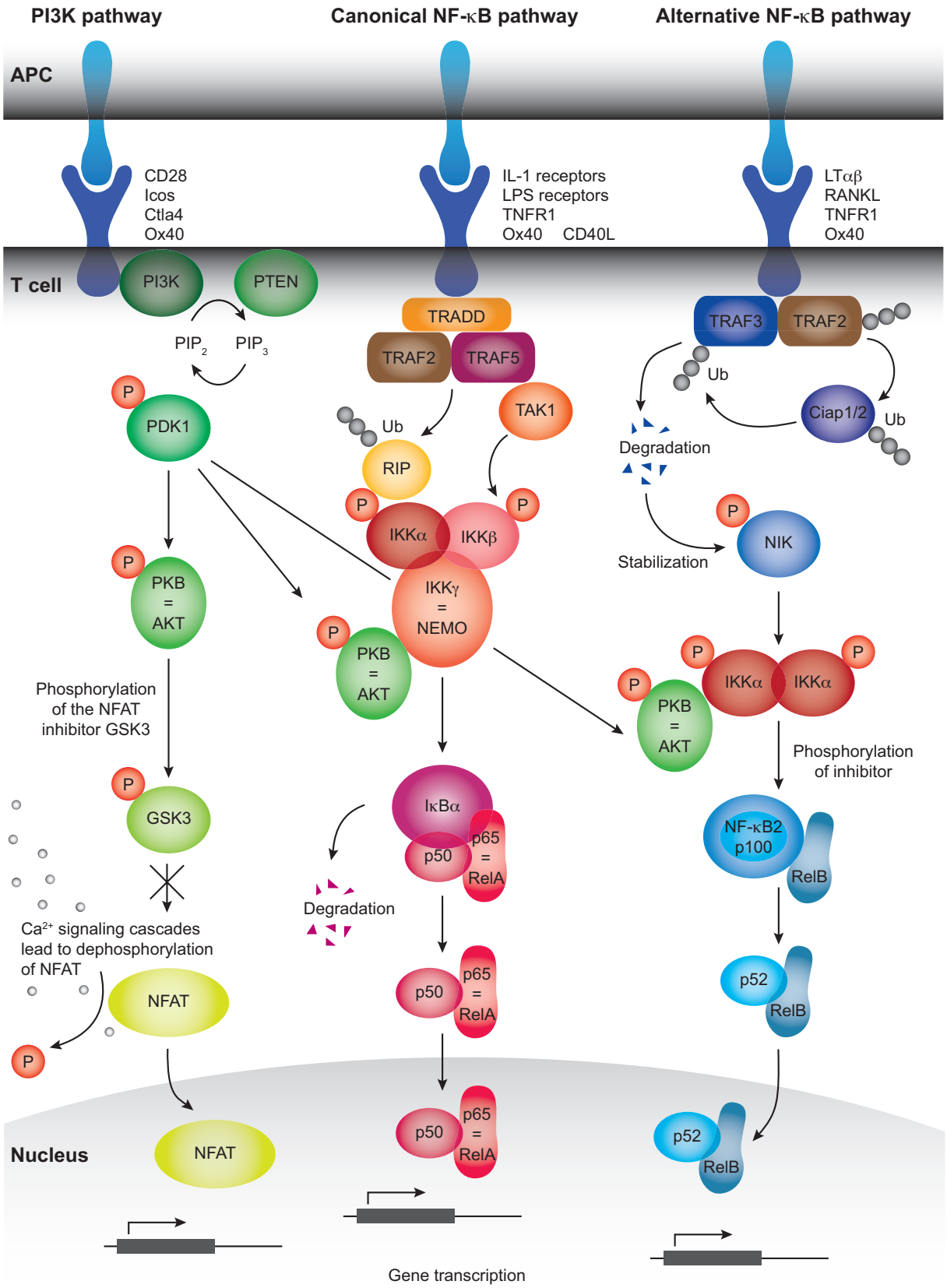

Figure 2: PI3K and NF-κB signaling. Activation of the PI3K pathway leads to a phosphorylation cascade and the initiation of transcription upon nuclear translocation of NFAT. Signaling via the canonical and alternative NF-κB pathway leads to the release of transcriptional activators from their inhibition and their translocation into the nucleus. A detailed description of these pathways is given in section 5.1.3.

Research in the field of NF-κB signaling is progressing fast, as defects in the signaling pathway are responsible for lymphoid malignancies. This adds numerous branches as well as negative and positive regulators to these pathways and elucidates cross-connections to other signaling pathways such as the PI3K pathway. The phosphorylation cascade of PI3K, PDK and PKB, for example, leads to the phosphorylation of IKKs and the subsequent degradation of IκBs, thereby activating the canonical or alternative NF-κB pathway [25]. This was demonstrated by disrupting CD28 receptor binding, which diminished the activation of IKK [62], while CD28 signaling normally enhances the activity of IKK [63,64].

5.1.4 Differentiation of T helper cells

By regulating cytokine transcription, the NF-κB pathways not only influence cell survival and proliferation, but also play an essential role in effector T cell differentiation [65]. $CD4^+$ T cells can differentiate into several distinct T helper (Th) cell subsets, depending on the environmental stimulus and type of infection. The cytokine profile of helper T cells together with specific "key" transcription factors are used to distinguish the different T helper cell subsets. It is generally understood that Th1 cells are characterized by the transcription factor T-bet, Th2 by Gata3, Th17 by RORγt and Treg cells by Foxp3. However, recent research has discovered remarkable plasticity among T helper cells [66-68]. Furthermore, new subsets were discovered, such as follicular T helper (Tfh) cells, which were not readily acknowledged by the community. While Tfh cells were accepted as a new T helper cell subset with the discovery of the transcription factor Bcl6 as essential transcription factor for their development [69-71], other subsets such as Th9 or Th22 cells are still not fully appreciated [66,68,72] (Figure 3).

The first subsets described were Th1 and Th2 cells [73]. Intracellular pathogens trigger the differentiation of Th1 cells producing IFN-γ. The release of IL-12 by innate immune cells and IFN-γ by NK and T cells induces the differentiation program of Th1 via the transcription factors T-bet, Stat1 and Stat4 [66,74,75]. Th2 cells secrete the cytokines IL-4, IL-5 and IL-13 and are effective against helminthes and extracellular pathogens. Their differentiation program is initiated by IL-4 and the transcription factor Stat6, both activating Gata3 expression [66,76-79]. However, even these seemingly stable Th1 and Th2 cell subsets can be converted upon certain stimuli. Th2 cells can be reprogrammed to T-bet/IFN-γ expressing cells in viral infections [80,81] and Th1 cells can convert into Th2 cells under certain circumstances [81]. Redirecting a transcriptional T cell profile might be beneficial for the host, as it provides certain flexibility to react appropriately to specific pathogens by simply shifting resources [66].

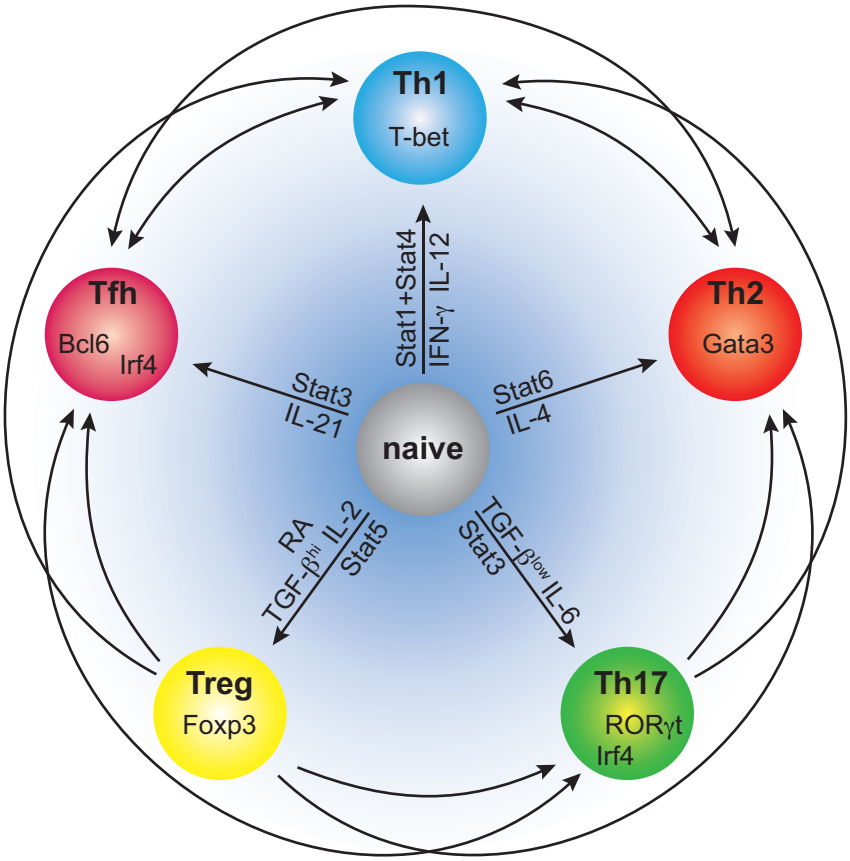

Figure 3: T cell differentiation and plasticity. The differentiation program of T cell subsets is governed by cytokines and transcription factors. However, recent studies reveal unexpected flexibility and plasticity of these differentiation programs. Seemingly stable T helper cell subsets were shown to completely switch their cytokine and gene expression profile or to express more than one key transcription factor. This flexibility might ensure a fast and specific response against invading pathogens. (Adapted from [66,67].)

Th17 cells are another subset important in the control of extracellular bacteria or fungi, especially at mucosal surfaces. The Th17 differentiation program is initiated by the cytokines TGF-β, IL-6, IL-21 and IL-23. The cytokine signaling activates the Th17 transcription factor RORγt via phosphorylation of the transcription factor Stat3 [82]. After an initial phase of effector cell expansion, regulatory T cells are induced to limit the immune response and to maintain immune homeostasis. Scurfy mice lacking thymus-derived ($CD4^+$ $CD25^+$) and TGF-β-induced Treg cells develop a severe autoimmune disease by producing excessive amounts of Th1 and Th2 cytokines [83-85].

Although originated by a reciprocal differentiation program [86,87], both peripheral Treg cells and Th17 cells depend on TGF-β. Th17 cells loose IL-17A and IL-17F expression in culture without addition of TGF-β or IL-6 and can convert into Th1 or Th2 cells in the presence of IL-12 or IL-4, respectively. Furthermore, mice, deficient for TGF-β, lack Treg cells as well as

Th17 cells and develop an autoimmune disease characterized by uncontrolled Th1 cell differentiation. TGF-β causes the up-regulation of both Foxp3 and RORγt, leading to the assumption that there might be a transient cell population, which can give rise to both Treg cells and Th17 cells [88]. Low TGF-β amounts together with pro-inflammatory cytokines up-regulate RORγt favoring Th17 differentiation and Foxp3 can no longer inhibit RORγt. High amounts of TGF-β, IL-2 and retinoic acid (RA) enhance Treg and inhibit Th17 differentiation [87]. However, these subsets are not terminally differentiated. In the gut, Treg cells can be converted into Th17 cells. This switch might be beneficial in response to specific pathogens such as fungi, which are known to induce this conversion [66,89]. Another transcription factor crucial for Th17 differentiation is Irf4 [90], which is also a direct target of Foxp3 [91]. Irf4 might also be involved in reprogramming Treg cells towards the Tfh cell phenotype [66]. Interestingly, a subgroup of Treg cells was discovered, expressing the Tfh transcription factor Bcl6. These regulatory Tfh cells constrain B cells in the germinal center, suggesting that Treg cells adapt to the transcriptional profile of their target cells [92,93].

In the germinal center reaction, T cells are required for humoral immune responses in which they give help to B cells. This function is provided by specialized Tfh cells that express the chemokine receptor CXCR5, the co-stimulatory molecules PD-1 and ICOS, the transcription factor Bcl6 and the cytokine IL-21 [94]. Tfh cell differentiation has been proposed to occur in a step-wise manner [94]. A strong TCR signal already drives T cells towards Tfh cell differentiation [95]. This priming by dendritic cells then triggers up-regulation of ICOS on the T cell, which is required for the subsequent expression of Bcl6. Induction of CXCR5 by Bcl6 [96] and down-regulation of the chemokine receptor CCR7 allows T cell migration towards the T-B cell boundary of follicles in the secondary lymphoid organs [97-99]. There, the contact with B cells and sufficient co-stimulation through several receptor-ligand pairs is required for the maintenance of Tfh cells [94]. The initial up-regulation and sustained expression of Bcl6 [100] is crucial for Tfh cell differentiation, but additional transcription factors such as c-Maf and Batf cooperate in the program [30,101-103]. Furthermore, mice deficient for Irf4 cannot develop follicular helper T cells [104,105] and Irf4 cooperates with Stat3 to regulate gene expression downstream of IL-21 stimulation [104]. In contrast, Blimp1 which is induced through IL-2 and Stat5 signaling, counteracts the commitment to this subset [69,70,106].

The transcription factors involved in Tfh cell differentiation also play a role in other subsets suggesting functional plasticity [30,31,90,107,108]. Furthermore, it was recently shown that cells in Th1 *in vitro* differentiation conditions pass through a stage shared with Tfh cells, which was marked by simultaneous expression of Bcl6, T-bet, IL-21 and IFN-γ. Subsequent input from

cytokines such as IL-12 and balanced regulation of epigenetics and gene expression then either enforces Th1 or Tfh commitment [108]. Moreover, plasticity of the differentiation program was also demonstrated in an IL-21 reporter mouse model *in vivo* [109].

5.1.5 Autoimmunity caused by inappropriate or defective co-stimulation and T cell differentiation

The cellular transition point to the Tfh cell subset has to be tightly controlled, since auto-reactive Tfh cells play a role in the development of autoimmune diseases [110,111]. In humans, a circulating Tfh-like population was found in 20–30% of patients with systemic lupus erythematosus. Patients with Sjogren's syndrome also displayed an increased population of circulating Tfh-like cells [112]. Tfh cells regulate the development of antigen-specific B cells and trigger germinal center formation. It is therefore not surprising that failed negative selection of somatically mutated germinal center B cells can also lead to lupus-like autoimmunity [113,114]. In systemic autoimmune diseases such as SLE, auto-reactive antibodies are often directed against nuclear antigens such as dsDNA [114,115]. Such auto-antigens are abundantly expressed on apoptotic cells present in the germinal center [116].

Systemic autoimmune diseases such as SLE are normally caused by the concurrence of several cellular abnormalities [117]. However, a single point mutation in the gene *Rc3h1* (named *Rc3h1*^{san}, expressing the protein Roquin-1^{san}) caused a lupus-like autoimmune phenotype in mice, involving enhanced numbers of Tfh cells and spontaneous germinal center formation. These findings imply an important role for Roquin-1 in Tfh cell differentiation or homeostasis. The san/san mice developed anti-nuclear and anti-DNA antibodies and showed elevated levels of Icos on all T cells [39]. This suggested that increased Icos co-stimulation could lead to the autoimmunity observed in the san/san mouse. In fact, a number of studies showed that experimentally induced constitutive co-stimulation, which is normally restricted in a spatial or temporal manner, can trigger autoimmunity. One example is Ox40 on T cells. Mice with ectopic co-expression of the Ox40 ligand on T cells develop autoimmune and auto-inflammatory phenotypes and have anti-DNA antibodies in the serum [44]. In line with this notion is that CD28 deficiency, which normally prevents germinal center reactions, was functionally reconstituted in the context of the san/san genotype [118]. Conversely, heterozygosity of Icos partially rescued san/san-associated phenotypes [119]. However, increased Icos levels on all T cells were also observed in mice that lack Roquin-1 in T cells or in the hematopoietic system, but failed to elicit elevated follicular helper T cell numbers or anti-nuclear antibody responses [120]. These findings question the previous concept in which

impaired post-transcriptional regulation of Icos mRNA by the Roquin-1^{san} protein leads to increased differentiation or expansion of auto-reactive Tfh cells, which then cause autoimmunity.

5.2 Post-transcriptional gene regulation

Transcriptional regulons control the first steps in gene expression and have been intensively studied over the past decades. This transcriptional regulation is rather a slow process, in which a gene is switched on, transcribed and translated or switched off and repressed. In the latter case, transcripts can persist long after transcription has been terminated, constituting a potential drawback if rapid responses are required [121]. Post-transcriptional gene regulation on the other hand ensures rapid changes in target gene expression in the course of changing environmental stimuli and is well established in the control of several cellular transition points in immune cells [122,123]. Such post-transcriptional mechanisms influence the stability and translation of mRNA and even include modifications at the protein level.

In immune responses for example, rapid induction of pro-inflammatory molecules is crucial to combat invading pathogens. However, of similar importance is the intensive control and timed shut down of pro-inflammatory molecules during the resolution phase of the inflammatory response to avoid excessive tissue damage [124]. For the coordination of such pro-inflammatory molecules in immune responses, post-transcriptional control mechanisms have evolved to play a dominant role [123].

Consequently, failed post-transcriptional control is associated with a number of human diseases such as cancer or Alzheimer's disease [125]. In many human tumors, the mRNAs of growth factors are stabilized, including GM-CSF (granulocyte-macrophage colony-stimulating factor), IL-1 and IL-6 [126]. Another example is the proto-oncogene *c-myc*, which is frequently mutated in cancer [127,128]. Hollis et al. discovered that a chromosomal translocation event in *c-myc*, causing the deletion of a 61 nucleotide AT-rich sequence in the 3'untranslated region (3'UTR), stabilized c-myc mRNA and led to T cell leukemia [127].

5.2.1 *Trans*-acting factors and *cis*-elements regulate mRNA stability

The structure and sequence of an mRNA crucially determines the way it is regulated. A 5' 7-methyl-guanosine (7^{me}G) cap and 3' poly(A) tail stabilize the mRNA, which further consists of a 5'UTR, a coding sequence (CDS) and a 3'UTR. Most *trans*-acting factors target the 3'UTR for mRNA regulation by binding to specific *cis*-elements [121] and the number of such

cis-elements in the 3'UTR greatly influences the stability of mRNA transcripts [123]. Therefore, activated T cells express mRNAs with shortened 3'UTRs to avoid destabilization by such *cis*-elements [129].

In eukaryotic cells, the first step of mRNA degradation is the shortening of the poly(A) tail. However, as long as the poly(A)-binding protein (PABP) is associated with the mRNA, it is protected against degradation [130,131]. PABP binds to eIF4G1 (eukaryotic initiation factor 4G1), which is associated with the cap-binding factor eIF4E leading to the circularization of the mRNA and stimulation of translation [121] (Figure 4).

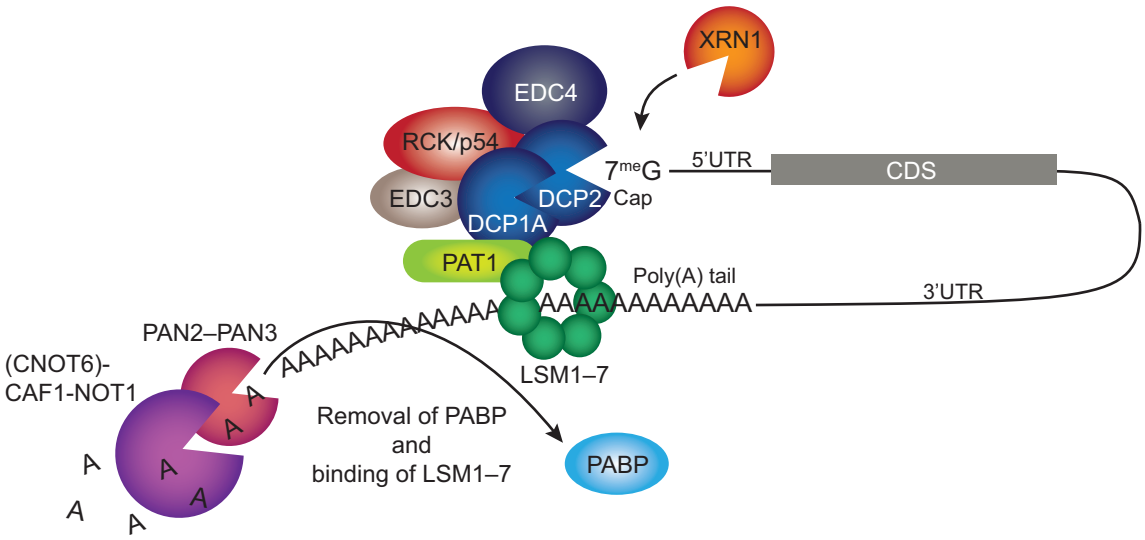

Figure 4: Regulation of mRNA stability. The first step in mRNA degradation is the shortening of the poly(A) tail by the deadenylase complexes PAN2–PAN3 and (CNOT6)-CAF1-NOT1. Subsequent replacement of the poly(A)-binding protein (PABP) and binding of the LSM1–7-PAT1 complex recruits and stimulates the decapping complex DCP1A–DCP2, which associates with EDC4, RCK/p54 and EDC3. The DCP1A–DCP2 complex subsequently removes the 5'cap structure of the mRNA and the mRNA is further degraded by the exoribonuclease XRN1. (Modified from [121].)

Degradation of mRNA is accomplished by the sequential action of two deadenylase complexes. Initially, the PAN2–PAN3 complex shortens the poly(A) tail to a size of 50–110 nucleotides, depending on the organism and the respective mRNA. These nucleotides are then further trimmed by the (CNOT6)-CAF1-NOT1 complex (CCR4-NOT transcription complex subunit 6 (CNOT6)-CAF1-NOT1 complex) with its catalytically active CCR4 and CAF1 (=POP2) subunits. The conversion of polyadenylation into oligoadenylation displaces PABP from the mRNA and enables the binding of the LSM1–7-PAT1 complex [121,132,133]. The binding of this complex stimulates the decapping activity of DCP2 and enables the decapping

complex DCP1A–DCP2 to remove the 5'cap structure. Assembly and activity of the DCP1A–DCP2 complex is also enhanced by EDC4 (enhancer of decapping 4, also named HEDLS), which interacts with the complex together with EDC3 and RCK/p54 [134]. The helicase RCK/p54 (also named DDX6) is essential for ATP-dependent unwinding of RNA structures or for displacing other factors bound at the mRNA [135]. The 5'-3' exoribonuclease XRN1 then degrades the mRNA (Figure 4). However, also 3'-5' exoribonucleases are involved in further mRNA degradation.

Trans-acting factors bind to certain *cis*-elements in their target mRNAs. Some of these *cis*-elements are well characterized, such as AU-rich elements (AREs). These AREs are characterized by clusters of AUUUA pentamers or UUAUUUAUU nonamers [136]. Well-known examples for ARE-binding proteins are HuR, AUF1 (ARE RNA-binding protein 1) and TTP (tristetraprolin), the latter one contains a tandem RNA-binding zinc finger domain. TTP destabilizes important inflammatory molecules such as TNFα, IL-2, IL-6, IL-10, IFN-γ or GM-CSF. Mice deficient for TTP suffer from arthritis, dermatitis and cachexia, a syndrome caused by the overexpression of pro-inflammatory cytokines including TNFα [137]. TTP negatively regulates TNFα by binding to its ARE and directly interacting with components of the mRNA decay machinery, including the decapping complex DCP1A–DCP2, the deadenylase CNOT6, the exoribonuclease XRN1, the exosome complex endonuclease PM-SCL75 and AGO2 [121]. Most *trans*-acting factors destabilize mRNA either by inducing mRNA decay by decapping or by interfering with translation initiation. However, HuR acts both as stabilizer and destabilizer. Three classic RNA recognition motifs (RRMs) allow binding of HuR to AREs in transcripts encoding IL-4, TNFα or IFN-γ, thereby stabilizing their expression [121,138]. In contrast, HuR represses c-Myc expression in cooperation with AGO2 and let-7 microRNA (miRNA) [139]. The terminal uridylyltransferase 4 (TUTase 4 or ZCCHC11) is another stabilizing factor, however, interfering with the miRNA-pathway. ZCCHC11 inhibits the miR-26 family of miRNAs by adding uridine residues to their 3'end. This leads to the de-repression of the IL-6 transcript [140].

MicroRNAs are another class of *trans*-acting factors. These small (ca. 22 nucleotides) non-coding single-stranded RNAs are generated from precursors, which are processed in the nucleus by the RNaseIII Drosha and the RNA-binding protein DGCR8, before they are exported into the cytoplasm. There, the RNaseIII Dicer performs the essential processing of the pre-miRNA into a mature miRNA duplex. One strand of this mature miRNA is loaded onto the AGO-containing RNA-induced silencing complex (RISC). The RISC-loaded miRNA then binds to partially complementary sequences mostly in the 3'UTR of target mRNAs and

represses their expression [122]. MicroRNAs regulate essential processes such as development, cell differentiation and immune cell homeostasis. Although most miRNAs are responsible for fine-tuning of gene expression, functional analyses revealed several single miRNAs with crucial roles in controlling cellular transition points [122]. The germinal center response, for example, is controlled by miR-155. Mice deficient for miR-155 develop less germinal center B cells in Peyer's patches and mesenteric lymph nodes. MiR-155 seems to be required for the efficient selection of cells producing high affinity antibodies [141]. Conversely, miR-155 is highly expressed in a wide range of B cell-derived lymphomas, including Burkitt's lymphoma or the aggressive diffuse large B cell lymphoma (DLBCL) [142]. Overexpression of the miRNA cluster miR-17–92 in mice also promoted lymphomagenesis and autoimmune disease, probably by suppressing the tumor suppressor PTEN and the pro-apoptotic protein Bim [143].

It is important to note that *trans*-acting proteins can bind to specific sequences as well as to structural elements. Watts et al., who have deciphered the entire structure of the HIV genome by SHAPE-analysis, pointed out that secondary RNA structures contain numerous unrecognized regulatory elements, playing essential roles in the genetic landscape [144]. An example for structure-specific binding is the GAIT element, a 29-nucleotide hairpin structure in the 3'UTR of inflammatory modulators. Inhibition of target transcripts can be induced by IFN-γ, which initiates the formation of the GAIT (IFN-γ activated inhibitor of translation) complex and the binding to the GAIT element. This complex consists of the four proteins glutamyl-prolyl tRNA synthetase EPRS, heteronuclear ribonucleoprotein Q1 (HNRNPQ1), glyceraldehyde 3 phosphate dehydrogenase (GAPDH) and the ribosomal protein L13A (RPL13A). The GAIT complex interferes with the initiation of translation: RPL13A binding to eIF4G1, a factor of the 48S pre-initiation complex, prevents the recruitment of eIF3, thereby inhibiting translation [121].

5.2.2 P bodies and stress granules regulate mRNA processing

The rate of translation or degradation of mRNAs is determined by a dynamic balance between polysomes (cluster of translating ribosomes bound to RNA) and processing (P) bodies. P bodies are membrane-less foci in the cytoplasm of cells, where mRNAs are stored for reversible repression or degradation [145]. Most of the factors described above (section 5.2.1) localize to these P bodies. However, no components of translation initiation such as PABP or ribosomal proteins are present in P bodies, indicating that P bodies are primarily places of mRNA decay and storage. Consequently, the decapping enzymes DCP1A–DCP2 localize to P bodies as well as decapping enhancers such as RCK/p54, EDC3 or EDC4. Furthermore, the

deadenylation complex (CNOT6)-CAF1-NOT1, LSM proteins and the 5'-3' exoribonuclease XRN1 localize to P bodies. Importantly, also factors of the miRNA-pathway are found within P bodies [145]. So far the exact mechanism of P body assembly has not been described, but is known to be dependent on the presence of RNA, since treatment of P bodies with RNase disrupts their structure. The contribution of other P body components is less clear, though. Knockdown of components of the miRNA biogenesis pathway as well as other P body-residing proteins such as RCK/p54 or LSM4 reduces P body numbers to a great extent [145]. However, P body formation is not per se dependent on those components, which rather might contribute to P body assembly by influencing the translationally inactive RNA pool. In addition, although RNA decay is generally associated with P bodies, the formation of the foci is not crucial for mRNA repression. Knockdown of RCK/p54, for example, disrupts P body formation, yet without affecting miRNA-mediated translational repression [146]. Therefore, P bodies might constitute compartments for the assembly of decay enzymes to increase their efficiency in two ways. First, compartmentalization brings interaction partners in close proximity and second, the protein–RNA complexes are isolated from the translation machinery.

In addition to P bodies, eukaryotic cells also contain other messenger ribonucleoprotein (mRNP) complexes such as stress granules. These granules accumulate adjacent to P bodies if cells undergo environmental stress conditions such as heat shock or oxidative stress. Stress causes the phosphorylation of eIF2α (eukaryotic translation initiation factor 2 alpha), which leads to a reduction of eIF2-GTP-$tRNA^{MET}$, the ternary complex that normally loads methionine onto the 48S pre-initiation complex to initiate translation. The T cell internal antigen-1 causes the assembly of stress granules by dissolving such translationally inactive pre-initiation complexes [147]. The lack of the decapping enzymes DCP1A–DCP2 and the presence of transcription initiation factors in stress granules indicate that these mRNP complexes function in the storage of stalled translation initiation complexes due to adverse environmental conditions. Interestingly, Roquin-1 was also proposed to localize to stress granules [39]. Stress granules and P bodies also share components such as XRN1 and TTP, the latter one being responsible for mRNA exchange between P bodies and stress granules [148]. However, there are still many open questions concerning the significance and assembly of P bodies and stress granules as well as the dynamics of mRNA exchange and degradation.

5.3 Objective of the research work

The protein Roquin-1 is one of the rare examples in which a single point mutation in a gene results in a complex autoimmune disease in mice [39]. Elevated Icos levels were held responsible for the spontaneous formation of follicular helper T cells and germinal centers in mice with the M199R mutation in Roquin-1^{san}. Although the same group could show that Roquin-1 limited the abundance of Icos mRNA [119], the exact mechanism how Icos was regulated remained unknown.

Before the start of this research project, extensive structure-function analyses were performed to investigate the role of each protein domain in Roquin-1. Furthermore, the molecular mechanism by which Roquin-1 represses Icos was investigated with respect to dependency on or cooperation with the miRNA pathway. These studies revealed that Roquin-1 functions independently of the miRNA pathway to repress Icos [149,150]. Amino-terminal sequences, especially the newly defined ROQ domain, are involved in mRNA interaction, whereas the carboxy-terminal parts are required for target repression and localization of Roquin-1.

In cooperation with this study [149], one part of this thesis work was the investigation of direct protein–RNA interactions *in vitro* as a crucial first step for Icos repression. Furthermore, the *in vitro* binding studies aimed at discovering the *cis*-element for Roquin-1 binding.

Contrary to earlier publications, which report localization of Roquin-1 to stress granules [39], Roquin-1 localizes in P bodies in various cell lines. Only after induction of cell stress by arsenite treatment Roquin-1 translocates into stress granules [149,150]. The present work corroborated these results by investigating localization of Roquin-1 in primary $CD4^+$ T cells.

These combined results allowed the elaboration of a molecular mechanism of Icos repression: Roquin-1 post-transcriptionally regulates Icos by directly binding to the Icos mRNA and by interacting with Rck and Edc4 [149], two factors of the decapping pathway (section 5.2), to induce Icos mRNA decay.

The second part of this thesis addresses the functions of Roquin-1 and its paralog Roquin-2 *in vivo*. Roquin-2, also named Mnab, was first described in 2000 as a nucleic acid binding protein with unknown function [151]. Interestingly, it exhibits remarkable similarities with Roquin-1. Roquin-1 and Roquin-2 share the same domain organization with high homology of the RING finger, the ROQ domain and the zinc finger in their amino-terminal parts. To investigate Roquin-2 functions *in vivo*, a conditionally targeted Roquin-2 knockout mouse was obtained to analyze Roquin-2 deficiency in different cell types.

At the same time, *Rc3h1*-deficient mice were generated and analyzed by a collaborating research group [120]. As described above, the M199R mutation in Roquin-1^{san} caused a lupus-like autoimmune disease with T cell-intrinsic phenotypes [39]. The complete loss of the Roquin-1 protein was therefore assumed to cause an even more severe phenotype. Indeed, systemic deletion of Roquin-1 resulted in perinatal death. However, loss of Roquin-1 in T cells, B cells or the hematopoietic system led to elevated Icos levels, but failed to induce anti-nuclear antibody responses [120].

We therefore speculated that Roquin-2 could compensate for the complete loss of Roquin-1, thereby preventing the development of an autoimmune disease. An essential part of this research project therefore aimed at investigating the potential redundancy of Roquin-1 and Roquin-2 by analyzing mice deficient for both *Rc3h1/Rc3h2* in T cells.

6 Material

6.1 Mice

Mice with *Rc3h2*$^{tm1a(KOMP)Wtsi}$ alleles were obtained from the International Knockout Mouse Consortium. For removing of the Frt-flanked Neo^{R} cassettes hACTB::FLPe.9205 mice were obtained from Jackson and CD4-Cre mice [152] were used for loxP site recombination. To obtain mice, which can be adenovirally transduced, standard targeting procedures were used to generate transgenic *CAG-CAR*$^{stop\text{-}fl}$ mice (Heger and Schmidt-Supprian, unpublished). Specifically, the targeting vector pROSA26-1 was modified to contain the CAG promoter, a loxP-flanked neomycin resistance gene/STOP cassette, the truncated human coxsackie adenovirus receptor (CAR), which is inactive in its intracellular signaling domain (CARΔ1) and the bovine growth hormone polyadenylation site. All mice were on a C57BL/6 genetic background or for *Rc3h2* also on a mixed C57BL/6-NMRI background. C57BL/6, DOCAR and DO11.10 mice were obtained from Taconic Farms. DOCAR (Tg(DO11.10)10Dlo Tg(CARΔ-1)1Jdgr) and DO11.10 mice bear a transgenic DO11.10 T cell receptor specific for a chicken ovalbumin (OVA) peptide. T cells from these mice are predominantly naive, if not experimentally activated by OVA-loaded APC or polyclonal stimulation. DOCAR mice additionally bear the truncated CARΔ1 receptor. All animals were housed in a special pathogen-free barrier facility in accordance with the Helmholtz Zentrum München institutional, state and federal guidelines.

6.2 Cell lines and cell culture

Human embryonic kidney cells (HEK293T) as well as human lung adenocarcinoma epithelial cells (A549) were purchased from ATCC. The HEK293A cell line was obtained from Invitrogen. Mouse embryonic fibroblasts (MEFs) were obtained from breedings of *Rc3h2*$^{+/neo}$ x *Rc3h2*$^{+/neo}$ and *Rc3h1*$^{fl/fl}$*; Rc3h2*$^{fl/fl}$ x *Rc3h1*$^{+/fl}$*; Rc3h2*$^{+/fl}$ mice, respectively and prepared as described in section 7.4 to produce MEFs deficient for Roquin-2 or both Roquin-1 and Roquin-2 proteins. Media used for cultivating cell lines (DMEM, supplemented with 10% FCS, 1% PenStrep and 1% HEPES) and primary T cells (RPMI, supplemented with 10% FCS and 1% of NEAA, β-mercaptoethanol-L-glutamine, vitamins, HEPES, PenStrep and sodium pyruvate) are described below (Table 1).

Table 1: Cell culture components

Name	Company
β-Mercaptoethanol	Sigma-Aldrich
Dulbecco's Modified Eagle Medium (DMEM)	Gibco, Invitrogen
Fetal calf serum (FCS)	PAN BIOTECH GmbH
RPMI 1640, without L-glutamine	BioWhittaker, Lonza
100x NEAA	BioWhittaker, Cambrex
GIBCO™ L-Glutamine-200 mM (100x), flüssig	Gibco, Invitrogen
GIBCO™ MEM Vitamin Solution (100x), flüssig	Gibco, Invitrogen
HEPES (1M)	Gibco, Invitrogen
PenStrep (10,000 U/ml)	Gibco, Invitrogen
Sodium pyruvate (100 mM)	BioWhittaker

6.3 Antibodies and cytokines

For intracellular staining and Western blotting of Roquin-1/2, we generated monoclonal antibodies against an amino-terminal fragment of Roquin-1 (aa 1–441) via immunization of rats. All antibodies described below were against mouse antigens unless otherwise stated.

Table 2: Antibodies and cytokines for stimulation and differentiation of primary mouse T cells

Antibody / cytokine	Company
Anti-CD3 (145-2C11)	In-house production
Anti-CD28 (37N)	In-house production
Anti-hamster IgG (goat)	MP biochemicals
Anti-IFN-γ (XMG1.2)	In-house production
Anti-IL-2	Miltenyi Biotec.
Anti-IL-4 (IIB11)	In-house production
Anti-IL-12 (C17.8)	In-house production
Anti-Ox40 antibody (Ox86)	In-house production
Anti-rat IgG	eBioscience
IL-4 supernatant	In-house production
Recombinant human IL-2 (ProleukinS)	Novartis
Recombinant human TGF-b1	R&D Systems
Recombinant mouse IL-6	PeproTech
Recombinant mouse IL-12	BD Biosciences

Table 3: Antibodies for histology

Antibody	Company
Anti-B220 (RA3-6B2)	BD Biosciences
Anti-CD4 (H129.19)	BD Biosciences
Anti-CD8a (53-6.7)	BD Biosciences
Anti-ER-TR7	Novus Biologicals, ImmunoResearch
Anti-FDC-M1 (4C11)	BD Biosciences
Anti-F4/80 (BM8)	BMA Biomedicals AG
Anti-IgD (11-26c.2a)	BD Biosciences
Anti-MOMA-1 (MOMA-1)	BMA Biomedicals AG

Table 4: Antibodies for Western blot analyses

Antibody	Company
Anti-Edc4 (RCD8)	Bethyl
Anti-GAPDH (6C5)	Calbiochem
Anti-histone H3 (C-term)	Millipore
Anti-IκBα (44D4)	Cell Signaling
Anti-Ikkβ (2C8)	Cell Signaling
Anti-Irf4 (P173)	Cell Signaling
Anti-NF-κB p65	Cell Signaling
Anti-NF-κB2 p100/p52	Cell Signaling
Anti-P-IκBα (Ser32/36; 5A5)	Cell Signaling
Anti-P-NF-κB p65 (Ser276)	Cell Signaling
Anti-Roquin-1/2 (3F12)	In-house production
Anti-RelB	Cell Signaling
Anti-tubulin (B-5-1-2)	Santa Cruz

Table 5: Antibodies for flowcytometric analyses

Antibody	Company
Anti-B220 (RA3-6B2)	eBioscience
Anti-Bcl6 (K112-91)	BD Biosciences
Anti-CAR (E1-1)	eBioscience
Anti-CD3 (145-2C11)	eBioscience
Anti-CD4 (GK1.5)	eBioscience
Anti-CD8 (53-6.7)	eBioscience
Anti-CD11c (N418)	eBioscience
Anti-CD21/35 (7G6)	eBioscience
Anti-CD23 (B3B4)	eBioscience
Anti-CD44 (IM7)	eBioscience
Anti-CD62L (MEL-14)	eBioscience
Anti-CD90.1 (Thy1.1, clone OX-7)	eBioscience
Anti-CD95 (Jo2)	eBioscience
Anti-CD134 (Ox40, clone OX-86)	eBioscience
Anti-CD278 (Icos, clone C398.4A)	eBioscience
Anti-CD279 (PD-1, clone J43)	eBioscience
Anti-CXCR5 (2G8)	eBioscience
Anti-F4/80 (BM8)	eBioscience
Anti-Foxp3 (FJK-16s)	eBioscience
Anti-GL-7 (GL7)	eBioscience
Anti-Gr-1 (RB6-8C5)	eBioscience
Anti-human IgG, Fcg-specific	Jackson ImmunoResearch
Anti-IFN-γ (XMG1.2)	eBioscience
Anti-MHCII (I-A/I-E; M5/114.15.2),	eBioscience
Anti-mIL-21R subunit FC chimera	R&D Systems
Anti-NK1.1 (PK136)	eBioscience
Anti-rat IgG (biotinylated)	Jackson ImmunoResearch
Anti-Roquin-1/2 (3F12)	In-house production
Anti-Siglec-F (E50-2440)	eBioscience
Anti-TCRβ (H57-597)	eBioscience
PBS57-loaded CD1d Tetramer	National Institutes of Health
Streptavidin	eBioscience

Table 6: Antibodies for confocal microscopy

Antibody	Company
Anti-Rck (A300-461A)	Bethyl
Anti-FMRP	Gift from U. Fischer
Anti-rabbit Cy5	Jackson Laboratories
Anti-mouse Cy3	Jackson Laboratories

6.4 Vectors and oligonucleotides

Most expression constructs were generated by TOPO® cloning. By cloning the sequence of interest into an entry vector (pCR8-GW, pENTR11, pCR2.1), the Gateway® system (Invitrogen) can be used to further insert the sequence into any destination vector by lambda recombination using LR clonase II (section 7.1.5). Point mutations were introduced into the insert of interest using site-directed mutagenesis (section 7.1.6).

6.4.1 Entry vector constructs

Entry vectors were generated for mouse Roquin-1 (AY948287) and human ICOS (NM_012092). Mouse Ox40 (NM_011659) and mouse Ctla4 (NM_009843.3) were amplified from cDNA and cloned into the entry vector pCR8-GW.

Table 7: Entry-plasmids for LR recombination into expression vectors.

Entry plasmid	Insert	Purpose
pCR8-GW	hICOS full-length	EMSA experiments and viral expression
pCR8-GW	hICOS CDS (nts 1–600)	EMSA experiments
pCR8-GW	hICOS nts 1–700	EMSA experiments
pCR8-GW	hICOS nts 1–800	EMSA experiments
pCR8-GW	hICOS nts 1–900	EMSA experiments
pCR8-GW	hICOS nts 1–1000	EMSA experiments
pCR8-GW	hICOS nts 1–1210	EMSA experiments
pCR8-GW	hICOS nts 1–1810	EMSA experiments
pCR8-GW	hICOS nts 1–2210	EMSA experiments
pCR8-GW	hICOS nts 600–700	SHAPE analysis
pCR8-GW	hICOS nts 700–800	SHAPE analysis
pCR8-GW	hICOS nts 800–900	SHAPE analysis
pCR8-GW	mCtla4 full-length	EMSA experiments
pCR8-GW	mOx40 full-length	EMSA experiments and viral expression
pCR8-GW	mRoquin-1 CDS	Viral expression
pCR8-GW	mRoquin-1 (aa 1–509)	Inactive mutant for viral expression
pCR8-GW	Cre w/o poly(A)	Viral expression
pCR8-GW	mMnab aa 1–1125	Viral expression
pCR8-GW	mMnab aa 1–1187	Viral expression
pENTR11	Roquin eGFP	Viral expression

6.4.2 Viral expression constructs

Retrovirus was expressed from pMSCV-IRES-Thy1.1, pLNCX2 or pDest12.2 vectors. The expression constructs had been equipped with a gateway cassette to allow for lambda recombination (LR) using the gateway system. Sequences of Roquin-1–eGFP and Cre recombinase were inserted using the LR clonase II Kit (Invitrogen) (7.1.5).

LR was also used to insert the following sequences into the adenoviral vector pCAGAdDu: Roquin-1 (aa 1–509 and WT), Roquin-2 (aa 1–1125 and aa 1–1187). The vector contained a bovine growth hormone poly(A)-signal in the context of the CAG (chicken actin promoter and CMV enhancer) promoter.

6.4.3 Additional constructs

Mouse Roquin-1 was cloned NcoI – XhoI into the bacterial expression vector pETM-11. The mouse Roquin-2 construct mMNAB pcDNA3 (IRCLp5011C0928D) was purchased from Source BioScience ImaGenes and the amino-terminal part (aa 1–438) cloned PciI – SalI into the pCR2.1 vector. By using the compatible restriction sites NcoI/PciI – XhoI/SalI, Roquin-2 (aa 1–438) was exchanged with Roquin-1 (aa 1–441) in the pETM-11 vector (Table 8).

Table 8: Plasmids for protein expression

Entry plasmid	Insert	Purpose
pETM-11	Roquin-1 full-length	EMSA experiments
pETM-11	Roquin-1 aa 1–414	EMSA experiments
pETM-11	Roquin-1 aa 1–441	EMSA experiments
pETM-11	Roquin-2 aa 1–438	EMSA experiments

For immortalization of MEF cells a large T-plasmid was used, kindly provided by W. Hammerschmidt (Helmholtz Zentrum München, Germany). Ecotropic or amphotropic packaging vectors were used for retrovirus production.

For adenoviral knockdown approaches, constructs were obtained from the Sirion GmbH. The vectors expressed hairpins from a U6 promoter and independently co-expressed GFP (Table 9).

Table 9: Sequences for adenoviral knockdown approaches

Target	Sequence
Sh-*Rc3h1*	CGCACAGTTACAGAGCTCATT
Sh-*Rc3h2*	GCCAAGAGTAACTCATTACTT
Sh-*U6*-Stop cassette	TTTTTGGCCTTTTTTAGCTG

6.4.4 Oligonucleotides synthesized by the company METABION

Table 10: Oligonucleotide sequences for DNA constructs

Name	Sequence (5'-3')	Application
mMNAB SalI forw	GTCGACCATGCCTGTGCAGGCAGCTC	Clone mRoquin-2
mMNAB NotI rev	GCGGCCGCTCAGCTGTTAACCATCTTCCCATTTG	Clone mRoquin-2
mMNAB PciI1-438for	CCCACATGTTACCTGTGCAGGCAGCTCAATGG	Clone mRoquin-2 N-term
mMNAB SalI1-438 rev	GTCGACCTATTCCTGAGAATGGGCAAATGTACAATTTG	Clone mRoquin-2 N-term
hICOS BamHI for	GAGAATCCGGACCATGAAGTCAGGCCTCTGGTATTTC	Clone hICOS
hICOS CDS XhoI rev	GAGACTCGAGGGTTATAGGGTCACATCTGTGAG	Clone hICOS CDS
hICOS1-700 XhoI rev	GAGACTCGAGTAAGTCAGACTCTCCGTGGTCC	Clone deletion construct
hICOS1-800 XhoI rev	GAGACTCGAGAGAGGACTCGGCAGTACCAAG	Clone deletion construct
hICOS1-900 XhoI rev	GAGACTCGAGGCACTGCTAGGAGCAGATGTG	Clone deletion construct
hICOS1-1210 XhoI rev	CTCGAGTGAGGGCACAAGAAAGCA	Clone deletion construct
hICOS1-1810 XhoI rev	CTCGAGATACCTAGTGGCCTCTGGCTC	Clone deletion construct
hICOS1-2210 XhoI rev	GAGACTCGAGGGTTAAGATAATATAAGTATGC	Clone deletion construct
hICOS full-length XhoI rev	GAGCTCGAGGGTTACTACTGTTAAAATCTCTTTG	Clone hICOS full-length
2deltaZincQCfor	GCCTCCACAGCATAGCAAATAGAAAACATACATGTGTCG	Quick change for Roquin-1ΔZn
2deltaZincQCrev	CTCGACACATGTATGTTTTCTATTTGCTATGCTGTGGAG	Quick change for Roquin-1ΔZn
hICOS PCR 600 for	TAATACGACTCACTATAGGTATGGAACTCTGGCACCCAGGCATG	T7 promoter for in vitro transcription
SHAPE-ICOS 700 rev	TGTAAAACGACGGCCAGTGTATGTAGTTAAGTCAGACTCTCCGTGG	M13 Primer sequence for probe annealing
hICOS PCR 700 for	TAATACGACTCACTATAGGACTACATACATCTTCTGCTGGTGTTTTGTTC	T7 promoter for in vitro transcription
SHAPE-ICOS 800 rev	TGTAAAACGACGGCCAGTGTTTGTTTTGAGAGGACTCGGCAGTAC	M13 Primer sequence for probe annealing
hICOS PCR 800 for	TAATACGACTCACTATAGGCAAAACAAACACCCTCTTGCAACCAGC	T7 promoter for in vitro transcription
SHAPE-ICOS 900 rev	TGTAAAACGACGGCCAGTCTGGCTGATGCACTGCTAGGAGC	M13 Primer sequence for probe annealing
Mouse Ox40 for	GAGGTCGACCATGTATGTGTGGGTTCAGC	Clone mouse Ox40
Mouse Ox40 FL rev	CTCGCGGCCGCTAGCATGTTTATTAGGAG	Clone mouse Ox40
Mouse Ctla4 for	GAGGTCGACCATGGCTTGTCTTGGACTC	Clone mouse Ctla4
Mouse Ctla4 FL rev	CTCGCGGCCGCAACAATCACAAGAAACTT	Clone mouse Ctla4
Zinc419Argfornew	GCAAATACAAAACATACATGCGTCGAGATATGAAAGGG	Quick change to mutate Zn finger of Roquin-1
Zinc416Argnewrev	CCCTTTGCTTCATATCTCGACGCATGTATGTTTTGTATTTGC	Quick change to mutate Zn finger of Roquin-1
M13 for	TGTAAAACGACGGCCAG	Sequence SHAPE assay
M13 rev	CAGGAAACAGCTATGAC	Sequence SHAPE assay

Table 11: Oligonucleotides for genotyping

Name	Sequence (5'-3')	Application
FlxFwN	TACAAGGTAGAGACGTTTGGGAAG	*Rc3h1* detection
RoqflxRv	AAAGCCCTCAAGATTCTTTGGGCA	*Rc3h1* detection
RoqloxFw	GTAAATGAGATTCAGTGTGTCCAG	*Rc3h1* detection
Rc3h2 5'arm	CTGCCTAATCTCTGCTAGATG	*Rc3h2* detection
Rc3h2 3'arm	CTCAATGACAGGCAGTGATTC	*Rc3h2* detection
LAR3	CAACGGGTTCTTCTGTTAGTCC	*Rc3h2* detection
ICOS1228for	GGTGTCCATCAAGAATCCAATG	*Icos* detection
ICOS1228rev	CCTTCTTAACTACTATTGGTACCTTG	*Icos* detection
Neo-for	GATTGAACAAGATGGATTGC	*Icos* detection
Neo-rev	CAGAAGAACTCGTCAAGAAG	*Icos* detection
IFNg MUT for	CCTTCTATCGCCTTCTTGACG	*IFN-γ* detection
IFNg WT for	AGAAGTAAGTGGAAGGGCCCAGAAG	*IFN-γ* detection
IFNg rev	AGGGAAACTGGGAGAGGAGAAATAT	*IFN-γ* detection
Car for	CAGGAGCGAGAGCCGCCTAC	*Car* detection
Car rev	CAGCCACTCGATGTCCAGCGGTC	*Car* detection
CD4Cre for	ACGACCAAGTGACAGCAATG	*CD4-Cre* detection
CD4Cre rev	CTCGACCAGTTTAGTTACCC	*CD4-Cre* detection
VavCre 1	GACAGGCAGGCCTTCTCTGAA	*Vav-Cre* detection
VavCre 2	CTTCTCCACACCAGCTGTGGA	*Vav-Cre* detection

Table 12: Oligonucleotides and probes (Universal probe library of Applied Biosystems) for qPCR

Gene	Forward primer (5'-3')	Reverse primer (5'-3')	Probe
Irf4	AGCACCTTATGGCTCTCTGC	TGACTGGTCAGGGGCATAAT	#3
RelB	GCCTTGGGTTCCAGTGAC	TGTATTCGTCGATGATTTCCAA	#103
Chuk (Ikkα)	GCACAGTAACCCCTCCAGTATC	CATTTGTGCTAACGTCTCTCCA	#46
Ikbkb (Ikkβ)	CCGGAAAGTGTCAGCTGTATC	CCTCAGCTGGAAGAAGGAGA	#92
Ikbkg (Ikkγ)	GGTACTCCTGAGACCCTCCA	CTGATTGCTCTGCCGGATA	#27
Map3K14 (NIK)	TCCACAGAATGAAGGACAAGC	TACCCGAAACACCTCGAGTC	#47
Birc2 (Ciap1)	GAAGAAAATGCTGACCCTACAGA	CATGACGACATCTTCCGAAC	#80
Birc3 (Ciap2)	CGATGCAGAAGACGAGATGA	TTTGTTCTTCCGGATTAGTGC	#68
Traf2	GCTCCTTCTGCCTGACCA	AGACACAGGCAGCACAGTTC	#73
Traf3	GTTCAGACTCTTCTAAGGAGTGAGG	TCCAGGGAGTTGCTCCAC	#62
Tradd	TGAATTACATCTTAGCCCAGAAGC	CACACGTCAGTTTGCAGAGC	#78
Icos	CGGCAGTCAACACAAACAA	TCAGGGGAACTAGTCCATGC	#6
Tnfrsf4 (Ox40)	GCTTGGAGTTGACTGTGTTCC	GGGTCTGCTTTCCAGATAAGG	#79
Ywhaz	CGCTAATAATGCAGTTACTGAGAGA	TGGAAGGCCGGTTAATTTT	#2

6.5 Chemicals, enzymes and kits

Table 13: Chemicals and reagents

Compound	Company
Ampicillin	Roche
Biozym DNA Agarose	Biozym Scientific GmbH
Brefeldin A	Sigma-Aldrich
BSA (Albumin Fraktion V)	Roth
Chloroform min. 99%	Sigma-Aldrich
Deoxynucleotide (dNTP) set	Fermentas
DEPC	Roth
Dimethyl Sulphoxide (DMSO)	Sigma-Aldrich

DNA Ladder 1 kb Plus	Invitrogen
DNA Ladder 2-Log (0.1–10.0 kb)	New England BioLabs
Dynabeads MyOne Tosylactivated	Invitrogen
ECL plus Western blotting reagent	GE healthcare
Ethidium bromide 1% (w/v)	Serva
Formaldehyde solution 36.5–38%	Sigma Life Science
FuGENE reagent	Roche
Ionomycin, Free Acid, Streptomyces conglobactus	Calbiochem
IPTG	VWR International GmbH
JetPI	Polyplus
Kanamycin sulfate	Roth
Milk powder	Roth
Paraformaldehyde	Sigma-Aldrich
Phorbol-12-myristate-13-acetate (PMA)	Calbiochem
RiboRuler™ High Range RNA Ladder	Fermentas
Saponin	VWR International GmbH
Tri®Reagent (Trizol)	Invitrogen
Trypsin 0.05% / EDTA 0.02% in PBS	Pan biotech GmbH
Trypton	Merck
Tween 20	Applichem
β-Mercaptoethanol 99%	Sigma-Aldrich

Table 14: Enzymes

Enzymes	Company
Gateway LR Clonase II Enzyme Mix	Invitrogen
Proteinase K	Invitrogen
Restriction enzymes	New England BioLabs
T4 DNA Ligase (10,000 U/ml)	New England BioLabs
Taq Polymerase (5,000 U/ml)	New England BioLabs
Taq Polymerase (5,000 U/ml)	Invitrogen
Vent Polymerase (2,000 U/ml)	New England BioLabs

Table 15: Kits

Kit	Company
Annexin V-Cy5 Apoptosis Detection Kit	BioVision
CD4+ CD62L+ T cell Isolation Kit II, mouse	Miltenyi Biotec
CD4+ T cell Isolation Kit (mouse)	Miltenyi Biotec.
DETACHaBEAD® Mouse CD4	Invitrogen
Dynabeads®Mouse CD4 (L3T34) Kit	Invitrogen
mMESSAGE mMACHINE(R) Kit	Ambion
Nucleobond®Xtra Maxi Kit	Macherey-Nagel GmbH & Co. KG
pCR™8/GW/TOPO® TA Cloning® Kit	Invitrogen
PureYield™ Plasmid Miniprep System	Promega
QIA®quick gel extraction Kit	Qiagen
RNeasy® Mini Kit	Qiagen
TaqManMicroRNA Assay	Applied Biosystems
TOPO® TA Cloning® Kit	Invitrogen
Universal Probe Library	Roche
XL QuickChange	Stratagene

6.6 Buffer and solutions

Table 16: Buffers and solutions

Standard solution	Composition
APS	10% APS w/v in ddH_20
Buffer A for nuclear fractionation	10 mM HEPES (pH 7.9), 10 mM KCl, 0.1 mM EDTA, 1 mM dithiothreitol, protease inhibitor mix without EDTA (Roche) in ddH_20
Coomassie staining solution	50% methanol, 40% H_2O, 10% glacial acid, 0.25 g/l brilliant-blue R-250
Destaining solution	50% methanol, 40% H_2O, 10% glacial acid
DNA dye (6x)	0.25 % bromophenol blue, 0.25 % xylene xyanol, 30% glycerol
Meister lysis buffer	20 mM Tris-HCl (pH 7.5), 150 mM NaCl, 0.25% (v/v) Nonidet-P40, 1.5 mM $MgCl_2$, 1 mM DTT, protease inhibitor mix without EDTA (Roche) in ddH_20
PBS	137 mM NaCl, 10 mM phosphate, 2.7 mM KCl
RIPA buffer	20 mM Tris-HCl (pH 7.5), 250 mM NaCl, 10 mM $MgCl_2$, 1% NP-40, 0.1% SDS, 0.5% Na-desoxycholate, 1 mM DTT, protease inhibitor mix without EDTA (Roche) in ddH_20
SDS (10%)	10% SDS (w/v) dissolved in ddH_20
SDS sample buffer (4x)	200 mM Tris/HCl (pH 6.8), 8% w/v SDS, 4% glycerol, 0.1% w/v bromophenol blue, 10% v/v β-mercaptoethanol in ddH_20
SDS-PAGE running buffer (5x)	25 mM Tris-Base, 200 mM Glycine, 10% (w/v) SDS in ddH_2O
TAC lysis buffer	13 mM Tris, 140 mM NH_4Cl (pH 7.2) in ddH_20
TBE (5x)	45 mM Tris-HCl, 1 mM EDTA (pH 8.0) in ddH_20
TBS (1x)	20 mM Tris-Base, 137 mM NaCl, 3.8 ml 1M HCl, dissolved in ddH_20
TBS-T (1x)	20 mM Tris-Base, 137 mM NaCl, 3.8 ml 1M HCl, 0.1% (v/v) Tween 20, dissolved in ddH_20
TE (10x)	100 mM Tris/HCl (pH 8.0), 10 mM EDTA (pH 8.0) in ddH_20
Western blot buffer	25 mM Tris-Base, 192 mM glycin, 20% v/v methanol (pH 8.4) in ddH_20

6.7 Instruments

Table 17: Instruments and devices

Instrument	Official name and company
Accuracy weighing machine	KERN ABJ-220-4M (Kern und Söhne GmbH) KERN EW 220-3NM (Kern und Söhne GmbH)
Agarose gel chambers	Peqlab Biotechnologie GmbH
Bacterial incubator	Brutschrank BINDER BF 53 (Binder Labortechnik) Innova 4400 incubator shaker (New Brunswick Scientific GmbH)
BD FACS AriaIII Cell Sorter	BD Biosciences
BD FACS Calibur Flow Cytometer	BD Biosciences
BD LSRFortessa Cell Analyzer	BD Biosciences
BD LSRII Flow Cytometer	BD Biosciences

Blotting chamber	BioRad
Centrifuges and rotors	Beckman Coulter Avanti-J-26XP (Beckman Coulter); JA-10 Rotor, Fixed Angle (Beckman Coulter) Allegra®X-12R Centrifuge (Beckman Coulter); Rotor SX 4750 (Beckman Coulter) Eppendorf Centrifuge 5810R (Eppendorf); Rotor A-4-62 and F-34-6-38 Multifuge Heraeus (Thermo Scientific); Rotor SN179
CO_2 incubator	Forma Direct Heat CO2 Incubator HEPA Class 100 (Thermo Electron Corporation)
Coasting mixer	Tube Roller-Mixers, SRT1 (Stuart) (ScienceLab)
Confocal microscopy	Type: 301-185.104-000 Order-No: 500277 (Leica)
Energy supplier	Stromgeber EC105 (Thermo Electron Corporation) BioRad energy supplier (BioRad)
Fluorescence microscope	Axiovert 200M (Zeiss) Olympus DP72 Hamamatsu NanoZoomer 2.0-HT
Gel documentation	(Peqlab Biotechnologie GmbH)
Ice machine	Scotsman AF 200 (Scotsman Icesystem)
Magnet stirrer	RCT basic safety control (IKA)
Microscope	Axiovert 40C (Zeiss)
Microwave	Bosch
pH meter	pH-Meter inoLab® pH 720 (Wissenschaftlich Technische Werkstätten)
Protein gel chamber	BioRad
Spectrophotometer	Eppendorf BioPhotometers (Eppendorf) Thermo Scientific NanoDropTM 1000 Spectrophotometer (Thermo Fisher Scientific Inc.)
Sterile-working bench	BDK, Luft und Reinraumtechnik
Table centrifuge	Centrifuge 5415D (Eppendorf) Centrifuge 5417R (Eppendorf)
Thermo cycler	DNA Engine 48/48 Dual Alpha Unit With Two Heated Lids (BioRad) Light Cycler 480II (Roche)
Thermo mixer	Thermomixer compact (Eppendorf) Thermomixer comfort (Eppendorf)
UV-lamp	Transilluminator model. TS-40 (Ultra-Violet Products Ltd.)
Vortexer	Vortex Genius 3 (IKA)
Water bath	WB7 (Memmert)

7 Methods

7.1 Molecular standard procedures

7.1.1 Bacterial culture

Chemically competent *E. coli* DH5alpha bacteria (Invitrogen) were used for plasmid DNA amplification. For the expression of recombinant protein, *E. coli* Rosetta(DE3)pLysS bacteria (Novagen) were used. The bacteria were transformed by incubation of 50 µl *E. coli* culture with plasmid DNA for 20 min on ice, followed by 30 s heat shock at 42°C. After brief equilibration on ice, 250 µl LB medium was added and cells were gently shaken (500 rpm) for 1 h at 37°C. The suspension was spread onto LB-agar containing the respective antibiotics and incubated at 37°C over night. For storage, a single colony was picked and used for inoculation of a fresh overnight culture. A mix of bacteria suspension and glycerol (1:1) was stored at –80°C.

LB media and LB agar were prepared with "ready to mix" powder (SERVA), supplemented with ampicillin (100 µg/ml), spectinomycin (50 µg/ml), kanamycin (30 µg/ml) or chloramphenicol (170 µg/ml) for the selection of bacterial resistance.

7.1.2 PCR for cloning and genotyping

For the generation of DNA constructs, PCR was performed according to standard protocols. The Taq polymerase (Invitrogen or New England BioLabs) was used for the amplification and generation of A-overhangs important for TA cloning. For more efficient proofreading, the Vent polymerase (New England BioLabs) was added to the Taq polymerase at a ratio of 1/10. Primers were designed with an annealing temperature of 53–62°C. A standard PCR reaction to amplify a DNA of interest contained: 10–150 ng DNA template, 0.25 µl of 100 pmol/µl forward primer, 0.25 µl of 100 pmol/µl reverse primer, 0.5 µl dNTP-mix (25 mM each), 2.5 µl 10xPCR Rxn Buffer, 1 µl 50 mM $MgCl_2$, 0.7 µl Taq DNA polymerase and 0.3 µl Vent polymerase. The mixture was filled up with H_2O to a volume of 25 µl. Cycling reactions were: 94°C for 2 min; 28 cycles of 94°C for 45 s, 58°C for 30 s, 72°C for 60 s (1 min per kb of DNA); 72° for 10 min and hold at 4°C.

For genotyping, the tip of the mouse tail was lysed overnight at 55°C in 200 µl genotyping buffer (100 mM Tris-HCl, pH 8.5, 5 mM EDTA, 0.2% SDS, 200 mM NaCl, 0.2 mg/ml proteinase K). After inactivation of the Proteinase K at 95°C for 15 min, 300 µl of water were

added and 0.4 µl were used as template for the PCR (see above). Primers for genotyping are listed in Table 11. For analysis or purification a minimum of 15 µl of the PCR product were loaded onto an agarose gel.

7.1.3 Preparation and purification of DNA

DNA was purified with the PureYield™ Plasmid Miniprep System (Promega). For larger amounts of DNA, the Nucleobond®Xtra Maxi Kit (Macherey-Nagel GmbH & Co. KG) was used, both according to the manufacturer's protocol.

7.1.4 DNA extraction from agarose gels

DNA was loaded on 1% agarose gels containing 3.5 µl ethidium bromide per 75 ml gel. The desired PCR product was excised under 254 nm UV light and purified using the QIAquick PCR Purification Kit according to the manufacturer's protocol (Qiagen).

7.1.5 TOPO® cloning and site-specific recombination

PCR products can be cloned in a very efficient and rapid way using TOPO® cloning. The linearized entry vector is supplied with overhanging 3'deoxythymidine (T) residues and the topoisomerase I covalently bound to the vector. Furthermore, the Taq polymerase has a terminal transferase activity that adds a single deoxyadenosine (A) to the 3'ends of PCR products. This allows efficient ligation of the PCR product into the vector.
Gateway® cloning allows the transfer of DNA sequences from an entry vector to a destination vector via lambda recombination (LR) based on specific recombination sites (Attl1 and 2, AttR1 and 2, respectively). A switch in antibiotic resistance between entry and destination vectors and the expression of a bacterial death gene (Toxin ccdB) ensure that only destination vectors are selected, which have recombined. TOPO® and Gateway® Cloning (Gateway LR Clonase II Enzyme Mix) reactions were carried out according to the manufacturer's protocol. For LR reactions of plasmids with more than 20 kb, the reaction was performed at 16°C overnight.

7.1.6 Site-directed mutagenesis with QuikChange® II XL

The QuickChange® II XL Kit (Stratagene) is designed to insert point mutations, deletions or insertions of single nucleotides into DNA constructs. Primers were chosen to match a melting

temperature above 75°C and a GC content of at least 40% (Table 10). The PCR was slightly altered to increase the number of colonies (Table 18), followed by a DpnI digested for 1 h to degrade the methylated and hemi-methylated parental template. Then, 4 µl of the PCR product were transformed into DH5alpha bacteria. One of the resulting plasmids was sequenced to check for the desired mutation.

Table 18: PCR conditions for site-directed mutagenesis

Cycles	Temperature	Time
1	95°C	1.2 min
18	95°C	1 min
	60°C	1 min
	68°C	1.1 min
1	68°C	7 min

7.1.7 Ligation of DNA fragments

For ligation of the digested pETM-11 vector with the mRoquin-2 (amino-terminus) insert, the fragments were incubated at 16°C overnight with 1 µl T4 DNA ligase (New England BioLabs) and 1 µl ligase buffer (10x), adjusted to a total volume of 10 µl.

7.1.8 Extraction of RNA

RNA for array approaches was extracted by using the mirVana™ miRNA Isolation Kit (Ambion). Up to 10^7 cells were lysed for 10 min on ice in 600 µl Lysis/Binding buffer with 60 µl Homogenate Additive. After adding 600 µl Acid-Phenol-Chloroform and vortexing for 60 s, the samples were centrifuged for 5 min, at 10,000 *g* and RT. The upper phase was transferred to a new tube and mixed with 1.25 volumes of 100% EtOH, loaded onto the filter cartridge and centrifuged 15 s at 10,000 *g*. After washing with Wash1 (one time) and Wash2/3 (two times), the samples were eluted with 100 µl hot elution buffer (95°C) at maximum speed for 20–30 s.

For quantitative real-time PCR, RNA was extracted from cells by using 1 ml of Trizol reagent (Invitrogen) according to the manufacturer's protocol. Shortly, the cells in Trizol reagent were mixed with 200 µl chloroform and incubated at RT for 2 min. The organic and aqueous phases were separated by centrifugation at 12,000 *g* for 15 min at 4°C. The aqueous phase was transferred to a new tube and subjected to isopropanol precipitation for 10 min at RT. RNA precipitates were centrifuged at 12,000 *g* for 10 min at 4°C, washed with 75% ethanol, air-dried and resuspended in 20 µl RNase-free water (treated with 0.1% DEPC).

7.1.9 Reverse transcription of RNA

RNA was reverse transcribed using the QuantiTect Reverse Transcription Kit (Qiagen) according to the manufacturer's instructions. Up to 1 µg purified RNA was incubated in gDNA Wipeout buffer at 42°C for 2 min. For the reverse transcription a mix prepared from QuantiTect Reverse Transcriptase, QuantiTect RT Buffer (5x) and 3 µg Random Primers (Invitrogen) was used. The reaction was performed at 42°C for 15 min and was then stopped by incubation at 95°C for 3 min. The resulting cDNA was diluted with H_2O (ad 100 µl) and stored at –20°C.

7.2 Cell culture

Mouse embryonic fibroblasts (MEFs), HEK293A/T and A549 cells were grown in DMEM with 10% (v/v) FCS, penicillin-streptomycin (1,000 U/ml) and HEPES (10 mM), pH 7.4 at 37°C in a 5% CO_2 humidified incubator.

For storage, cells were frozen in a mixture of 90% FCS and 10% DMSO in NUNC-freezing tubes. The cells were first slowly cooled down to –80°C and then transferred into a liquid nitrogen container for long-time storage.

7.3 Preparation and stimulation of primary T cells

Organs were pressed through rough nets and filtered (rough and fine nets obtained from BD Falcon) before analysis by FACS or isolation and differentiation of $CD4^+$ T cells. For Th1 differentiation, $CD4^+$ T cells were isolated from spleens and lymph nodes using CD4 dynabeads and detachabeads (Invitrogen) according to the manufacturer's protocol. For differentiation into Th0, Th1, Th2, Th17 and Treg subsets, cells were enriched in $CD4^+$ T cells using CD4 dynabeads and then sorted on a BD FACS AriaIII Cell Sorter to obtain naive $CD4^+$ T cells ($CD4^+$ $CD25^-$ $CD62L^+$ $CD44^-$). The cells were stimulated on pre-coated plates (goat anti-hamster IgG; MP biochemicals) with anti-CD3 (145-2C11; 0.1–0.25 µg/ml) and anti-CD28 (37N; 1–2.5 µg/ml) or with anti-CD3/anti-CD28 antibodies coupled to magnetic beads (Dynabeads M-450 Tosylactivated, Invitrogen) at a ratio of 1:1 (beads:cells). Skewing antibodies and cytokines for the respective differentiation conditions are listed in Table 19. Suppliers are given in Table 2. Two days after activation, $CD4^+$ T cells skewed for Th0, Th1 or Th2 subsets were cultured in the presence of recombinant hIL-2 (20 U/ml, ProleukinS, Novartis). An anti-Ox40 antibody (Ox86, 10 µg/ml) or isotype control antibody (rat IgG, 10 µg/ml, eBioscience) was used for NF-κB activation.

Table 19: Antibodies and cytokines for T cell differentiation

Differentiation condition	Antibody / cytokine	Concentration
Th0	–	–
Th1	anti-IL-4	10 µg/ml
	IL-12	10 ng/ml
Th2	anti-IL-12	10 µg/ml
	anti-IFN-γ	5 µg/ml
	IL-4 hybridoma supernatant	1:10 (v/v)
Th17	anti-IL-12	10 µg/ml
	anti-IFN-γ	5 µg/ml
	anti-IL-4	10 µg/ml
	anti-mIL-2	2.5 µg/ml
	IL-6	5 ng/ml
	TGF-β	1 ng/ml
Treg	TGF-β	1 ng/ml
	IL-2	100 U/ml

7.4 Generation of mouse embryonic fibroblasts

Mouse embryonic fibroblasts (MEF) were generated by intercrossing *Rc3h2*$^{+/neo}$ mice or *Rc3h1/2*$^{+/fl}$ mice and removing the embryos at 13.5 dpc. The trunk of the embryos excluding the head and the liver was sliced into very small pieces, incubated with trypsin for 15 min at 37°C and then cultivated in DMEM medium. Cells were directly taken for experiments or immortalized via ecotropic retroviral infection with an SV40 large T antigen plasmid followed by hygromycin selection at 100 µg/ml for two weeks. *Rc3h1/2*$^{-/-}$ cells were obtained by retroviral Cre transduction of *Rc3h1/2*$^{fl/fl}$ MEFs.

7.5 Virus production and transduction

7.5.1 Adenovirus

Type 5 replication-deficient adenovirus was produced by transfection of linearized adenovirus-encoding plasmids into HEK293A (Invitrogen) with JetPI (Polyplus) transfectant according to the manufacturer's instructions. Adenovirus-producing cells were harvested after ten days and, subjected to three freeze-thaw cycles to release virus particles. In order to obtain a higher virus titer, the resulting virus lysate was amplified by infection of $2*10^7$ HEK293A cells. After 48 h, cells were harvested and resuspended in 800 µl medium before freeze-thaw cycles to generate the amplified virus lysate. $2*10^6$ $CD4^+$ CAR^+ T cells were incubated for 2 h at 37°C with 100–300 µl virus lysate if the virus did not contain a marker for titration or with an MOI (multiplicity of infection) of 100–300.

7.5.2 Retrovirus

Retroviral supernatants were produced by calcium-phosphate transfection of HEK293T cells with the retroviral expression plasmid and an ecotropic packaging vector. After 48 h the supernatant was harvested, filtered (0.45 μm; Millipore) and concentrated (6,000 *g*; 4°C; o/n). Transfection of T cells with retrovirus is described below (section 7.6).

7.6 *In vitro* deletion of loxP-flanked *Rc3h1/2* alleles

$CD4^+$ T cells were transduced 40 h after Th1 stimulation with concentrated MSCV-Cre-Thy1.1 retrovirus by spin-infection (830 *g*; 1 h; 18°C) in the presence of 9 μg/ml polybrene (SIGMA). After 6–7 h incubation the virus supernatant was removed and cells were cultured with recombinant hIL-2 (20 U/ml, ProleukinS, Novartis). 3–4 days after retroviral transduction, cells were lysed to generate protein extracts for Western blot analysis or were used for adoptive transfer. In this process, $CD4^+$ T cells ($10–15*10^6$ per mouse) were injected i.v. into $Icos^{-/-}$ animals. For analyzing cell proliferation, cells were labeled before transfer with the Cell Proliferation Dye eFlour450 (eBioscience) according to the manufacturer's protocol.

7.7 Confocal microscopy

$CD4^+$ T cells were transfected with LNCX2-Roquin-1-eGFP constructs using FuGENE reagent (Roche) according to the manufacturer's protocol. Cells were then seeded on Diagnostica glass cover slips and subjected to oxidative stress for 1 h at 37 °C with 0.5 mM sodium arsenite (Sigma). Diagnostica glass cover slips were coated first with 0.01% (w/v) poly-L-lysine and then with anti-CD3 (2.5 μg/ml) and anti-CD28 (5 μg/ml) before the addition of T cells in a volume of 50 μl. Cells were fixed with 4% (w/v) paraformaldehyde and were washed three times in 0.5% (v/v) Nonidet-P40, 0.01% (w/v) NaN_3 and 10% (v/v) FCS in PBS. Antibodies to Rck or FMRP were used for staining in combination with the secondary antibodies anti-rabbit Cy5 and anti-mouse Cy3. Images were captured on a Leica DM IRBE microscope and were analyzed with LCS Lite software.

7.8 Protein purification

Roquin-1 (aa 1–441) was expressed from the pETM-11 bacterial expression vector (modified; Novagen) in *E. coli* Rosetta (DE3) pLysS bacteria. After induction of the protein expression with 1 mM IPTG (VWR International) and disruption of the cells by sonification, the protein

was purified by histidine-tag chromatography (GE Healthcare) and desalted via PD10 gel filtration (GE Healthcare). Roquin-2 (aa 1–438) was expressed from the vector pETM-11 in *E. coli* Rosetta2 (DE3) and purified by affinity chromatography (HiTrap Chelating column) and size exclusion chromatography (16/60 HiLoad Superdex 200 column). The purification buffer was 50 mM Tris-HCl pH 8.0, 300 mM NaCl, 0.01% (v/v) 1-thioglycerol. Protein was visualized on SDS-polyacrylamide gels by Coomassie staining and subsequent de-staining.

7.9 *In vitro* RNA transcription

For *in vitro* transcription, constructs containing the CDS with or without parts of the 3'UTR were introduced into the destination vector pDest17 (Invitrogen) by LR. The vector was linearized by digestion with restriction enzymes. The mMessage mMachine T7 transcription kit was used according to the manufacturer's instructions (Ambion) and RNA was purified with an RNeasy Kit (Qiagen).

7.10 Electrophoretic mobility shift assay (EMSA)

Samples were separated by electrophoresis through native 0.75% agarose gels and were stained with ethidium bromide after the run. Recombinant protein (0.5–200 pmol) was incubated for 20 min on ice with *in vitro* transcribed mRNA (0.6 or 1 pmol) in a buffer of 150 mM KCl, 50 mM Tris-HCl (pH 7.4), 1 mM $MgCl_2$, 1 mM EDTA and 1 mM DTT, and was then adjusted to a concentration of 16% (v/v) glycerol. The buffer conditions were optimized at a later time point to: 150 mM NaCl, 20 mM HEPES (pH 7.4), 1 mM $MgCl_2$ and 1 mM DTT, adjusted to 16% (v/v) glycerol.

7.11 SHAPE assay

The selective 2'-hydroxyl acylation analyzed by primer extension (SHAPE) assay was used to model the secondary structure of an mRNA [153]. As readout radioactive sequencing was chosen. For that purpose M13-primer DNA and a LMW DNA-ladder (New England BioLabs) were tagged with γ^{32}P ATP. For the assay 2 pmol of the RNA of interest was first denatured at 95°C for 2 min and then refolded on ice for 2 min in 0.5xTE buffer (total volume 12 µl). 6 µl folding mix (333 mM HEPES (pH 8.0), 20 mM $MgCl_2$, 333 mM NaCl) were added and the sample was incubated for 20 min at 37°C. The RNA was modified with either 1 µl of 130 mM NMIA or DMSO as a control for 45 min at 37°C. The RNA was precipitated with

EtOH for 30 min at –80°C and dissolved in 0.5xTE buffer. For the primer extension reactions, 0.5 µM of the radiolabeled M13-primers were added to the NMIA (N-methylisatoic anhydride) or control reaction, incubated for 5 min at 65°C, slowly cooled down to 35°C and put on ice. 6 µl of SHAPE enzyme mix (4 parts Superscript III FS buffer, 1 part 0.1 M DTT and 1 part 10 mM dNTP mix) were added for 1 min at 52°C, followed by 1 µl Superscript III RT for 10 min at 52°C. After adding 1 µl 4 M NaOH for 5 min at 95°C, the reaction was stopped with 29 µl acid stop mix and subjected to a polyacrylamide sequencing gel. To assign the bands in the NMRI and control reaction, sequencing lanes were generated by adding 2.5 µl ddNTP mix to the NMRI and control reactions. One or two sequencing reactions (here ddA and ddT) are usually sufficient to infer the entire sequence.

7.12 Flow cytometry and intracellular staining

7.12.1 Surface staining

Single cell suspensions of thymus and spleen were pre-incubated with 10 µg/ml Fc-block (CD16/31; 2.4G2; in-house production) in staining buffer (PBS, 2% FBS, 2 mM EDTA) for 10 min at 4°C and stained with antibodies for 20 min at 4°C in staining buffer. Antibodies, listed in Table 5, were diluted according to the manufacturer's suggestion. The PBS57-loaded CD1d Tetramer was kindly provided by the National Institutes of Health.

For the CXCR5 staining, cells were incubated for 1 h at 4°C with rat anti-mouse CXCR5 hybridoma supernatant in staining buffer followed by stainings with biotinylated mouse anti-rat IgG and Streptavidin–APC or –PerCP.

7.12.2 Intracellular staining

For intracellular cytokine staining, splenocytes or $CD4^+$ T cells were stimulated either with PMA/ionomycin (20 nM and 1 µM, respectively) or antiCD3/antiCD28 (0.25 µg/µl and 2.5 µg/µl, respectively) for 5 h adding BrefeldinA (10 µg/ml) for at least 2 h. After the surface staining, cells were fixed with 4% PFA and permeabilized with PBS containing 0.5% saponin and 1% BSA. This buffer was used for all following steps. The samples were pre-incubated with Fc-block (10 µg/ml) for 10 min and antibody stained for 30 min at the concentration suggested by the manufacturer. IL-21 was detected by staining with a mIL-21R subunit FC chimera for 30 min at room temperature, followed by a FITC-conjugated anti-

human IgG, Fcγ-specific antibody. Bcl6 (45 min) and Foxp3 (30 min) stainings were performed at RT using the Foxp3 staining kit (eBioscience).

For intracellular staining of Roquin-1/2, an in-house-produced biotinylated antibody (3F12) against the amino-terminus of both proteins was used. After 20 min fixation with 2% formaldehyde, cells were permeabilized in PBS containing 0.5% saponin and 1% BSA. 3F12 supernatant was applied for 1 h (dilution 1:50), followed by staining with Streptavidin–APC. Biotinylation of the 3F12 antibody was performed with the EZ-Link NHS-PEG Solid-Phase Biotinylation Kit (Thermo Scientific) according to the manufacturer's instructions.

Samples were acquired on a FACSCalibur, LSRII or LSRFortessa (BD Biosciences) and analyzed with FlowJo software (Tree Star).

7.13 Co-immunoprecipitation and immunoblotting

For co-immunoprecipitations MEFs were lysed on ice in an NP-40 lysis buffer, shock frozen in liquid nitrogen, thawed and the lysates were cleared by centrifugation (10,000 *g*, 4°C, 10 min). Anti-Roquin-1/2 antibody (Q4-2, in-house production) coupled to magnetic beads (MyOne Tosylactivated Dynabeads, Invitrogen) was incubated for 4 h at 4°C with lysate containing 3–5 mg protein in the presence of 20 U RNasin. Beads were washed three times with lysis buffer. For protein elution the beads were taken up in lysis buffer containing SDS sample buffer and boiled at 95°C for 5 min. The supernatant was used for Western blotting.

For Western blot lysates, cells were washed in PBS at 4°C and lysed in a minimum of 15 µl RIPA or Meister lysis buffer. Lysates were incubated for 15 min on ice, vortexed every 2 min and then centrifuged at 10,000 *g*, 4°C for 10 min. The protein amount in the supernatant was determined by the Bradford protein assay. Protein samples were boiled in SDS sample buffer for 5 min at 95°C and loaded into the slots of a SDS-polyacrylamide gel. In addition, a protein size maker (Precision Plus Protein All Blue Standards, Biorad) was loaded. The gels consisted of a lower separating and an upper stacking part. The separating part consisted of 8–12% acrylamide, 0.1% SDS, 0.1% APS and 0.06% TEMED in 375 mM Tris-HCl (pH 8.8). The stacking part contained 5% acrylamide, 0.1% SDS, 0.1% APS and 0.1% TEMED in 126 mM Tris-HCl (pH 6.8). After loading the samples, the electrophoresis was first run for 15 min at 80 V and then for 1.5 h at 120 V. The proteins were blotted on methanol-activated PVDF membranes at 40 V over night in Western blot buffer using a wet gel blotting chamber (Biorad). For protein detection, membranes were first blocked in 5% milk dissolved in TBS for two hours at RT. The blocked membranes were washed with TBS-T (3 x 10 min) and the diluted primary antibody was applied for 2 h at RT or over night at 4°C. The membranes were

washed again and incubated with the secondary antibody, conjugated with horseradish peroxidase, for 1 h at RT. After three more washing steps (TBST-T, TBS, H_2O for 10 min each) the blots were developed with ECL plus Western blotting reagent (GE healthcare) or quantified on an Odyssey infrared imaging system.

7.14 Nuclear fractionation

For cytoplasmic and nuclear fractionation, cells were resuspended in 200 µl buffer A (Table 16), incubated 15 min on ice and dounced 10 times. After centrifugation (10 min, 4°C, 20,000 *g*), the supernatant containing the cytoplasmic fraction was used for Western blotting as described. The pellet that contained the nuclear fraction was washed two times with buffer A and was lysed for 15 min on ice in RIPA buffer (Table 16) and applied to Western blotting.

7.15 Histology

Spleens were shock-frozen in HBS solution (Hank's Balanced Salt Solution w/o Phenol Red; Lonza) and 4 µm sections were processed. Stainings were performed with BOND-MAX M210871 (Leica) and pictures were taken on Olympus DP72. Antibodies used for staining the sections are given in Table 3.

7.16 Quantitative real-time PCR

RNA was isolated from Th1 cell lysates with Trizol (Invitrogen) and reverse transcribed with the Quantitect kit (Qiagen). Quantitative PCR (qPCR) assays were run on a Light Cycler 480II device with the Light Cycler 480 SW 1.5 software. Primers and universal probes (Roche) are given in Table 12.

7.17 Statistical analysis

Statistical analyses were performed with GraphPad Prism 5.0d and p values were calculated by Student's t-test, one-way analysis of variance (ANOVA) or Tukey's multiple comparisons test.

8 Results

8.1 Characterization of protein–RNA interactions in post-transcriptional gene regulation

Post-transcriptional gene regulation is a crucial element in the control of immune responses. Compared to regulation on the level of transcription, regulation on the post-transcriptional level can respond faster and quickly alter gene expression [121]. A striking example of failed post-transcriptional control is the san/san mouse, in which a single point mutation (san mutation) in the ROQ domain of the protein Roquin-1 led to a severe autoimmune disease [39]. Although it was demonstrated that Roquin-1 limited the abundance of the inducible co-stimulator (Icos) transcript [119], the exact mechanism of this regulation could not be resolved. It had been proposed that Roquin-1-dependent Icos repression was mediated by miR-101, which contained a putative binding site in the 3'UTR of the Icos mRNA [119]. However, recent studies using cells deficient for Dicer or Ago1–Ago4, which were devoid of miRNAs [149] or defective in miRNA-mediated gene silencing [154], clearly demonstrated that Roquin-1 was able to repress Icos independently of the miRNA pathway [149]. We therefore investigated the possibility of direct Roquin-1 protein interaction with Icos mRNA as a crucial first step in the so far unknown mechanism of Roquin-1-mediated Icos repression.

8.1.1 Roquin-1 is able to directly bind to RNA and has an intrinsic preference for the 3'UTR of ICOS mRNA

Direct interaction of Roquin-1 with the human ICOS mRNA was investigated *in vitro* using electrophoretic mobility shift assays (EMSA), in which *in vitro* transcribed ICOS mRNA was combined with purified recombinant Roquin-1 protein. It was important to test the interaction with ICOS full-length (FL) mRNA to avoid any bias by using only fragments of the ICOS mRNA. Recent studies showed that a region encompassing one-third at the end of the ICOS 3'UTR responded to high Roquin-1 overexpression when transplanted into the context of a reporter gene [119]. Within this fragment Roquin-1 was mapped to bind at a 47-nt sequence immediately adjacent to the miR-101 binding site mentioned above [155]. Because of this correlation, the focus was laid on the 47-nt sequence in the investigation of direct protein–RNA binding and functional response. However, Roquin-1 overexpression down-regulated the reporter construct containing the putative 47-nt response element to a lesser extent than

the larger construct containing the full last third of the ICOS 3'UTR [119]. Bearing in mind that Roquin-1-mediated Icos repression was demonstrated to be independent of the miRNA pathway [149], it was crucial to investigate Roquin-1 binding to the entire ICOS mRNA.

As the ICOS FL mRNA (nts 1–2540) was too large to run on polyacrylamide gels, EMSAs were performed on a standard agarose gel and RNA or RNA–protein complexes were visualized by staining the gel with ethidium bromide. For these experiments, ICOS mRNA constructs were *in vitro* transcribed and purified (Figure 5 A). Furthermore, a truncated recombinant Roquin-1 (aa 1–441) protein was generated, comprising the RING finger, the ROQ domain and the zinc finger (Figure 5 B and Figure 15 B showing the protein domain organization).

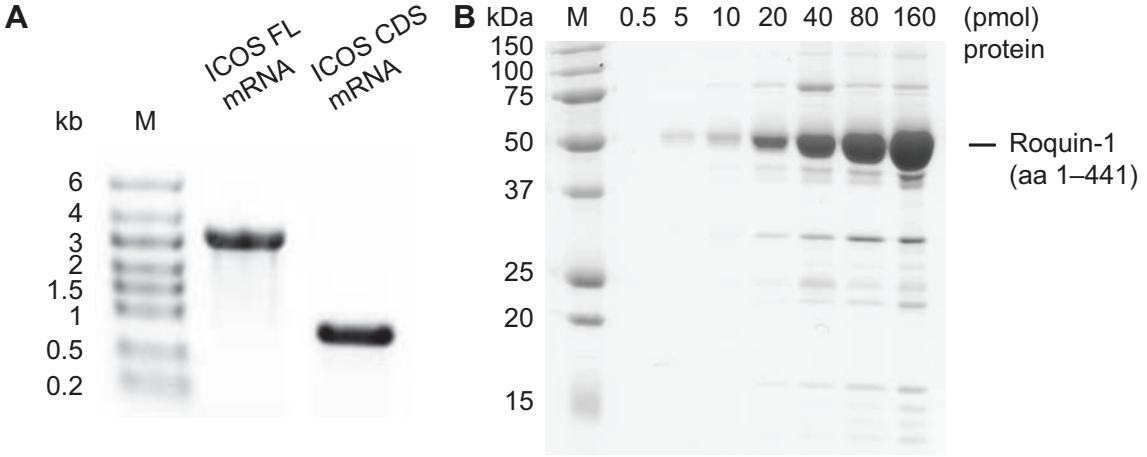

Figure 5: *In vitro* transcribed ICOS mRNA and recombinant Roquin-1 (aa 1–441) protein. (A) *In vitro* transcribed and purified ICOS full-length (FL) or coding sequence (CDS) mRNA, analyzed on a denaturing agarose gel. (B) SDS polyacrylamide gel showing the purity of increasing amounts (pmol) of Roquin-1 (aa 1–441) after purification and desalting.

In immunoprecipitation experiments from cell lysates, in which Roquin-1 mutants were overexpressed, this amino-terminal fragment of Roquin-1 had been shown to efficiently bind to ICOS mRNA, while the carboxy-terminus was not involved in ICOS mRNA binding [149]. However, this interaction of the amino-terminus of Roquin-1 with the ICOS mRNA could also occur indirectly via binding of other factors present in these lysates. Testing the truncated recombinant Roquin-1 construct in the EMSA *in vitro* system would therefore constitute the first proof of a direct protein–RNA interaction via the amino-terminus of Roquin-1.

The band shift experiments demonstrated indeed that the amino-terminus of Roquin-1 (aa 1–441 of full-length (FL) protein isoforms aa 1–1130 or 1–1121) was capable of directly binding to ICOS mRNA *in vitro*. The ICOS FL mRNA band only shifted in the presence of varying amount of Roquin-1 (5, 7.5 and 10 µg), but not in the presence of equal amounts of BSA protein (Figure 6 A). Furthermore, the Roquin-1-binding was specific for mRNA, as tRNA used as a competitor did not compete the observed band-shift (Figure 6 B).

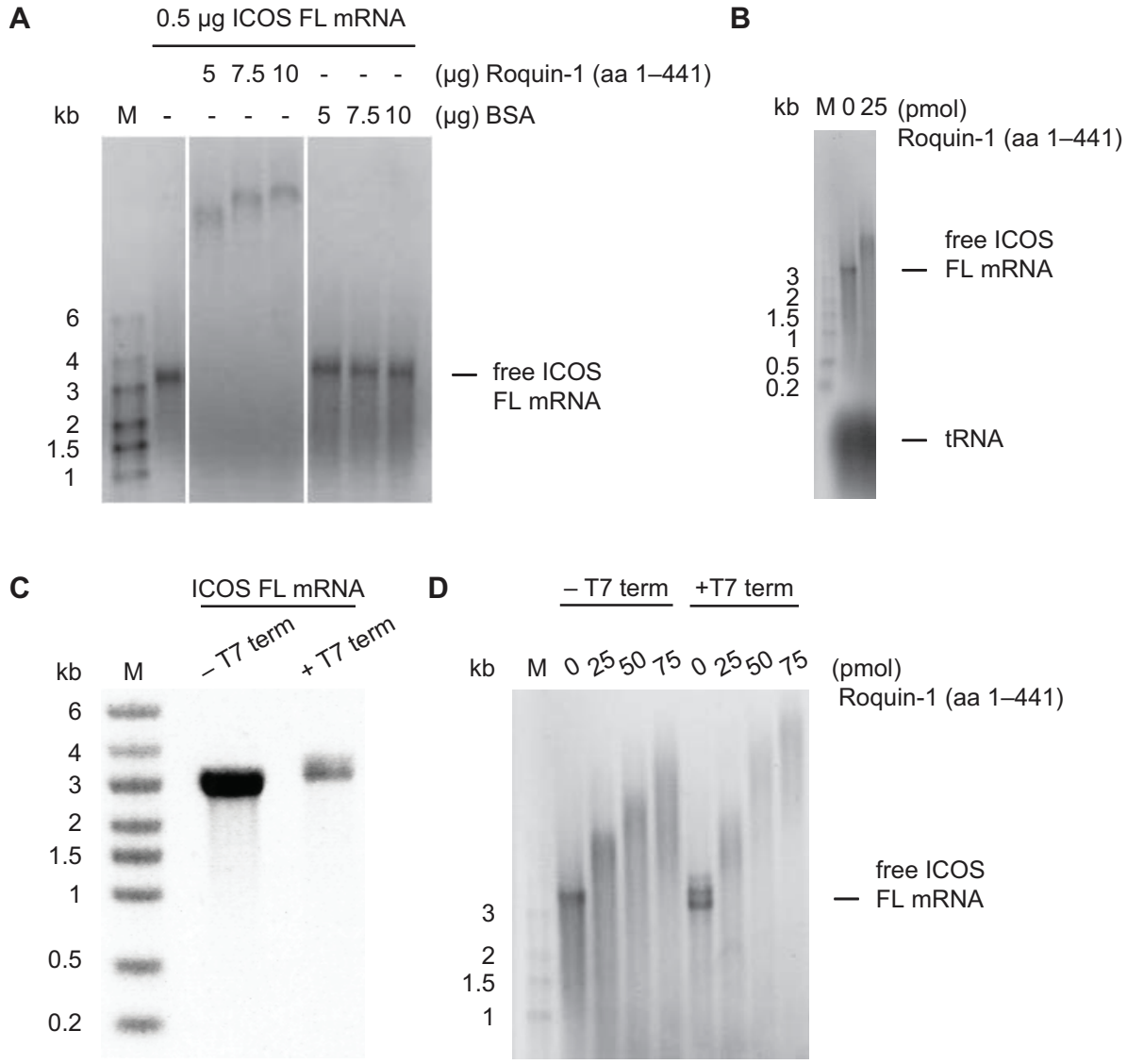

Figure 6: Roquin-1 interacts with ICOS mRNA. (A–B, D) EMSAs of Roquin-1 protein interacting with ICOS mRNA were performed in the presence of 65-fold excess competitor yeast transfer RNA (tRNA). Varying amounts of Roquin-1 (aa 1–441) (A, D) and unrelated protein (BSA=bovine serum albumin) (A) were incubated with ICOS FL mRNA. (C–D) The DNA template used for *in vitro* transcription and subsequently for EMSA, was linearized to produce mRNA with or without the T7-terminator sequence.

Nevertheless, the use of restriction sites behind the T7-terminator sequence to linearize the DNA template for *in vitro* transcription occasionally led to the *in vitro* transcription of the T7-terminator sequence, which might allow Roquin-1 binding to the secondary structure of the T7-terminator sequence. To exclude this possibility, a restriction site was cloned behind the respective ICOS sequence, but before the T7-terminator sequence. Importantly, ICOS mRNA bands were equally well shifted when the DNA template for *in vitro* transcription was cut before or after the terminator sequence. Therefore, the binding was not dependent on the T7-terminator sequence (Figure 6 C–D).

As most *trans*-acting factors target *cis*-elements in the 3'UTR of mRNAs [121], the binding preferences of Roquin-1 were investigated. Roquin-1 bound effectively to RNA sequences from the ICOS FL or 3'UTR, while ICOS CDS mRNA was not well recognized *in vitro* (Figure 7 A). Furthermore, a band representing an artificial mRNA with a tandem repeat of the ICOS CDS was also not efficiently shifted *in vitro* (Figure 7 B). This excluded the possibility that binding depended solely on the length of the transcript. Moreover, this indicated that a specific *cis*-element for Roquin-1-binding was localized in the 3'UTR of ICOS mRNA. Roquin-1-specific binding of mRNA was shown by the complete absence of free mRNA and could be quantified by titration of different amounts of Roquin-1 protein. 1 pmol of full-length ICOS mRNA could be fully shifted with 20 pmol protein, while ICOS CDS was not shifted below 160 pmol protein (Figure 7 C). This indicated an at least eightfold binding preference of Roquin-1 to the 3'UTR of ICOS mRNA compared to ICOS CDS mRNA. The continuous shifting upon higher protein concentrations might be due to cooperative binding of several Roquin-1 molecules at the same RNA. Notably, using higher protein concentrations even resulted in an excessive shift of ICOS FL and the disappearance of free ICOS CDS. This gel retardation might be caused by an additional low binding affinity of Roquin-1 to RNA in general, as was observed for the ICOS CDS. This suggested a bimodal binding kinetic with a high affinity binding at low molar protein concentrations and a low binding affinity of Roquin-1 to RNA in general at high protein concentrations.

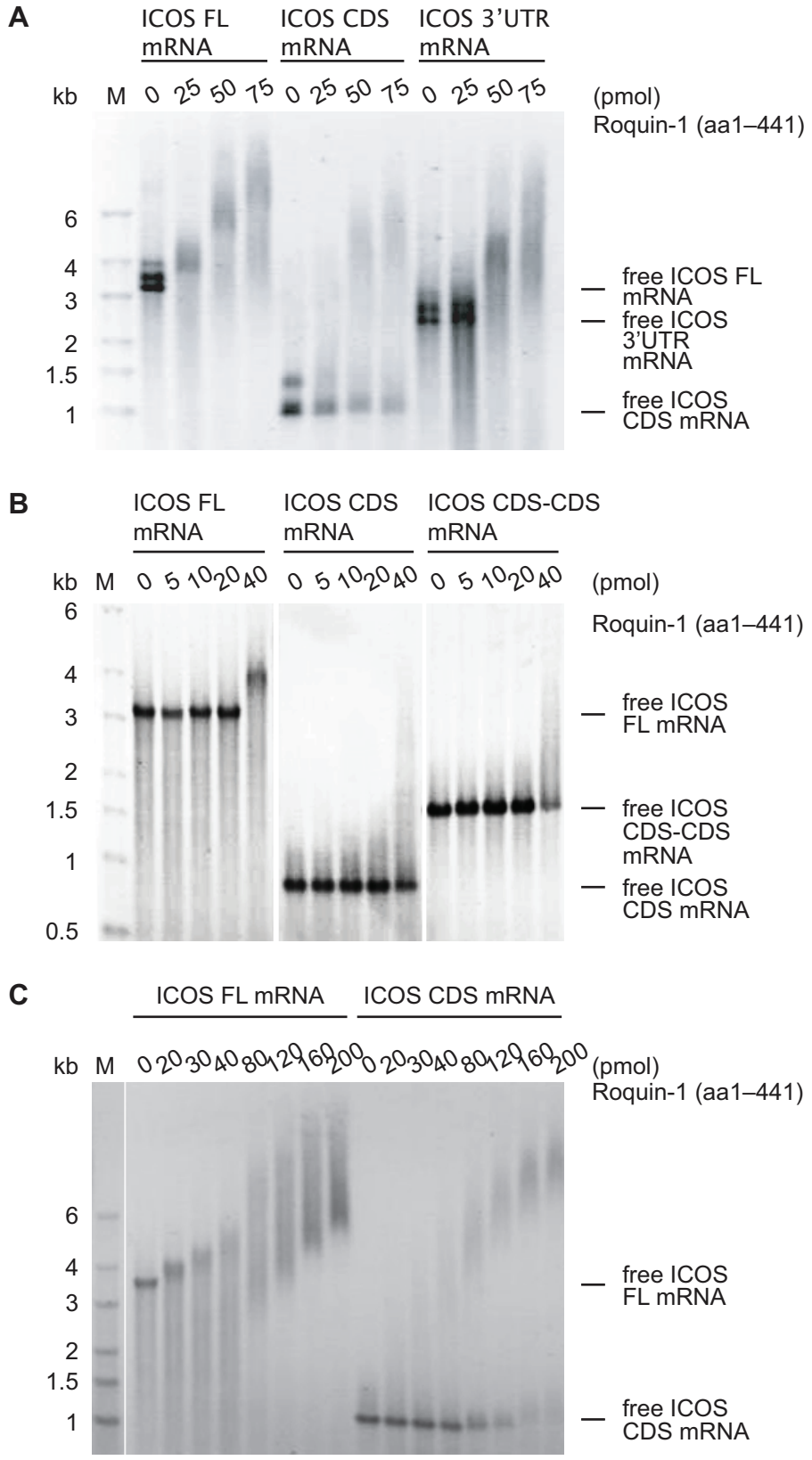

Figure 7: Roquin-1 specifically binds to the 3'UTR of ICOS mRNA. (A–C) EMSA showing a titration of increasing amounts (0–200 pmol) of recombinant Roquin-1 (aa 1–441) protein, incubated with *in vitro* transcribed ICOS mRNAs (1 pmol per lane). The ICOS mRNAs contained either full-length mRNA (1–2540), coding sequence only (1–600) or the 3'UTR only (601–2540). As an artificial mRNA, the CDS was cloned in tandem omitting a second start codon (B).

The band shift experiments above in addition to immunoprecipitation studies [149] demonstrated that the ROQ domain of Roquin-1 was essential for the direct binding to ICOS mRNA. Furthermore, the previous overexpression and immunoprecipitation experiments indicated that the zinc finger contributed to the binding [149]. Therefore, the function of the zinc finger had also been studied *in vitro* using electrophoretic mobility shift assays. Recombinant Roquin-1 protein lacking the zinc finger (aa 1–414) showed a reduced gel-retardation of the ICOS FL mRNA compared to Roquin-1 (aa 1–441) (Figure 8 A). This difference could be interpreted as a reduced binding activity of Roquin-1 (aa 1–414). However, several proteins can interact with the same mRNA. Therefore, the alteration might equally be due to the reduced molecular weight of the Roquin-1 (aa 1–414)–ICOS mRNA complex. To discriminate between both possibilities, recombinant Roquin-1 (aa 1–441) was generated with a mutation of the first cysteine of the zinc finger. This protein fragment with equal mass but without zinc finger activity did not show decreased binding affinity to ICOS FL mRNA (Figure 8 B), explaining why addition of EDTA did also not interfere with Roquin-1 binding (EDTA was present in the EMSA in Figure 8 A, but not in B; also see section 7.10). The zinc finger therefore did not significantly contribute to the binding of ICOS FL mRNA *in vitro*, but may accomplish functions *in vivo* of so far unknown specificity.

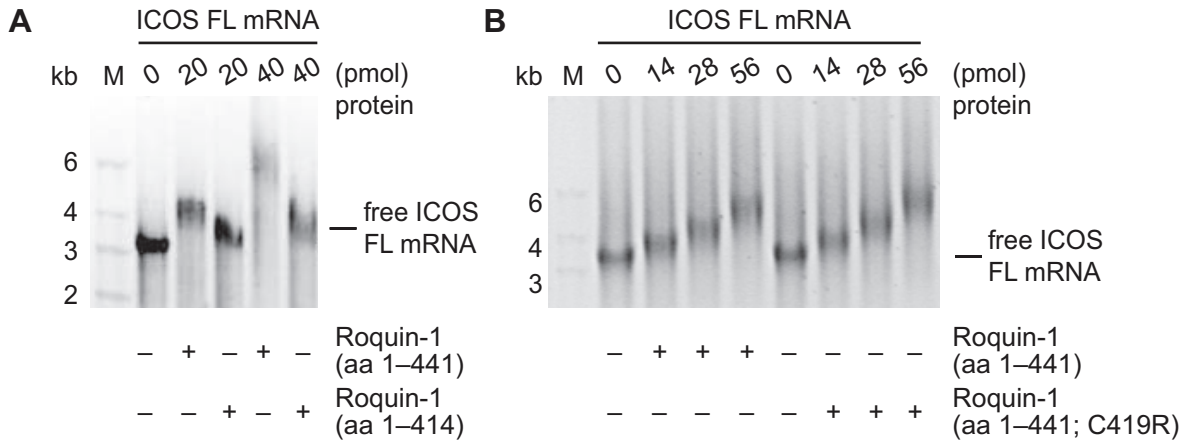

Figure 8: The zinc finger in Roquin-1 does not significantly contribute to RNA binding. (A–B) EMSA showing the binding of recombinant Roquin-1 to 1 pmol of ICOS FL mRNA. Recombinant Roquin-1 was generated with (aa 1–441) or without (aa 1–414) the zinc finger domain (A) or with a point mutation in the first cysteine of the zinc finger (C419R mutation) causing loss of zinc finger function (B). In (A) the original EMSA buffer with EDTA was used and in (B) the optimized binding buffer without EDTA was used (section 7.10).

Moreover, the carboxy-terminal part of Roquin-1 did not play a significant role in RNA binding, as full-length Roquin-1 (aa 1–1130) shifted ICOS mRNA only slightly better than the truncated version of Roquin-1 (aa 1–441) (Figure 9). This difference in the binding could equally be explained by the increased size of the Roquin-1 FL–ICOS mRNA complex compared to Roquin-1 (aa 1–441) binding to the ICOS mRNA.

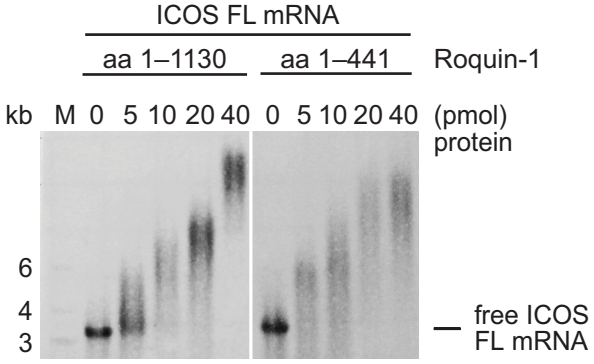

Figure 9: Both Roquin-1 FL (aa 1–1130) and Roquin-1 (aa 1–441) bind comparably well to the ICOS mRNA. EMSA of Roquin-1 proteins (0–40 pmol) with 1 pmol ICOS FL mRNA.

Interestingly, the Roquin-1^{san} protein (aa 1–441) with the M199R mutation did not show an altered binding behavior to ICOS FL mRNA (Figure 10 A). Roquin-1^{san} had been proposed to bind to ICOS with higher affinity than Roquin-1 wild-type [155]. However, these studies used PAGE and radioactively labeled RNA fragments for the investigation of the RNA-binding and therefore focused on the isolated 47-nt sequence in the ICOS 3'UTR, which correlated with the miR-101 complementary sequence [155]. In contrast, agarose EMSAs allowed the unbiased investigation of full-length ICOS mRNA. In this system, binding differences between Roquin-1 wild-type (aa 1–441) and Roquin-1 M199R (aa 1–441) protein could not be reproduced even in a very fine titration of Roquin-1 M199R vs. wild-type Roquin-1 protein (Figure 10 B).

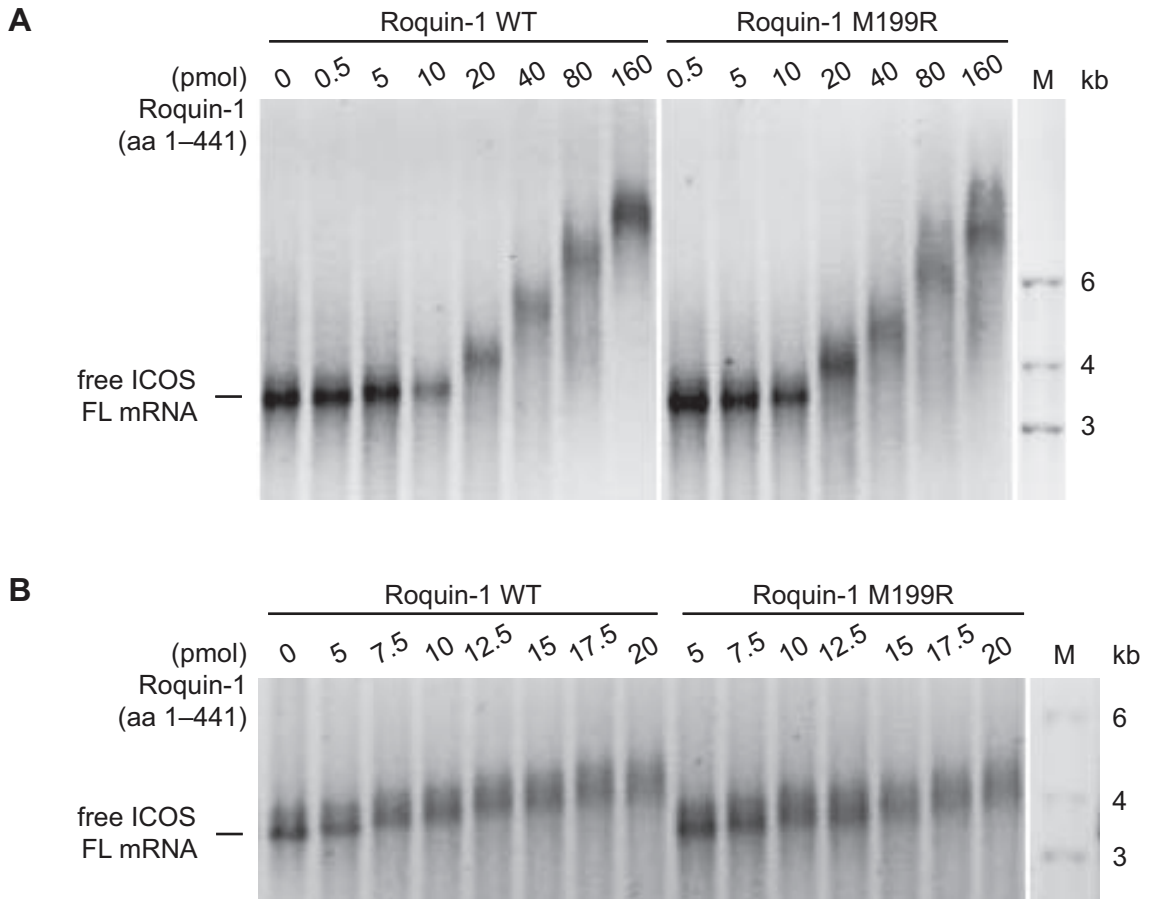

Figure 10: Roquin-1 (aa 1–441) protein with the M199R mutation binds equally well to ICOS mRNA as wild-type protein. (A–B) EMSA of Roquin-1 (aa 1–441) protein with or without M199R mutation (0–160 pmol) binding to 1 pmol ICOS FL mRNA.

8.1.2 Roquin-1 binds to a specific *cis*-element in the 3'UTR of ICOS

To identify the specific *cis*-element for Roquin-1 binding, the 3'UTR of ICOS mRNA was sequentially shortened by 600 nucleotides (nts), starting from the 3'end. ICOS mRNA transcribed from all deletion constructs was shifted equally well by Roquin-1 (aa 1–441) protein compared to ICOS FL mRNA, with the shortest one containing the ICOS CDS plus additional 610 nts of the 3'UTR (ICOS 1–1210) (Figure 11 A). Importantly, Roquin-1 (aa 1–441) bound to ICOS 1–1210 with higher affinity than to an irrelevant mRNA of comparable length (Figure 11 B). Similarly, the artificial construct with the tandem CDS of ICOS mRNA comprising 1200 nucleotides did not response to Roquin-1 binding (Figure 7 B), corroborating the observation that the band shift did not depend on the length of the RNA.

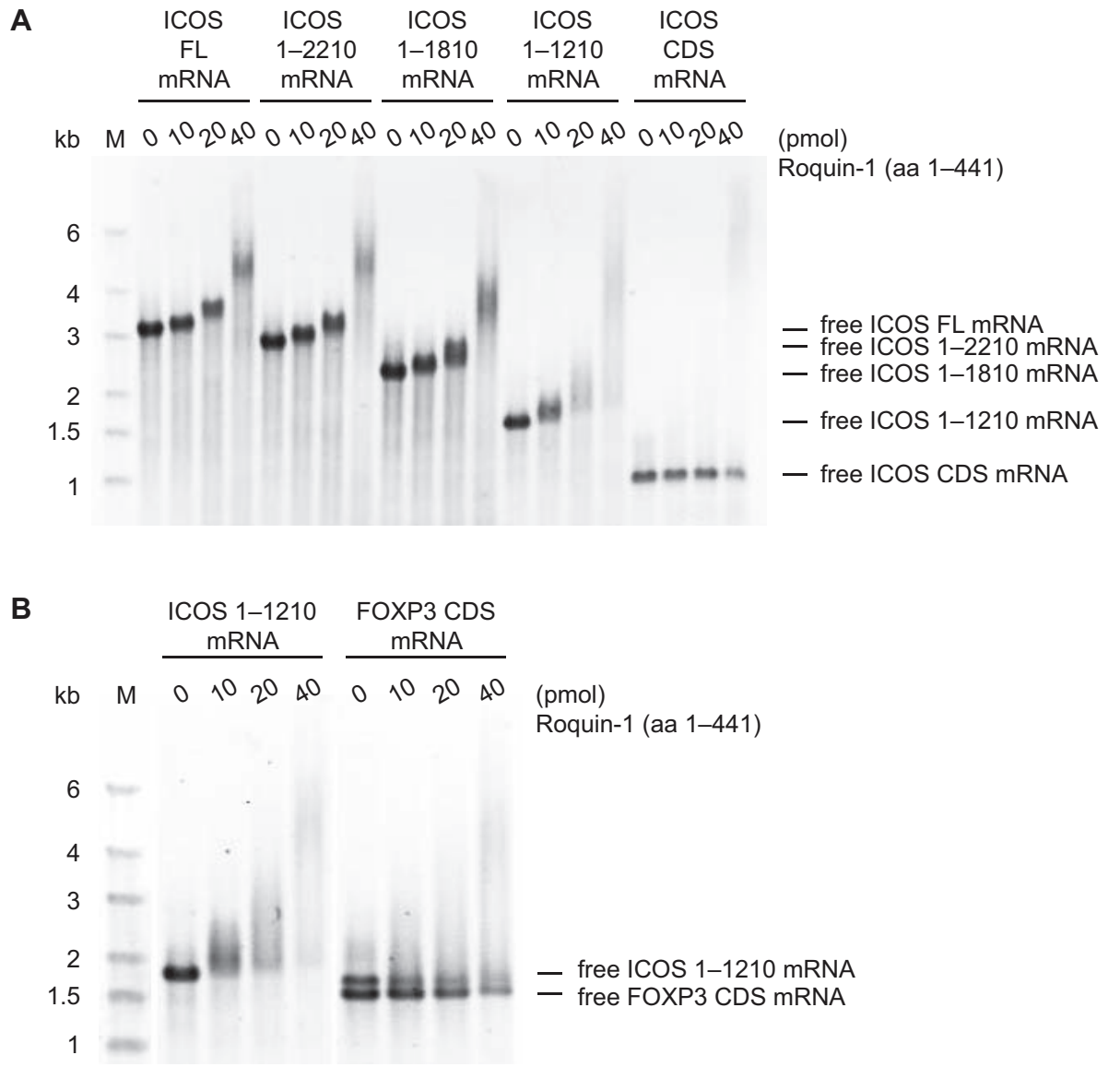

Figure 11: Roquin-1 specifically binds to a *cis*-element in the 3'UTR of ICOS mRNA. EMSA of increasing amounts (0–40 pmol) Roquin-1 (aa 1–441) protein with ICOS mRNAs (1 pmol per lane). (A) ICOS mRNAs were progressively shorted from the 3'end to investigate the binding preference of Roquin-1 to different parts of the ICOS mRNA. ICOS FL = 1–2540, ICOS CDS = 1–600. (B) FOXP3 CDS mRNA was used as a non-specific binding control compared to an ICOS mRNA fragment of similar size (nts 1–1210).

Additional deletion constructs of ICOS mRNA were generated to localize the responsive *cis*-element. ICOS 1–1210 was further shortened in a step-wise manner by 100 nts each. As the construct ICOS 1–800 was still effectively bound, but ICOS 1–700 was not, one crucial *cis*-element could be assigned to 100 nts 3' to the stop codon of the ICOS CDS (Figure 12).

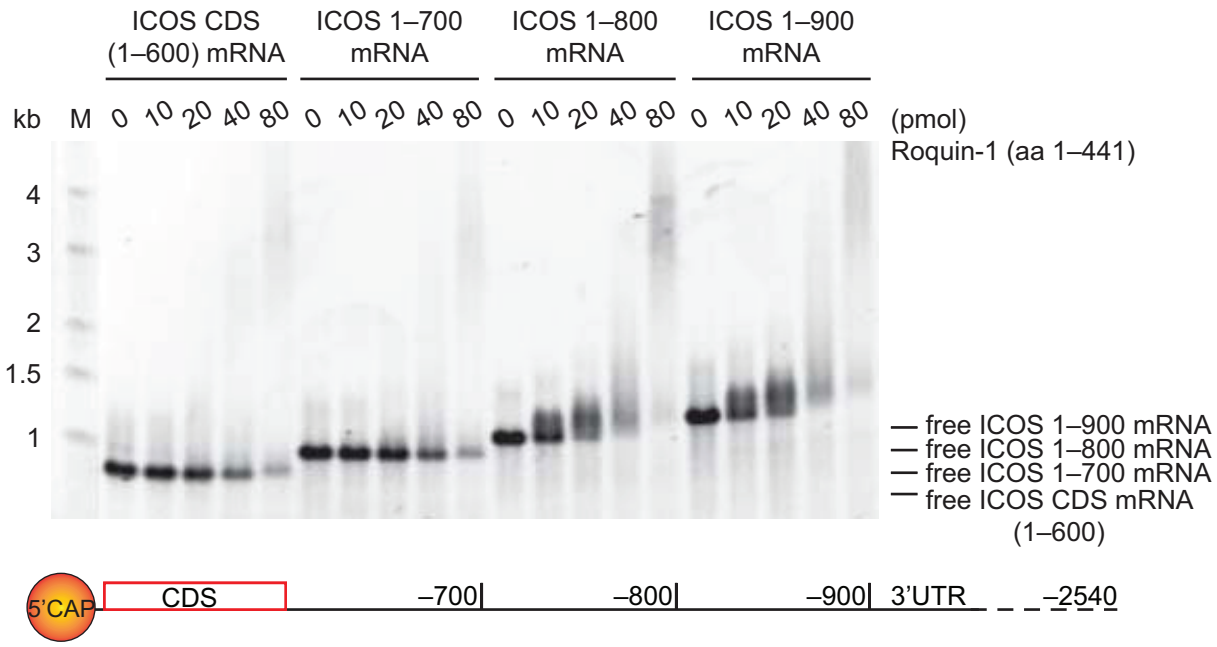

Figure 12: A crucial *cis*-element for Roquin-1 binding is localized 100 nts 3' to the stop codon. EMSA of increasing amounts (0–40 pmol) Roquin-1 (aa 1–441) recombinant protein with *in vitro*-transcribed ICOS mRNA. The 3'UTR of ICOS mRNA was progressively shortened from 900 bases (ICOS 1–900 mRNA) to 700 bases (ICOS 1–700 mRNA) as indicated in the scheme.

8.1.3 The RNA sequence in the ICOS *cis*-element adopts a finger-like structure

Trans-acting factors can either bind to specific sequences in their target mRNA, or recognize certain structural motifs [121]. It can therefore be difficult to describe a valid *cis*-element just on the basis of a mapped sequence. The 3'UTR of the ICOS mRNA is unusually long and was found to contain six highly conserved regions [119]. There are few conserved and several poorly conserved miRNA binding sites in the ICOS 3'UTR and miR-101 was initially proposed to play a role in Roquin-1-mediated Icos repression [119]. However, as was shown thereupon in *Dicer*-deficient cells, Roquin-1 repressed Icos independently of miRNAs. Instead it directly bound to the 3'UTR of the ICOS mRNA (section 8.1.1, 8.1.2 and [149]).

The ICOS 3'UTR was then scanned for known RNA-binding motifs, using the IBT tool *UTRscan*. Beside the polyadenylation site at the end of the ICOS 3'UTR, the scan only revealed six putative Musashi binding elements. Musashi is a stem cell factor involved in the post-transcriptional control of early developmental processes [156]. Despite this motif, there was no evidence for other sequence-specific motifs such as AU-rich elements. Therefore, the secondary structure of ICOS mRNA was determined to identify possible structures, which might play a role in Roquin-1/2 protein binding. The SHAPE assay (selective 2'-hydroxyl

acylation analyzed by primer extension) [153] was used to model structural motifs of the ICOS 3'UTR. Electrophilic components, such as N-methylisatoic anhydride (NMIA), are attracted by the nucleophilic reactivity of 2'-hydroxyl groups of unpaired RNA nucleotides. Acylation of these groups by NMIA leads to a stop in a primer extension reaction. It is therefore possible to directly obtain the site, where nucleotides are present in an unpaired conformation. With this information, the secondary structure of an mRNA can be modeled at a single nucleotide resolution [153]. As described in section 7.11, RNA was modified with NMIA or DMSO as a control and primer extension as well as sequencing reactions for nucleotide assignment were performed with radioactively labeled primers. As there is a limit to the length of the RNA that can be resolved on the gel, we focused on the mapped *cis*-element ICOS 700–800 as well as on two additional fragments 5' (ICOS 600–700) and 3' (ICOS 800–900) to the *cis*-element (Figure 13 A–B). The intensity of the ^{32}P-labeled nucleotides was determined for the NMIA and DMSO reaction (Figure 13 C) and the signal was normalized to the DMSO background levels (Figure 13 D). In Figure 13 D, yellow bars represent relative SHAPE reactivities above 0.2 and red bars above 0.3. However, background levels strongly vary. Therefore, we defined that relative SHAPE reactivities above 0.3 indicate possibly unpaired nucleotides, while relative SHAPE reactivities above 0.5 represent truly unpaired nucleotides. The strength of nucleotide pairing can be influenced by wobbly structures in the RNA. A single free nucleotide neighbored by two paired nucleotides could loosen the base pairing of its neighbors, which might be a reason why nucleotides appear as unpaired but might not truly be free.

The additional information of unpaired nucleotides can be entered into the RNA folding form of "The mfold Web Server" program to model the secondary structure of the RNA. The platform offers the possibility to constrain the folding by certain formulas. Here, the formula P i 0 k was used with *i* being the first base that must not pair and *k* the number of consecutive bases that must not pair starting with *i*.

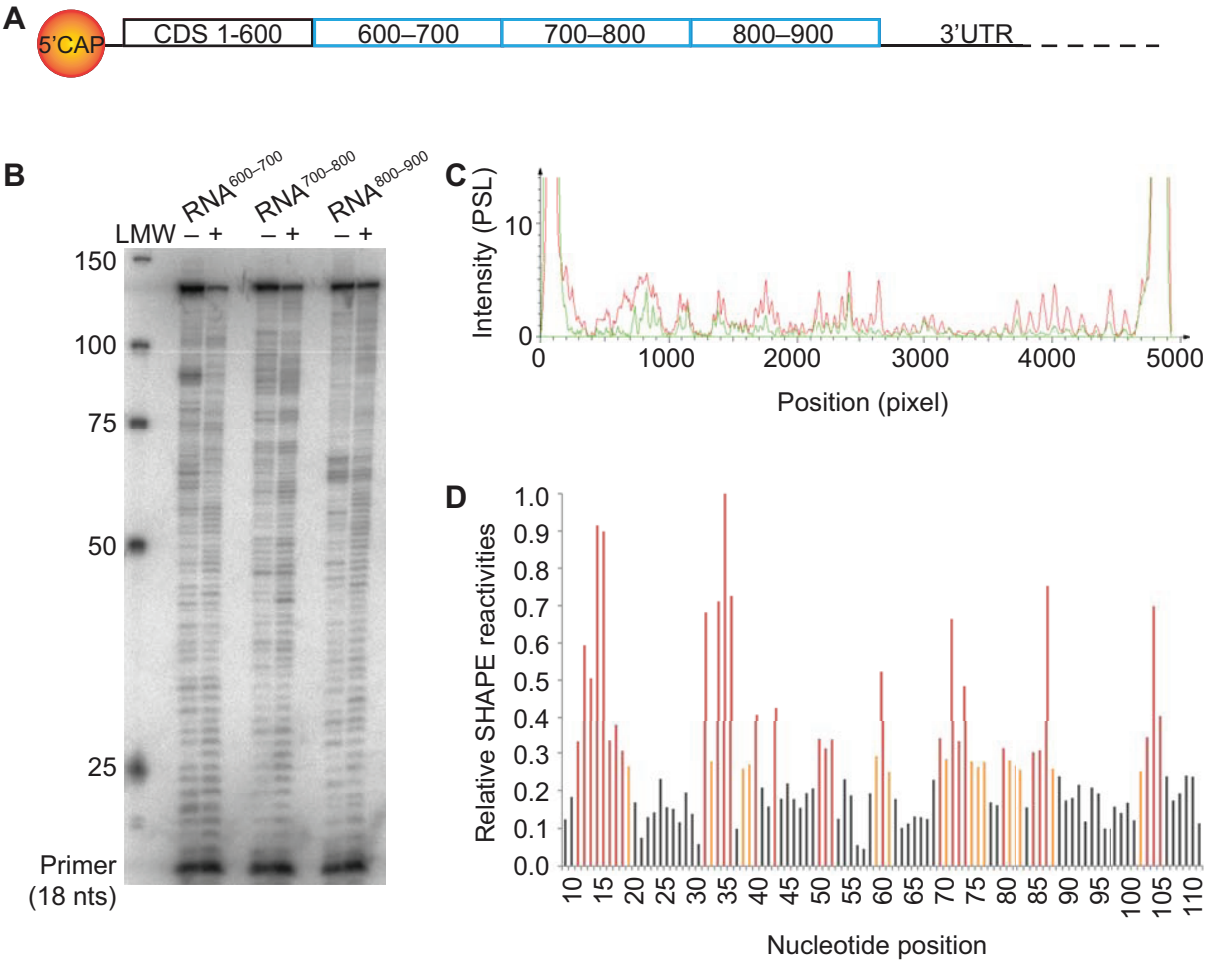

Figure 13: SHAPE analyses of ICOS mRNA fragments. (A) Scheme of ICOS mRNA indicating the analyzed fragments in blue. (B) DNA-sequencing gel for the ICOS fragments 600–700, 700–800 and 800–900 showing reactions with NMIA (+) or with DMSO as a control (–). LMW=low molecular weight marker. (C) Intensity (PSL) of the radioactive nucleotides in the sequencing reaction of ICOS 700–800 with (+, red) or without (–, green) NMIA. (D) Relative SHAPE reactivities indicating unpaired nucleotides of ICOS 700–800 normalized to the DMSO-control reaction. Primer extension and sequencing reactions as well as data analyses were done by Dr. Maximilian Hartl, Department of Biopolymers, Universität Bayreuth.

For the analyzed fragments, only one or two thermodynamic stable structures were predicted (Figure 14 A–C). Both ICOS 600–700 (Figure 14 A) and ICOS 800–900 (Figure 14 C) displayed a long, stretched secondary structure with small loops, while ICOS 800–900 could also exert a structure with wider loops. However, only ICOS 700–800 exhibited an interesting two-finger-like structure, which might serve as a binding groove for Roquin-1 protein (Figure 14 B, finger-like structure highlighted in blue).

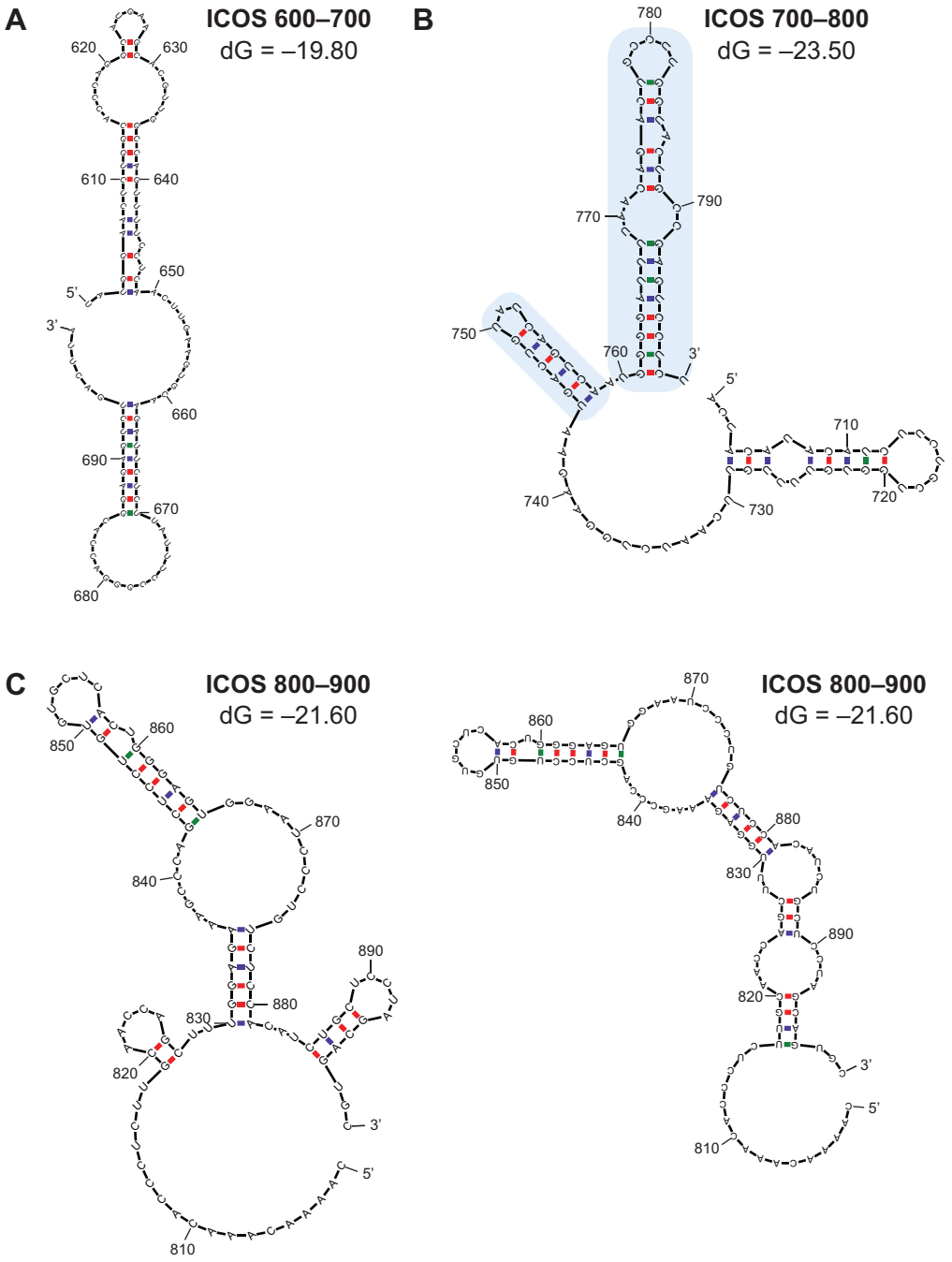

Figure 14: Secondary structures of ICOS mRNA fragments. (A–C) Using the additional information of free, unpaired nucleotides determined in section 8.1.3 (cutoff >0.5), the secondary structure of ICOS 600–700, ICOS 700–800 and ICOS 800–900 was modeled with "The mfold Web Server" program using the formula P i 0 k with *i* being the first base that must not pair and *k* the number of consecutive bases that must not pair starting with *i*. Only one thermodynamic stable conformation was predicted for (A–B) and two conformations were predicted for (C) with the same Gibbs free energy (dG) value. ICOS 700–800 was mapped in EMSAs to contain a crucial *cis*-element for protein binding. Data analyses were done by Dr. Maximilian Hartl, Department of Biopolymers, Universität Bayreuth.

This idea matched with the mapping of the region in the ICOS 3'UTR, which contained a crucial *cis*-element for Roquin-1 binding, approximately 100 nts 3' to the stop codon of ICOS CDS (Figure 12). However, a limitation of this method is clearly the separated view onto distinct RNA constructs, which add up to the whole secondary structure of the ICOS mRNA. It is therefore reasonable to investigate overlapping segments of the sequence of interest to optimize the modeling procedure.

8.1.4 Roquin-2 binds equally well to the 3'UTR of Icos mRNA

Roquin-2, the paralog of Roquin-1, was first described as a membrane-associated nucleic acid-binding protein (Mnab) [151]. The amino acid sequences of both proteins are highly conserved in the amino-terminal regions and less conserved in their carboxy-termini (Figure 15 A). Furthermore they share a similar domain organization with a RING finger, ROQ domain and zinc finger and similarly a proline-rich region in their carboxy-termini (Figure 15 B). Roquin-2 is the only other protein in the mouse containing this ROQ domain with 77% identity to the Roquin-1 ROQ domain-transcript and even 94% identity on the amino acid level.

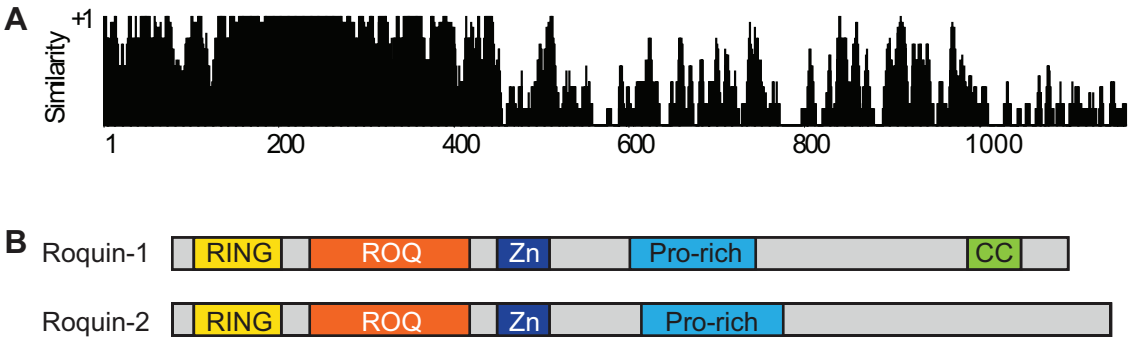

Figure 15: The paralogs Roquin-1 and Roquin-2 share sequence and domain organization. (A) Alignment of mouse Roquin-1 and the long isoform of mouse Roquin-2 (aa 1–1187) for amino-acid similarity. (B) Depiction of the domain organization in Roquin-1 and Roquin-2 with the RING finger, the ROQ domain, a zinc finger (Zn), a proline-rich region (Pro-rich) and a Coiled coil (CC) domain.

To investigate the binding of Roquin-2 to RNA, specifically to the ICOS mRNA, a recombinant Roquin-2 protein (aa 1–438) was generated and tested in EMSAs, which was homologous to the amino-terminal fragment of Roquin-1 (aa 1–441). Interestingly, Roquin-2 bound equally well to ICOS mRNA as Roquin-1 (aa 1–441) with an intrinsic preference to the

3'UTR of ICOS (Figure 16). This indicated that Roquin-2 might target the same or similar mRNAs, or might be able to substitute for Roquin-1.

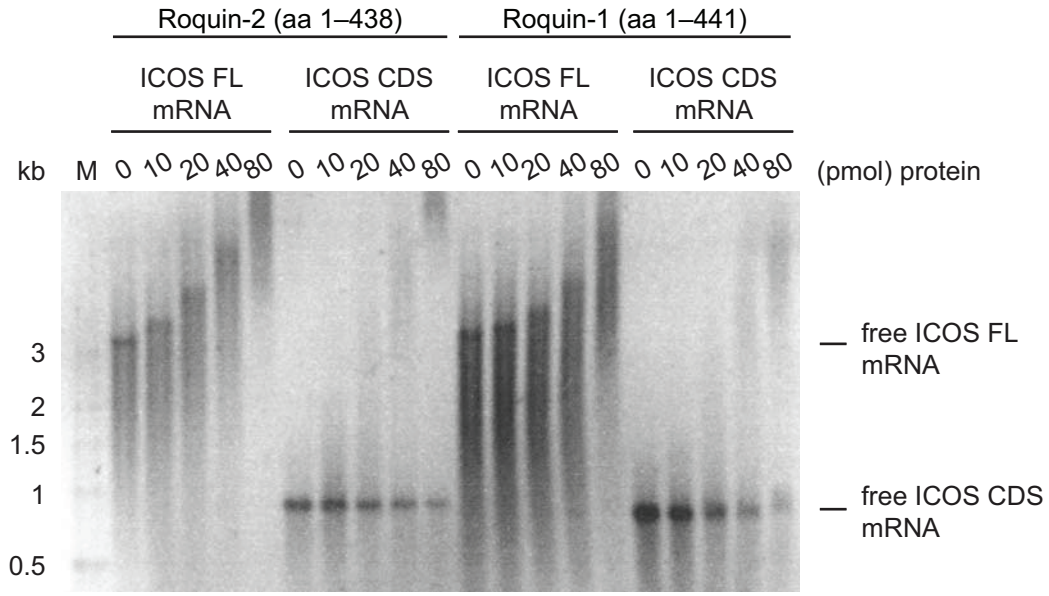

Figure 16: Roquin-1 and Roquin-2 bind equally well to the 3'UTR of ICOS mRNA. EMSA of varying amounts of recombinant Roquin-1 (aa 1–441) or Roquin-2 (aa 1–438) protein with 1 pmol ICOS FL or CDS mRNA.

8.1.5 An array-approach to identify new targets of Roquin-1

ICOS mRNA was the first confirmed target of Roquin-1. Very recently IFN-γ had been proposed to be an additional Roquin-1 target, as indicated by increased half-life of IFN-γ mRNA in *Rc3h1*$^{san/san}$ mice [157]. However, IFN-γ has not been functionally evaluated as a potential target in respect to direct protein–RNA interaction or direct repression by Roquin-1. The important function of Roquin-1 in the immune system necessitated the search for more targets, especially because Icos de-repression could not exclusively explain the massively disturbed phenotype of the *Rc3h1*$^{san/san}$ mouse. To address this question, Roquin-1 was knocked down in CD4^{+} T cells from mice bearing a transgene for a truncated human coxsackie adenovirus receptor (CAR). This receptor enabled the transfection of cells with a control or Roquin-1-knockdown adenovirus. The knockdown construct independently co-expressed GFP as a marker and the 10% highest infected cells were sorted for RNA isolation. In three repeats a relatively small set of targets was identified. Knockdown of Roquin-1 revealed 43 genes, which were de-repressed, while the expression of only 8 genes was reduced by the knockdown (Figure 17), indicating that Roquin-1 acted predominantly as

repressor of targets. As a knockdown control, Roquin-1 was efficiently down-regulated and the known target Icos was up-regulated. Interestingly, several other T cell co-stimulatory receptors were deregulated, including 4-1bb and Ox40. Additionally, the knockdown of Roquin-1 revealed several genes involved in oxidative stress, the glucose metabolism or diverse signaling pathways.

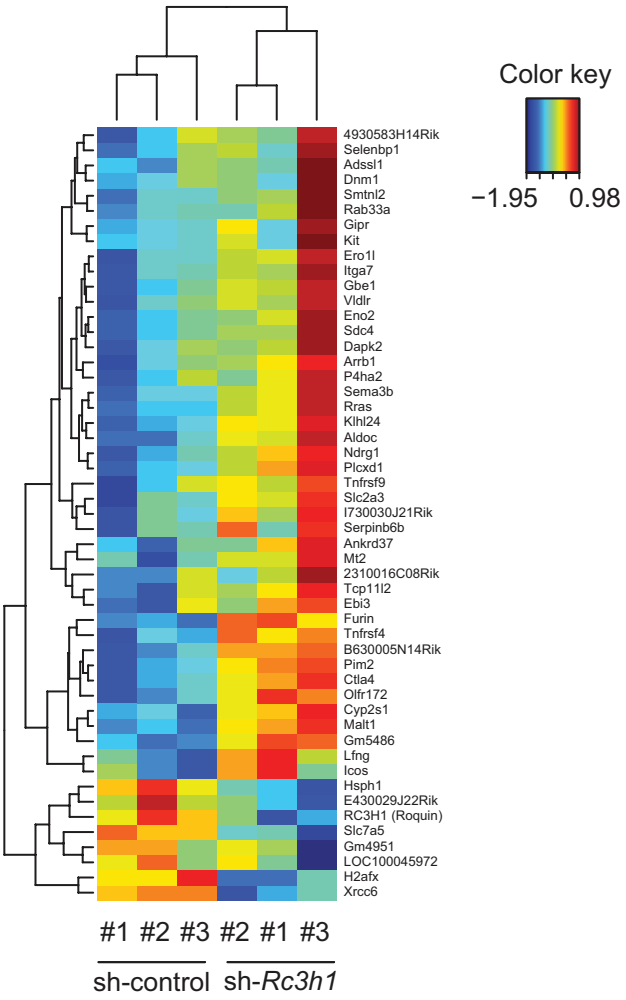

Figure 17: Expression levels of putative Roquin-1 target mRNAs. In an array approach, *Rc3h1* was adenovirally knocked down to search for deregulated targets. The color key indicates the fold-change as 2^x. Arrays were performed in three replicates and are ordered in the heat map according to similarity among each other. Gene expression analyses were done at the Laboratory for Functional Genome Analysis, Munich under the direction of Dr. Helmut Blum. The statistical analyses and heat map were done by Dr. Dirk Repsilber, Leibniz Institute for Farm Animal Biology, Dummerstorf.

Quantitative PCR was used to further validate several of the putative targets, which were identified in the knockdown approach. Expression levels of target mRNAs were determined in $CD4^+$ T cells from *Rc3h1*$^{fl/fl}$*; CD4-Cre* mice, which lacked Roquin-1 expression or as a control from wild-type mice. This approach confirmed seven targets of Roquin-1. Roquin-1 acted therefore as repressor of Pim2, Kit, Ox40, Lfng, Ctla4, Icos and Ebi3 amongst other possible targets (Figure 18).

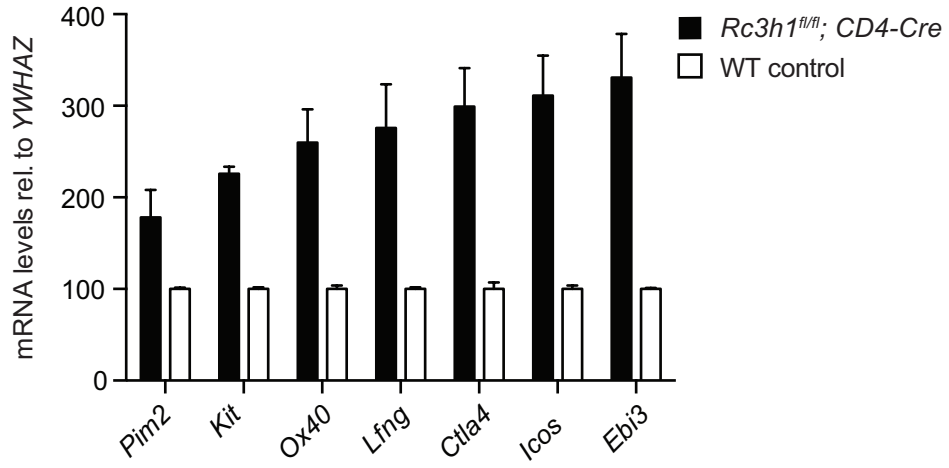

Figure 18: De-repressed targets of Roquin-1. To validate targets unique to Roquin-1, RNA was prepared from wild-type $CD4^+$ T cells or $CD4^+$ T cells of mice deficient for Roquin-1. The mRNA expression levels of the indicated genes relative to *YWHAZ* were analyzed by qPCR. The qPCR analyses were performed by Dr. Kai Höfig.

8.1.6 Roquin-1 binding to new mRNA targets

Based on the qPCR results, two very promising candidates of Roquin-1 binding are Ctla4 and Ox40, as they are both co-receptors on T cells. Furthermore, Ctla4 is structurally related to Icos [25]. Both belong to the CD28 receptor family and interact with PI3K (section 5.1.2 and [25]). However, they diversify in function as Icos provides positive co-stimulation whereas Ctla4 exerts negative co-stimulation [158]. Ox40 does not share a common structure with Icos, but is also an activation marker on T cells, providing co-stimulatory signals for cell division and survival [42]. In EMSA experiments, Roquin-1 (aa 1–441) could actually bind to both mouse Ox40 and mouse Ctla4 FL mRNA (Figure 19). While the binding of ICOS or Ctla4 seemed to exhibit similar characteristics, Ox40 mRNA shifted higher than ICOS with the same protein concentration. These studies corroborate Ox40 and Ctla4 as new direct targets of Roquin-1.

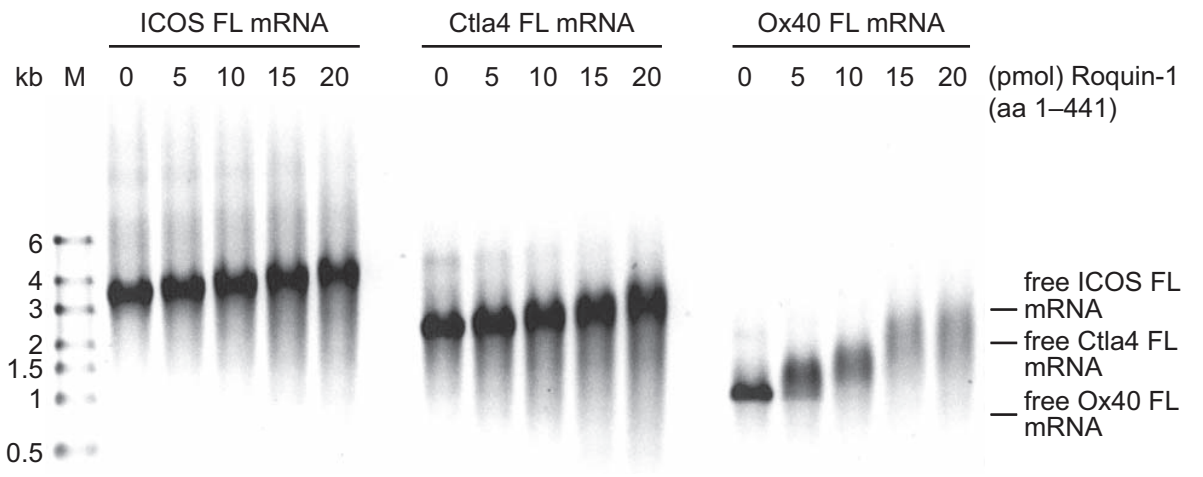

Figure 19: Roquin-1 binds to ICOS, Ctla4 and Ox40 mRNA. EMSA showing binding of increasing amounts of recombinant Roquin-1 (aa 1–441) protein to 1 pmol ICOS, Ctla4 or Ox40 full-length (FL) mRNA. EMSA was performed by Gitta Heinz.

8.2 Function of Roquin-1 and Roquin-2 *in vivo*

After analyzing the essential RNA-binding activity of Roquin-1 and Roquin-2 *in vitro*, the focus was laid on the function and mechanism of both proteins *in vivo*. Roquin-1 deficiency had already been analyzed at several levels (section 5.3) [120]. In contrast to the *Rc3h1*$^{san/san}$ mouse, the conditional Roquin-1 knockout in T cells, B cells or in the hematopoietic system did not show signs of autoimmunity. However, Icos levels were uniformly elevated in all knockouts [120]. This showed that de-repression of Icos was not sufficient to break tolerance and that other factors significantly contributed to the lupus-like autoimmune phenotype in san/san mice. This was also supported by a recent publication, which demonstrated that loss of Icos in the context of the *sanroque* alleles even increased splenomegaly and led to the predominant occurrence of anti-nuclear antibodies in *Rc3h1*$^{san/san}$ mice, which normally show anti-nuclear as well as anti-cytoplasmic autoantibodies [159].

Furthermore, the striking homology of Roquin-1 and Roquin-2 (Figure 15), Roquin-2 binding to ICOS mRNA (Figure 16) as well as the mild phenotype in *Rc3h1*-deficient mice [120] strongly suggested that Roquin-2 might be able to substitute for loss of Roquin-1 function in the knockout situation, but not when Roquin-1 is still present in its mutated form. Therefore, conditional knockout mice were analyzed to determine the redundant and non-redundant functions of Roquin-1 and Roquin-2 *in vivo*.

8.2.1 Expression levels of Roquin-1 and Roquin-2 in mouse tissues

First, the expression levels of both proteins were investigated. For that purpose, a monoclonal antibody was generated that detected both proteins with similar efficiency. The antibody was raised against the amino-terminal part of Roquin-1, which comprised highest sequence homology to Roquin-2. It recognized endogenous Roquin-1 and Roquin-2 proteins equally well as the recombinant protein fragments Roquin-1 (aa 1–441) and Roquin-2 (aa 1–438) (Figure 20 A).

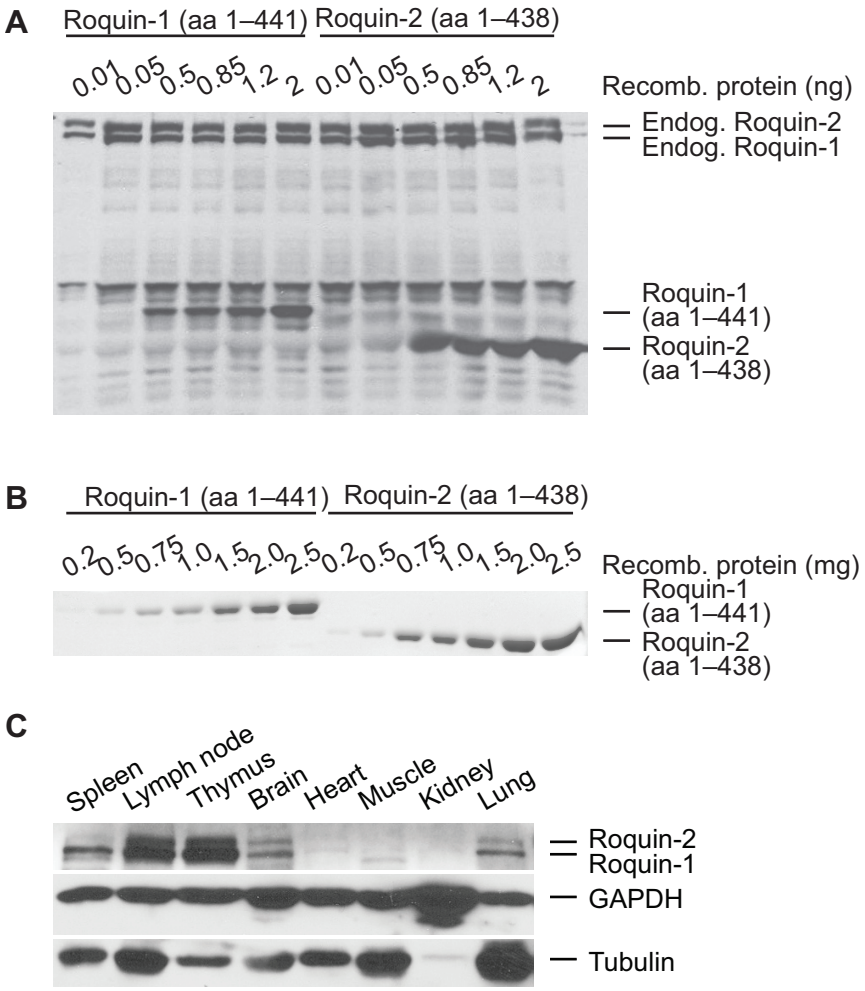

Figure 20: Roquin-1 and Roquin-2 are similarly expressed in different tissues. (A) To evaluate the antibody clone 3F12 against the amino-terminal part of Roquin-1 and Roquin-2, increasing amounts of recombinant Roquin-1 (aa 1–441) or Roquin-2 (aa 1–438) protein were spiked into wild-type MEF cell lysates. (B) Increasing amounts of purified recombinant Roquin-1 (aa 1–441) or Roquin-2 (aa 1–438) were analyzed by PAGE and protein was stained with Coomassie. (C) Protein expression levels of Roquin-1 and Roquin-2 in different mouse tissues with tubulin and GAPDH as loading controls (A–B) were performed by Nina Martin and (C) in cooperation with Claudia Lohs.

Figure 20 B shows a Coomassie staining of Roquin-1 and Roquin-2 proteins as a loading control. The expression levels of Roquin-1 and Roquin-2 were then studied in lysates with equal protein amount from different mouse tissues. Roquin-1 and Roquin-2 proteins showed highest expression levels in extracts from lymph nodes and thymus and significant levels in extracts from brain, lung and spleen. Both proteins were only weakly detectable in extracts from heart, muscle and kidney. Interestingly, in all tissues analyzed, Roquin-1 was present at higher protein levels than Roquin-2 (Figure 20 C). In MEF cells, however, both proteins were endogenously expressed to a similar extent (Figure 20 A).

8.2.2 In $CD4^+$ T cells Roquin-1 localizes to P bodies

To investigate the expression of Roquin-1 in T cells, confocal microscopy was used to study localization of Roquin-1. Primary CAR-transgenic $CD4^+$ T cells were transduced with adenoviruses expressing GFP-tagged Roquin-1. The GFP signal marking Roquin-1 expression was found to co-localize with the helicase Rck, a P body marker (Figure 21, upper panel). Upon stress-induction by arsenite treatment, stress granules formed, which showed co-expression of Roquin-1. In only 5.5% of these cells, Roquin-1 remained co-localized with Rck (Figure 21, lower panel).

This demonstrated that Roquin-1 primarily localized to P bodies, but could translocate into stress granules, if the cell was subjected to stress. It had also been shown that Roquin-1 directly interacted with Rck to induce the decay of its mRNA target [149]. As both Roquin-1 and Roquin-2 can bind RNA and are similarly expressed in different tissues, we asked whether Roquin-2 was also restricted to P bodies. Indeed, co-localization of Roquin-1 and Roquin-2 could be demonstrated by overexpression studies in A549 cells [150]. Furthermore it was shown that there was no difference in the localization of Roquin-1, Roquin-1^{san} and Roquin-2 [155]. Though Athanasopoulos et al. described localization of these proteins to stress granules instead of P bodies, this could be explained by the transient transfection systems they used, which tended to induce cell stress.

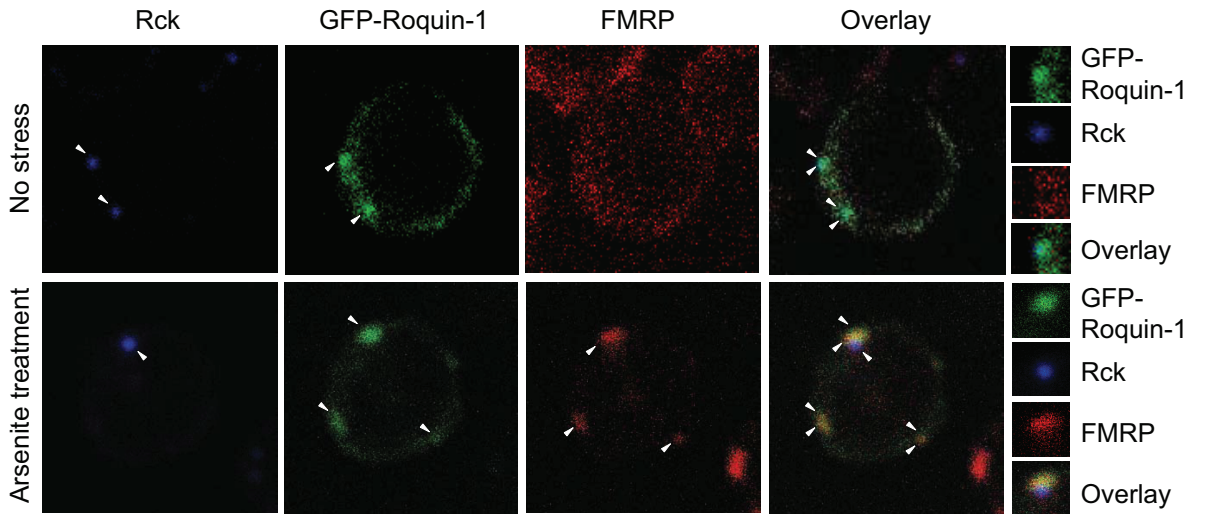

Figure 21: Roquin-1 co-localizes with Rck in P bodies. Confocal microscopy showing co-localization of Rck (blue) and FMRP (red) with GFP-tagged wild-type Roquin-1 (GFP-Roquin-1; green) in primary CD4$^+$ T cells. Cells were stimulated for 48 h with plate-bound anti-CD3 and anti-CD28 antibodies and treated with (Arsenite treatment) or without (No stress) arsenite. White arrowheads indicate Rck-, GFP- and FMRP-marked foci, respectively. Zoom (far right) shows selective enlargement of the images on the left. Original magnification: x23 (main images) or x262 (enlarged images).

8.2.3 Evaluation of the complete Roquin-2 knockout

To evaluate the function of Roquin-2 *in vivo*, conditional knockout mice were obtained with targeting exon 4 of *Rc3h2*. Targeting was confirmed by Southern blotting using standard procedures (EUCOMM mouse IKMC Project - ID: 30078, Figure 22 A–C).

The complete absence of Roquin-2 was assessed by immunoblotting. For this, MEF cells were generated from crossings of mice with an *Rc3h2*$^{+/neo}$ genotype to obtain wild-type *Rc3h2*$^{+/+}$, heterozygous *Rc3h2*$^{+/neo}$ or *Rc3h2*-deficient *Rc3h2*$^{neo/neo}$ MEF cells (Figure 22 D). The neomycin cassette (Neo) with a polyadenylation signal in the Roquin-2 targeting vector already created a null allele and completely eliminated Roquin-2 protein. The absence of Roquin-2 in *Rc3h2*$^{neo/neo}$ MEF cells could even be demonstrated by intracellular FACS staining with the 3F12 antibody (described in section 8.2.1), which recognized both Roquin-1 and -2 in wild-type or only Roquin-1 in *Rc3h2*$^{neo/neo}$ MEF cells (Figure 22 E).

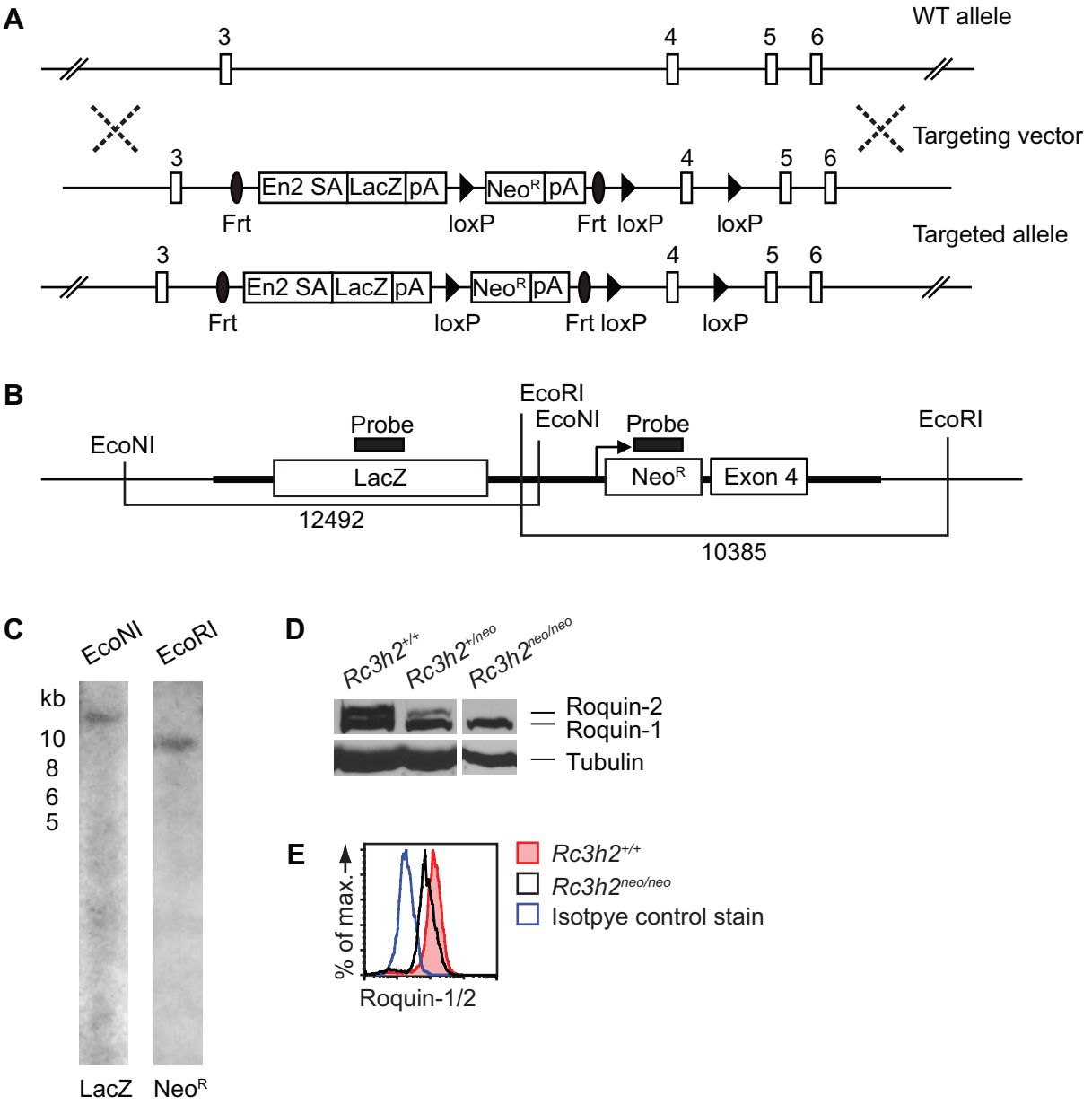

Figure 22: Targeting strategy of the *Rc3h2* allele. (A) Schematic representation of the gene-targeting construct. (B) Position of the restriction sites used to validate the *Rc3h2* gene-targeting. (C) Southern blot analysis showing the conversion to the *Rc3h2*$^{tm1a(KOMP)Wtsi}$ allele by using a probe to LacZ (left panel) and Neo^R (right panel) after digestion with the indicated restriction enzymes (top). The genomic restriction sites are adjacent to the targeting vector arms. Expected sizes: 5' EcoNI (12492 bp) and 3' EcoRI (10385 bp). Southern blots were performed by Dr. Joel Schick, Institute of Developmental Genetics, Helmholtz Zentrum München. (D) Western blot analysis of Roquin-2 and tubulin expression in *Rc3h2*$^{+/+}$, *Rc3h2*$^{+/neo}$ and *Rc3h2*$^{neo/neo}$ immortalized MEF cells. (E) Intracellular FACS staining of Roquin-1/2 proteins with the 3F12 antibody described in section 8.2.1 in MEF cells of the indicated genotype. Wild-type cells were also stained with an isotype control antibody.

Having confirmed correct targeting of *Rc3h2*, the consequences of Roquin-2 deficiency were investigated. The most obvious phenotype in *Rc3h2*$^{neo/neo}$ mice on a pure C57BL/6 background was postnatal death. Though postnatal death in *Rc3h2*-deficient mice was clearly a non-redundant phenotype, *Rc3h1*-deficient mice similarly exhibited early death, only several hours after birth [120]. The exact cause of death in *Rc3h2*$^{neo/neo}$ mice, however, could not be resolved yet. As lethality in *Rc3h1*-deficient mice could partially be rescued on an outbred strain genetic background, a similar strategy was used to rescue death in *Rc3h2*$^{neo/neo}$ mice. The higher genetic variance in mixed C57BL/6–NMRI-outbred strain mice was assumed to allow for compensatory mechanisms. Indeed, the viability of homozygous *Rc3h2*-deficient animals was restored in one single cross with mice from an NMRI outbred strain genetic background and a subsequent intercross of the F1 generation. The offspring was born at a Mendelian ratio and survived until weaning age (P21) and longer (Figure 23 A). Physically, the mice appeared normal, with decreased body weight only seen in male individuals. This difference in weight constituted 24–29% at each point of measure starting at day 1 after birth up to adulthood (Figure 23 B).

A

Age	#	*Rc3h2*$^{+/+}$ (NMRI)	*Rc3h2*$^{+/neo}$ (NMRI)	*Rc3h2*$^{neo/neo}$ (NMRI)
P21	58	16 (27.6%)	30 (51.7%)	12 (20.7%)

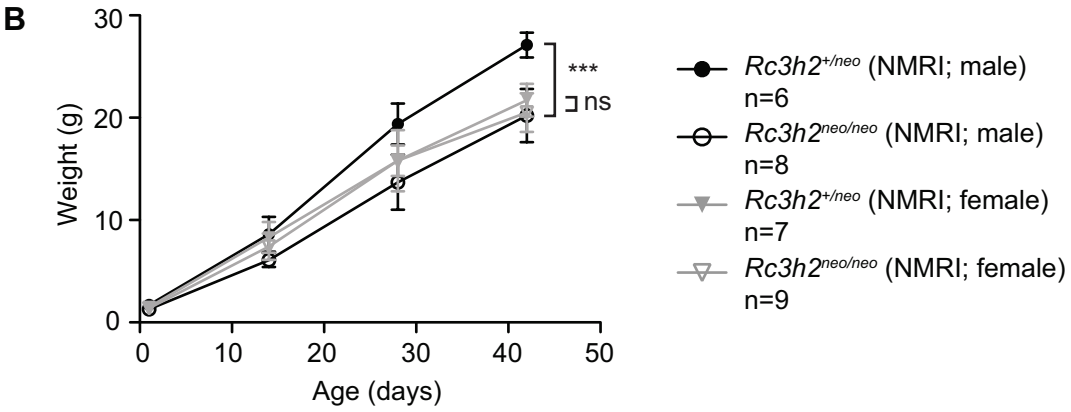

Figure 23: Crossing *Rc3h2*$^{neo/neo}$ mice to an NMRI outbred strain background rescues lethality. (A) Genotype frequency of offspring from a heterozygous mating of *Rc3h2*$^{+/neo}$ mice on an NMRI outbred strain background. (B) Body weight curve of male or female *Rc3h2*$^{+/neo}$ and *Rc3h2*$^{neo/neo}$ mice on an NMRI outbred strain background. Weight reduction in male *Rc3h2*$^{neo/neo}$ mice was already significant at each point of measure starting at day 1 after birth. Statistical significances were calculated by Student's t-test (*p < 0.001).**

Surprisingly, further analysis of these mice did not reveal an obvious immune phenotype. There was no difference in total splenocyte (Figure 24 A) or thymocyte (Figure 24 B) numbers between *Rc3h2* knockout, heterozygous or wild-type (WT) mice on a mixed background.

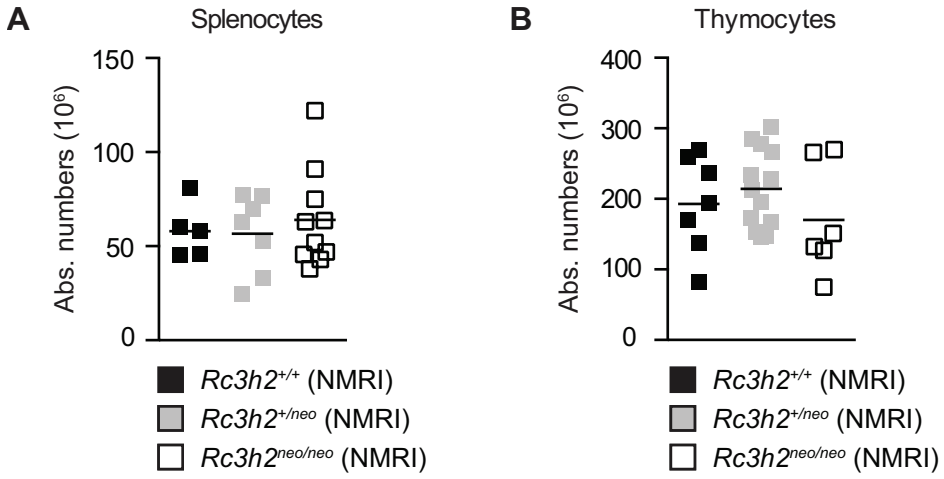

Figure 24: Splenocyte and thymocyte numbers are normal in *Rc3h2*$^{neo/neo}$ (NMRI) mice. (A) Splenocyte numbers in mice with the indicated phenotypes. (B) To count thymocyte numbers, littermate mice with the indicated phenotypes were analyzed at an age of three weeks. The bar represents the mean value in each group.

Additionally, different lymphocyte subsets were investigated. However, no abnormalities could be found in populations of $CD4^+$, $CD8^+$, Treg, B, NK, NKT or dendritic cells as well as in eosinophils, neutrophils and macrophages (Table 20). This clearly shows the importance of genetic variation. Introducing new alleles of various genes into *Rc3h2*-deficient C57BL/6 mice was sufficient to rescue death and possible immune cell phenotypes.

Table 20: Phenotyping of *Rc3h2*$^{neo/neo}$; NMRI mice. Absolute cell numbers with standard deviation of various cell types from *Rc3h2*$^{+/+}$, *Rc3h2*$^{+/neo}$ and *Rc3h2*$^{neo/neo}$ mice, which were all bred to an NMRI outbred strain to rescue lethality. Statistical significances were calculated by one-way analysis of variance (ANOVA).

	Rc3h2$^{+/+}$ (NMRI) (n=5)	*Rc3h2*$^{+/neo}$ (NMRI) (n=7)	*Rc3h2*$^{neo/neo}$ (NMRI) (n=10)	p value (one-way ANOVA)	Significance
CD4$^+$ T cells (CD4$^+$)	7.8*10^6 ±3.9*10^6	7.3*10^6 ±4.4*10^6	6.4*10^6 ±2.1*10^6	0.7305	ns
CD8$^+$ T cells (CD8$^+$)	3.0*10^6 ±1.6*10^6	2.6*10^6 ±1.1*10^6	2.3*10^6 ±1.0*10^6	0.5164	ns
Treg (CD4$^+$ Foxp3$^+$)	9.8*10^5 ±2.7*10^5	9.0*10^5 ±4.2*10^5	9.2*10^5 ±2.8*10^5	0.9104	ns
B cells (B220$^+$)	7.0*10^6 ±3.2*10^6	8.1*10^6 ±4.6*10^6	8.9*10^6 ±3.7*10^6	0.6707	ns
NKT (B220$^-$ TCRβ^{int} CD1d-PBS57$^+$)	4.4*10^5 ±3.0*10^5	5.0*10^5 ±3.3*10^5	4.0*10^5 ±2.1*10^5	0.7489	ns
NK (B220$^-$ CD3$^-$ NK1.1$^+$)	6.4*10^5 ±6.1*10^5	11.1*10^5 ±7.5*10^5	9.2*10^5 ±8.3*10^5	0.5876	ns
DC (CD11c$^+$ MHCII$^+$)	3.3*10^5 ±1.8*10^5	3.4*10^5 ±2.0*10^5	4.0*10^5 ±1.7*10^5	0.7212	ns
Eosinophils (SiglecF$^+$ GR-1^{int})	2.1*10^5 ±0.9*10^5	1.8*10^5 ±0.7*10^5	3.1*10^5 ±1.7*10^5	0.1336	ns
Neutrophils (SiglecF$^-$ GR-1^{hi} F4/80$^-$)	11.4*10^5 ±13.0*10^5	8.6*10^5 ±5.7*10^5	9.6*10^5 ±3.6*10^5	0.8052	ns
Macrophages (SiglecF$^-$ GR-1^{int} F4/80^{hi})	1.4*10^6 ±0.8*10^6	1.4*10^6 ±0.8*10^6	1.8*10^6 ±0.8*10^6	0.4147	ns

8.2.4 Conditional Roquin-2 knockout in T cells

As the mixed C57BL/6–NMRI-outbred strain genetic background might disguise immune phenotypes, Roquin-2 was conditionally deleted in T cells on a pure C57BL/6 background using CD4-Cre recombinase. The CD4-Cre recombinase is expressed as soon as CD4 is switched on in T cells. This occurs early in TCRαβ thymocyte development upon the transition of DN to DP thymocytes. Although the *CD4* gene is silenced in immature DN thymocytes, the CD4 enhancer and promoter are already active in the DN3 precursor stage [160]. This implies that CD8$^+$ cells were also devoid of Roquin-2 in *Rc3h2*$^{fl/fl}$*; CD4-Cre* mice, while the *CD4* gene was later on silenced again in this lineage.

Roquin-2 protein expression was completely absent in peripheral CD4$^+$ T cells from conditionally targeted mice and already reduced in total thymocytes. In wild-type peripheral T cells and thymocytes, Roquin-2 was typically lower expressed than Roquin-1 (Figure 25 A).

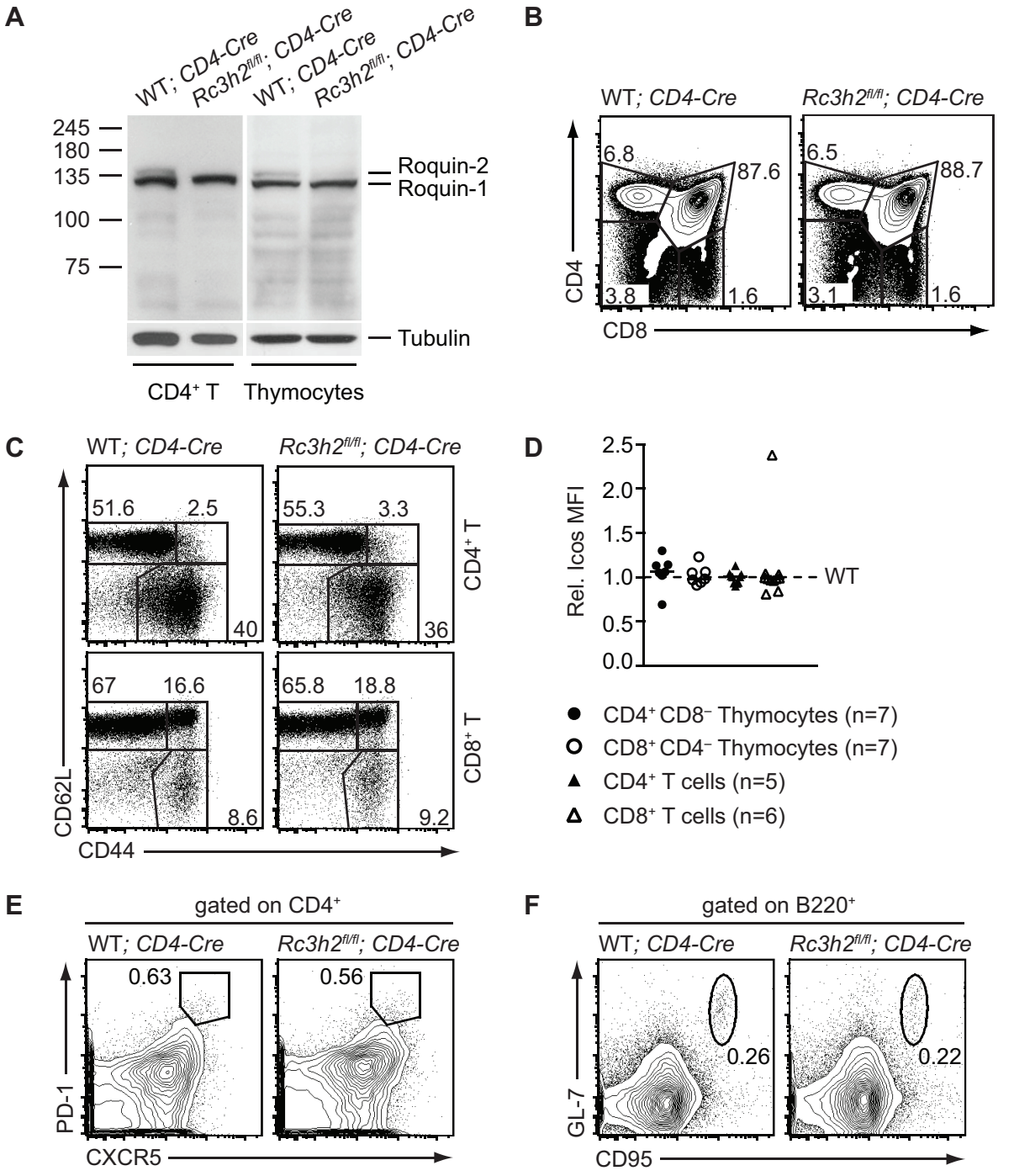

Figure 25: Deletion of Roquin-2 in T cells does not affect T cell development and activation or Icos levels. (A) Western blot analysis of Roquin-1 and Roquin-2 expression in CD4$^+$ T cells (left) or thymocytes (right). Representative contour plots showing the frequencies of CD4$^+$ or CD8$^+$ thymocytes (B) or the activation status of peripheral CD4$^+$ or CD8$^+$ T cells (C). (D) Relative median fluorescence intensity (MFI) of Icos in CD4$^+$ CD8$^-$ or CD8$^+$ CD4$^-$ thymocytes or peripheral T cells from *Rc3h2$^{fl/fl}$; CD4-Cre* mice, normalized to the ICOS MFI in wild-type; *CD4-Cre* mice. The bar represents the median value of each column. (E–F) Representative contour plots of follicular helper T cells (PD-1^{hi} CXCR5^{hi}), pre-gated on CD4$^+$ B220$^-$ (E) or germinal center B cells (GL-7^{hi} CD95^{hi}), pre-gated on B220$^+$ (F) splenocytes. Genotypes are indicated in the figure and data are representative for 3 (A) independent experiments or 10 (B), 12 (C) and 5 (E–F) individual mice per genotype.

Infrared imaging quantification revealed that Roquin-1 protein was expressed 5 times more (5.3 ± 0.5 SD) than Roquin-2 in peripheral $CD4^+$ T cells. Despite the fact that thymocytes had already reduced Roquin-2 levels, thymus development occurred normal in respect to absolute number and percentage of T cell populations (Figure 25 B). Furthermore, there was no defect in the development of peripheral T cells. Percentage and absolute number of naive ($CD62L^{hi}$ $CD44^{lo}$), effector-like ($CD62L^{lo}$ $CD44^{hi}$) and memory-like ($CD62L^{hi}$ $CD44^{hi}$) T cells was not altered (Figure 25 C). This is in contrast to *Rc3h1*$^{fl/fl}$*; CD4-Cre* T cells showing highly enhanced effector-like $CD8^+$ T cells [120]. These animals also displayed increased Icos levels on T cells, which could not be observed in *Rc3h2*-deficient thymocytes or peripheral T cells (Figure 25 D). The percentage of follicular helper T cells as well as germinal center B cells was also not altered (Figure 25 E–F). Altogether, no abnormal T cell phenotypes and no signs of autoimmunity could be detected, revealing any role for Roquin-2.

8.2.5 Conditional Roquin-2 knockout in the hematopoietic system

Because the ablation of Roquin-2 in T cells did not reveal an immunological phenotype, Roquin-2 was deleted in the hematopoietic system using Vav-Cre recombinase. Deleting Roquin-2 in hematopoietic cells might reveal a new function of Roquin-2 in other cell types. However, similar to complete absence of Roquin-2 in mice with mixed C57BL/6–NMRI background, there was no significant change in total splenocyte (Figure 26 A) or thymocyte (Figure 26 B) numbers.

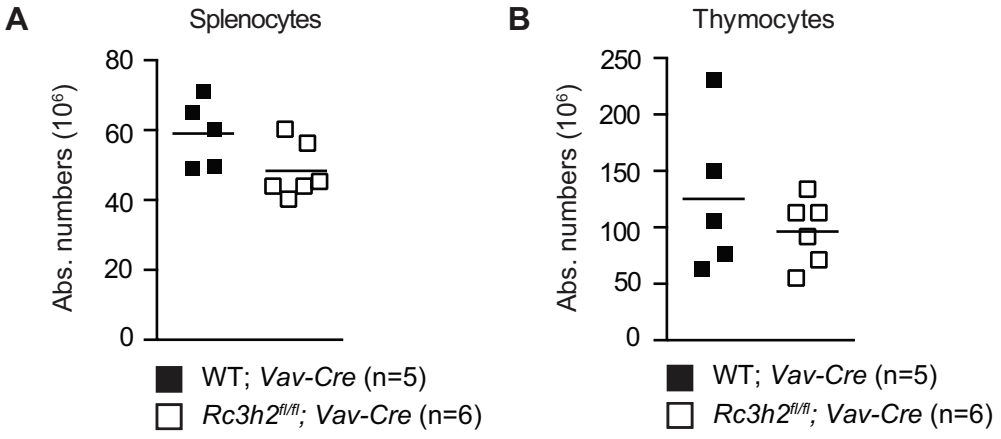

Figure 26: Splenocyte (A) and thymocyte (B) numbers are not significantly altered in *Rc3h2*$^{fl/fl;}$ *Vav-Cre* mice compared to wild-type controls (WT; *Vav-Cre*). The bar represents the mean value of each column.

Furthermore, cell subsets defined by CD4, CD8, B, NK, NKT or dendritic cell markers as well as markers for eosinophils, neutrophils and macrophages did not reveal differences in frequency of absolute cell numbers (Table 21).

Table 21: Phenotyping of *Rc3h2$^{fl/fl}$; Vav-Cre* mice. Absolute cell numbers with standard deviation of various cell types from *Rc3h2$^{fl/fl}$; Vav-Cre* and WT; *Vav-Cre* mice. Statistical significances were calculated by Student's t-test (p < 0.01).**

	WT; *Vav-Cre* (n=5)	*Rc3h2$^{fl/fl}$; Vav-Cre* (n=6)	p value (Student's t-test)	Significance
$CD4^+$ T cells ($CD4^+$)	$7.76*10^6$ $1.48*10^6$	$5.77*10^6$ $1.87*10^6$	0.0669	ns
$CD8^+$ T cells ($CD8^+$)	$4.21*10^6$ $0.27*10^6$	$3.94*10^6$ $1.02*10^6$	0.5346	ns
Treg ($CD4^+$ $Foxp3^+$)	$11.0*10^5$ $1.61*10^5$	$7.15*10^5$ $1.65*10^5$	0.0026	**
B cells ($B220^+$)	$22.5*10^6$ $5.65*10^6$	$17.4*10^6$ $5.44*10^6$	0.1334	ns
NKT ($B220^-$ $TCR\beta^{int}$ CD1d-$PBS57^+$)	$2.69*10^5$ $0.72*10^5$	$2.36*10^5$ $0.63*10^5$	0.3295	ns
NK ($B220^-$ $CD3^-$ $NK1.1^+$)	$8.06*10^5$ $4.09*10^5$	$7.02*10^5$ $2.93*10^5$	0.6444	ns
DC ($CD11c^+$ $MHCII^+$)	$5.16*10^5$ $2.15*10^5$	$3.66*10^5$ $1.36*10^5$	0.1504	ns
Eosinophils ($SiglecF^+$ $GR\text{-}1^{int}$)	$3.33*10^5$ $1.93*10^5$	$3.20*10^5$ $1.67*10^5$	0.9675	ns
Neutrophils ($SiglecF^-$ $GR\text{-}1^{hi}$ $F4/80^-$)	$6.84*10^5$ $3.84*10^5$	$7.03*10^5$ $2.88*10^5$	0.9632	ns
Macrophages ($SiglecF^-$ $GR\text{-}1^{int}$ $F4/80^{hi}$)	$5.74*10^5$ $2.74*10^5$	$7.48*10^5$ $2.80*10^5$	0.4015	ns

Interestingly, peripheral Treg cell numbers were significantly decreased in *Rc3h2$^{fl/fl}$; Vav-Cre* mice (Table 21 and Figure 27 A). This reduction in Treg cell numbers is most likely an indirect effect as Treg cells appeared unaltered in *Rc3h2$^{fl/fl}$; CD4-Cre* mice (Figure 27 B). Furthermore, it contrasts the elevated Treg cell numbers in *Rc3h1$^{fl/fl}$; CD4-Cre* mice [120]. However, as this research project primarily focuses on Roquin-1/2 function in T cells, it remains to be elucidated which cell population is responsible for altered Treg cell numbers and what the functional consequences might be.

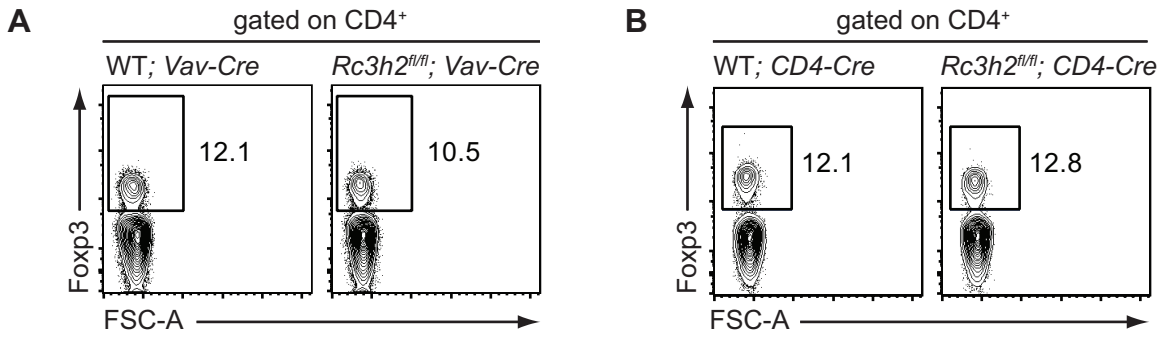

Figure 27: Frequencies of peripheral Treg cells in *Rc3h2*-deficient cells. (A–B) Representative contour plots of peripheral Treg cells, pre-gated on CD4$^+$ splenocytes from mice deficient for Roquin-2 in hematopoietic cells (A) or T cells (B). Genotypes are indicated in the figure and data are representative for 5 (A, wild-type) and 6 (A, knockout) as well as 2 (B) individual mice per genotype.

8.2.6 Conditional knockout of Roquin-1 and Roquin-2 in T cells resembles phenotypes of the *Rc3h1$^{san/san}$* mouse

Until now, it had not been answered why the *Rc3h1$^{san/san}$* mouse developed such a severe autoimmune disease, while mice deficient for Roquin-1 in T, B and hematopoietic cells display only a mild immune deregulation. Likewise, mice deficient for Roquin-2 in T and hematopoietic cells do not show a significant phenotype at all. Although the san mutation affects all cells in the mouse, some phenotypes such as the activation of T cells and de-repression of Icos were T cell intrinsic [39]. Therefore, T cell-specific ablation of Roquin-1 and Roquin-2 together was chosen to investigate functional redundancy of both paralogs. Complete absence of Roquin-1 and Roquin-2 protein was shown in T cell extracts from *Rc3h1$^{fl/fl}$; Rc3h2$^{fl/fl}$; CD4-Cre* (*Rc3h1/2$^{fl/fl}$; CD4-Cre*) mice (Figure 28 A). Interestingly, all *Rc3h1/2$^{fl/fl}$; CD4-Cre* mice developed splenomegaly and lymphadenopathy (Figure 28 B), already at an age of four weeks. Spleens increased in weight and total splenocyte numbers (Figure 28 C).

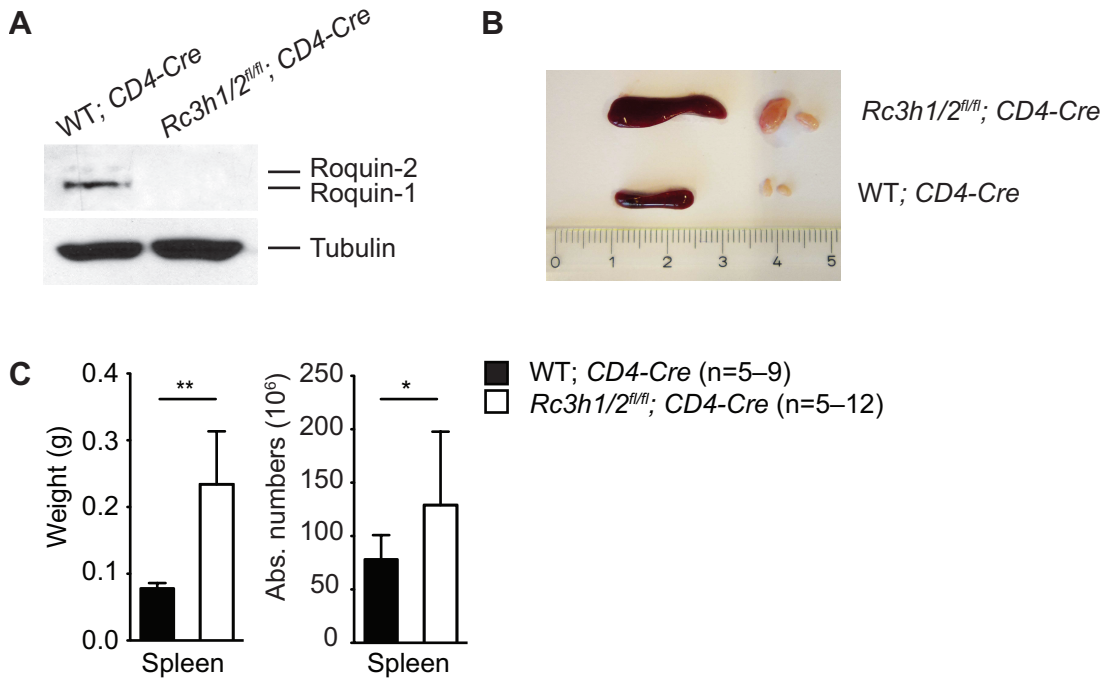

Figure 28: Combined deficiency of Roquin-1/2 in T cells causes splenomegaly and lymphadenopathy. (A) Western blot analysis confirming the ablation of Roquin-1 and Roquin-2 in CD4$^+$ T cells. Tubulin was used as a loading control. (B) Spleen (left) and lymph node (right) sizes. (C) Mean splenic weight (left graph) and mean splenocyte number (right graph). Genotypes are indicated in the figure and data are representative for four (A) independent experiments. Significances are calculated by Student's t-test (*p < 0.05; **p < 0.01). (B–C) Data were collected in cooperation with Dr. Stephanie Edelmann.

Analyzing the T cell compartment by flowcytometry, it was observed that all T cells were highly activated. CD4$^+$ T cells displayed an increased frequency of effector-like (CD44^{hi} CD62L^{lo}) T cells. This was even exacerbated in CD8$^+$ T cells, which lacked almost all naive (CD62L^{hi} CD44^{lo}) T cells and had a reduced frequency of memory-like (CD62L^{hi} CD44^{hi}) T cells. Furthermore, there was a reduction in absolute numbers of total CD4$^+$ T cells as well as naive CD4$^+$ and CD8$^+$ T cells and a significant increase in CD8$^+$ effector-like T cells (Figure 29 A–B). The phenotype of *Rc3h1/2*-deficient mice exceeded that of *Rc3h1$^{fl/fl}$; CD4-Cre* mice by far. Importantly, Roquin-1 and Roquin-2 expression levels were similar in CD4$^+$ and CD8$^+$ T cells and Roquin-2 was not altered in *Rc3h1*-deficient CD4$^+$ or CD8$^+$ T cells (Figure 29 C). Furthermore, peripheral regulatory T cells exhibited a marked increase in frequency, although absolute numbers were normal presumably due to the overall reduction in CD4$^+$ T cells (Figure 29 D). The increase in effector-like CD4$^+$ and especially CD8$^+$ T cells resembles prominent phenotypes of the *Rc3h1$^{san/san}$* mouse. Furthermore, *Rc3h1/2$^{fl/fl}$; CD4-Cre* as well

as *Rc3h1*$^{san/san}$ mice develop splenomegaly and lymphadenopathy. Altogether, these data suggest functional redundancy of Roquin-1 and Roquin-2.

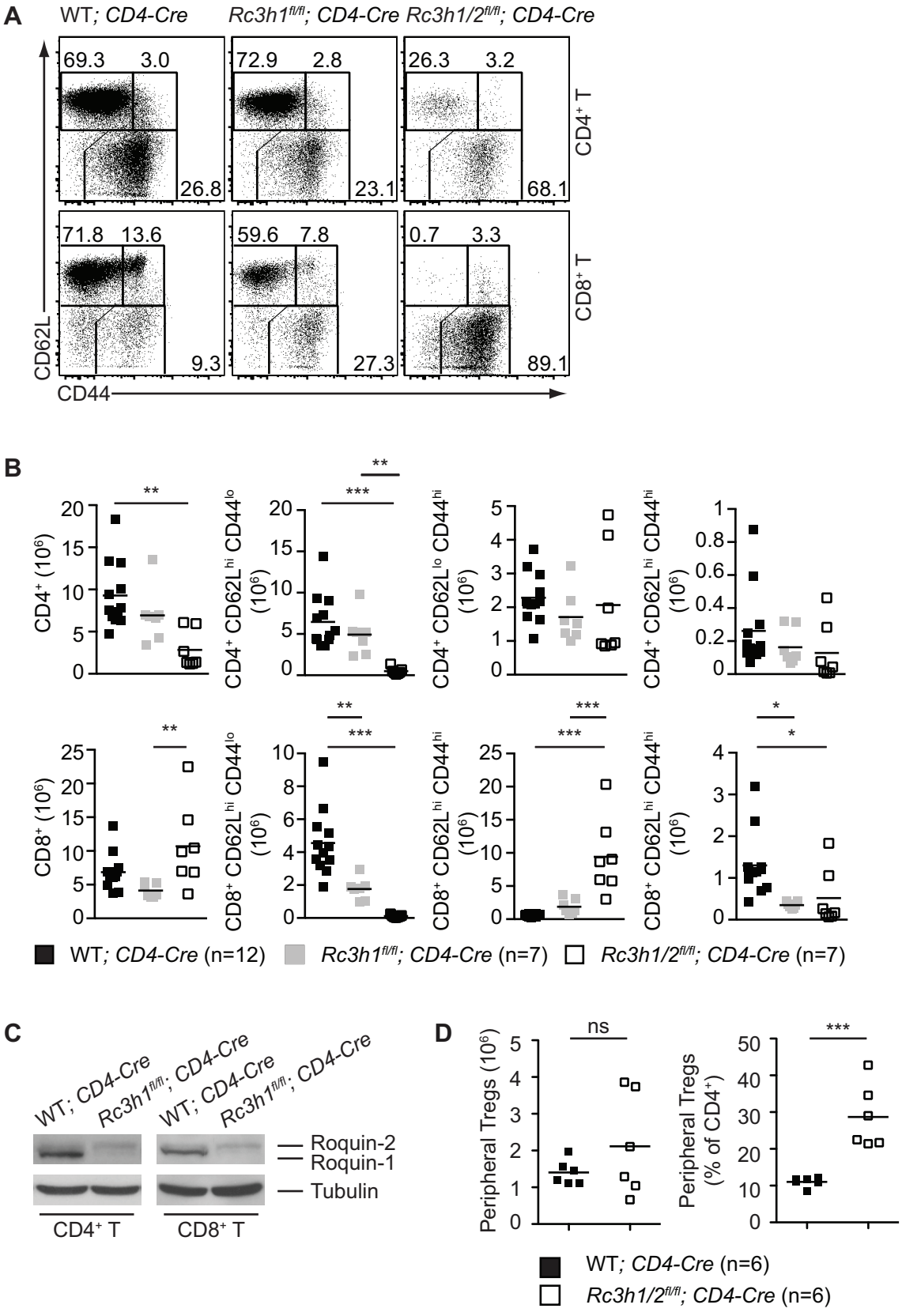

Figure 29: Combined ablation of Roquin-1 and Roquin-2 in T cells reveals functional redundancy. Representative contour plots (A) and corresponding cells numbers (B) from CD4$^+$ (upper panel) or CD8$^+$ (lower panel) T cells, showing CD62L^{hi} CD44^{lo}, CD62L^{lo} CD44^{hi} or CD62L^{hi} CD44^{hi} T cells from spleen. (C) Western blot analysis of Roquin-1 and Roquin-2 expression levels in CD4$^+$ (left) or CD8$^+$ (right) T cells. (D) Absolute cell number (left panel) or percentage (of CD4$^+$ T cells, right panel) of peripheral Treg cells (CD4$^+$ Foxp3$^+$). Genotypes are indicated in the figure and data are representative for two (C) independent experiments. The number of mice analyzed in (A) is indicated in (B). Statistical significances were calculated by Tukey's multiple comparisons test (B) or Student's t-test (D) (*p < 0.05; **p < 0.01; ***p < 0.001). (B, D) The bar represents the mean value of each column. (A–B, D) Data were collected in cooperation with Dr. Stephanie Edelmann and the Western blot (C) was developed with help of Claudia Lohs.

8.2.7 Roquin-1 and Roquin-2 both repress ICOS mRNA

A hallmark of the autoimmune disease in *Rc3h1*$^{san/san}$ mice was elevated Icos levels on all T cells. Analysis of Icos levels in *Rc3h1/2* double-deficient mice showed increased Icos expression on all CD4$^+$ and CD8$^+$ T cells. Icos protein levels were highest on effector-like (CD44^{hi} CD62L^{lo}) CD4$^+$ or CD8$^+$ T cells (Figure 30 A–B).

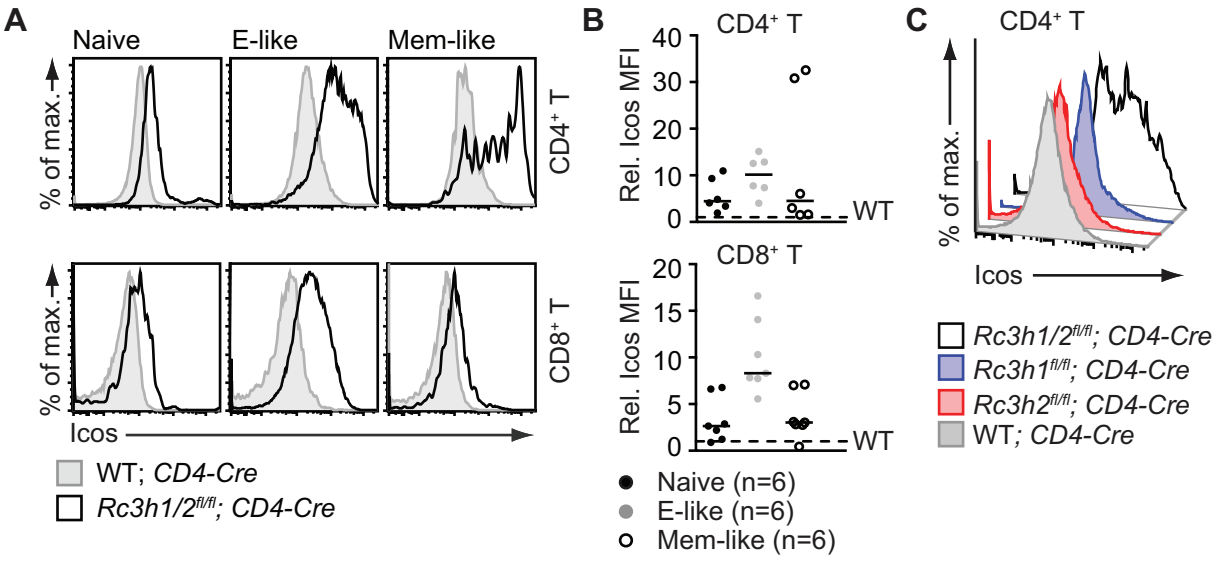

Figure 30: Icos levels are extremely elevated in *Rc3h1/2$^{fl/fl}$; CD4-Cre* mice. Representative histograms (A) and relative median fluorescence intensity (MFI) (B) of Icos in naive (CD62L^{hi} CD44^{lo}), E-like (CD62L^{lo} CD44^{hi}) or Mem-like (CD62L^{hi} CD44^{hi}) CD4$^+$ (upper panel) or CD8$^+$ (lower panel) T cells from *Rc3h1/2$^{fl/fl}$; CD4-Cre* mice, each compared to an equal number of wild-type; *CD4-Cre* animals. The bar represents the median value of each column. (C) Histogram overlay of Icos levels on CD4$^+$ T cells. Genotypes are indicated in the figure and data are representative for six (A) and two (C) independent experiments. Data were collected in collaboration with Dr. Stephanie Edelmann.

Interestingly, Icos levels were massively enhanced in double knockout $CD4^+$ T cells compared to Roquin-1-single knockout cells [120]. Expression levels seemed even higher than in the *Rc3h1*$^{san/san}$ mouse [39]. *Rc3h2*-deficient cells showed normal wild-type levels of Icos expression (Figure 30 C).

This difference in Icos expression between *Rc3h1*-deficient and *Rc3h1/2* double-deficient mice could be explained by functional redundancy of both paralogs or by an indirect negative effect of Roquin-2. To address this question, biochemical analyses investigated and compared the molecular mechanism of Roquin-1 and Roquin-2. As shown in section 8.1, both proteins had a general binding affinity to RNA, but showed a specific binding preference for the 3'UTR of ICOS mRNA. Indeed, Roquin-1 and Roquin-2 exhibited an identical binding behavior to the ICOS mRNA, inferred from the upshifting RNA band (Figure 16).

In addition, direct repression of Icos expression was investigated by overexpressing Roquin-1 wild-type (WT), an inactive version of Roquin-1 (aa 1–509) and two different isoforms of Roquin-2 (aa 1–1125 and 1–1187). To achieve sufficient overexpression of both proteins in $CD4^+$ T cells, mice were generated bearing a truncated human CAR on $CD4^+$ T cells (Heger and Schmidt-Supprian, unpublished). The CAR was only expressed after Cre-mediated recombination of a floxed stop-cassette. To reduce endogenous protein backgrounds, $CD4^+$ T cells were isolated from *Rc3h1*$^{fl/fl}$*; CAG-CAR*$^{stop\text{-}fl}$*; CD4-Cre* mice and transduced with adenovirus encoding the indicated proteins. Roquin-1/2 protein expression was analyzed by intracellular staining with a Roquin-1/2 specific antibody (clone 3F12). Icos levels were repressed by Roquin-1 wild-type and both isoforms of Roquin-2, but not by the inactive version of Roquin-1 (aa 1–509) (Figure 31 A–B).

Furthermore, Roquin-1 had been demonstrated to interact with factors of the mRNA decapping pathway, such as Edc4 [149]. Immunoprecipitation experiments revealed that both proteins could independently and equally interact with Edc4 in MEF cell extracts deficient for Roquin-1 or Roquin-2. In extract from wild-type MEF cells, Edc4 was immunoprecipitated approximately twice as efficiently as in single-deficient cells. In double-deficient MEF cells, no Edc4 was immunoprecipitated by anti-Roquin-1/2 antibodies (Figure 31 C).

In summary, both proteins could independently bind to a *cis*-element in the 3'UTR of ICOS mRNA and repressed Icos expression after overexpression on $CD4^+$ T cells. They furthermore both interacted with Edc4, which is involved in mRNA decay. Therefore, Roquin-1 and Roquin-2 exhibited identical molecular characteristics, suggesting that they may function redundantly in guiding target mRNAs to the decapping pathway and inducing their decay.

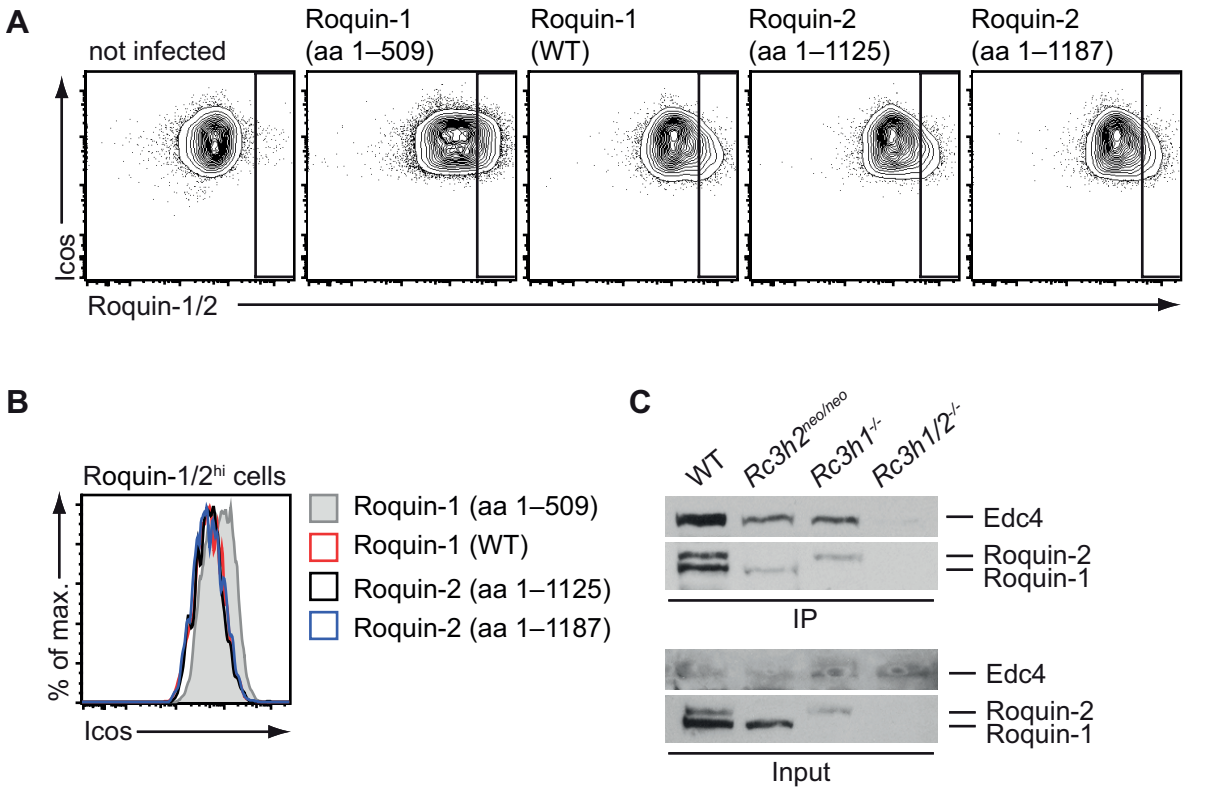

Figure 31: Roquin-1 and Roquin-2 proteins interact with Edc4 protein and redundantly regulate Icos expression. (A) Adenoviral transduction of CD4$^+$ T cells from *Rc3h1$^{fl/fl}$; CAG-CAR$^{stop-fl}$; CD4-Cre* mice with adenovirus encoding an inactive Roquin-1 (aa 1–509), Roquin-1 wild-type (WT) or two isoforms of Roquin-2 (aa 1–1125 or aa 1–1187). (B) shows a histogram overlay of Roquin-1/2^{hi} cells gated in (A). All blots in (A–B) are pre-gated on CAR$^+$ cells. (C) Immunoprecipitation (IP) with magnetic beads coupled to an antibody, which recognizes both Roquin-1 and Roquin-2, of protein extracts from MEF cells. Edc4, Roquin-1 and Roquin-2 proteins were detected by Western blot analysis in IP and input. Genotypes are indicated in the figure and data are representative of three (A–B) and two (C) independent experiments. (C) IP was performed by Christine Wolf.

8.2.8 *Rc3h1/2*-deficient mice show increased follicular helper T and germinal center B cells, but no auto-antibodies

Similar to the *Rc3h1$^{san/san}$* mouse, *Rc3h1/2*-deficient mice showed an increased frequency and number of follicular helper T cells, characterized by CXCR5^{hi} and PD-1^{hi} (Figure 32 A–B). Interestingly, double-deficient CD4$^+$ T cells showed an overall increase in PD-1 expression, indicating either that more cells are about to adopt a Tfh cell phenotype or that the T cells are overall more activated (Figure 32 A, left). The functionality of CXCR5^{hi} PD-1^{hi} cells was further evaluated by staining the Tfh cell transcription factor Bcl6 (Figure 32 A, right).

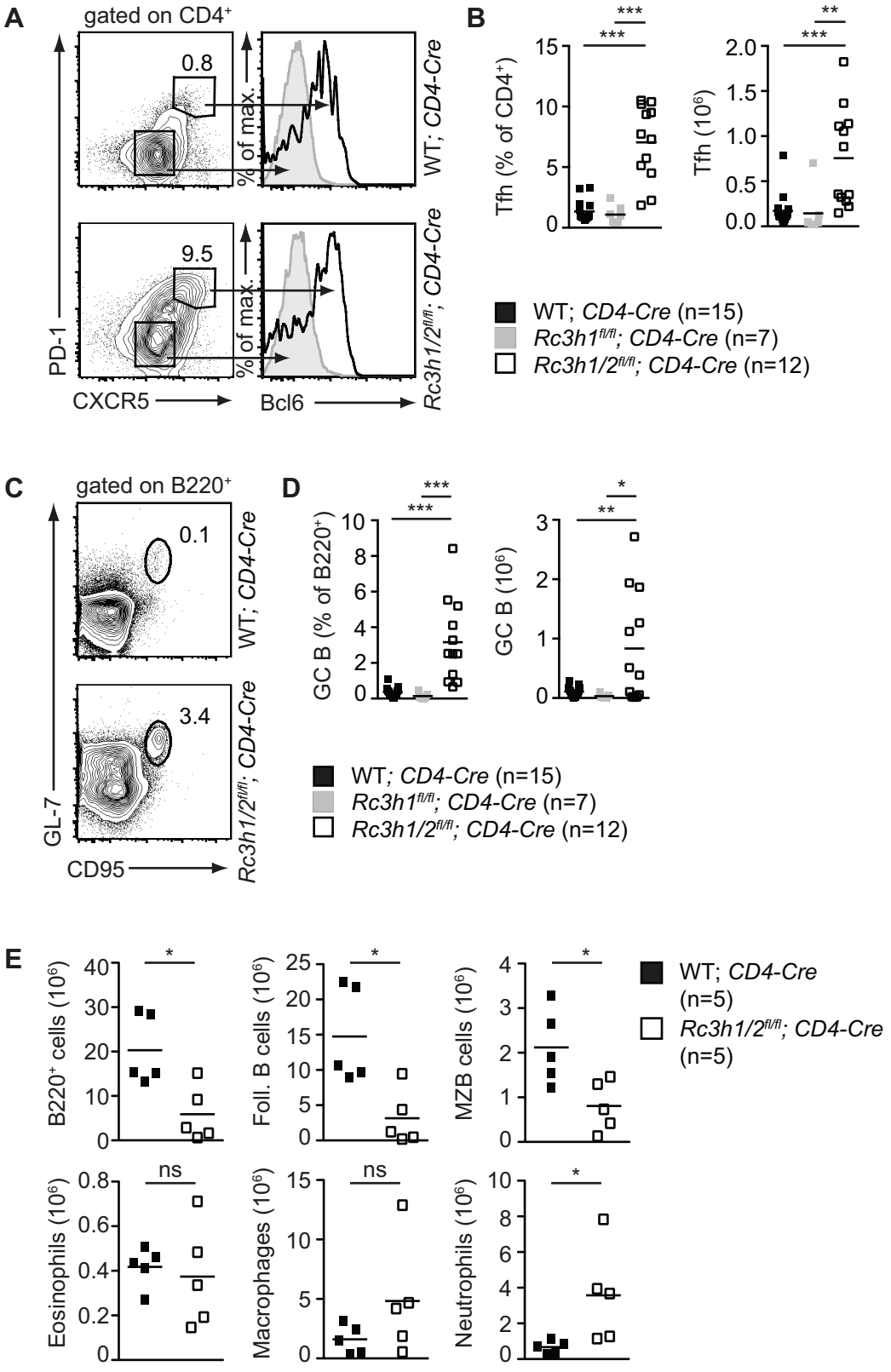

Figure 32: Combined loss of Roquin-1 and Roquin-2 causes an increase in Tfh and GC B cells as well as immune dysregulation. (A) Representative contour plots of splenic Tfh cells (PD-1^{hi} CXCR5^{hi}), pre-gated on CD4^{+} with histogram overlays showing Bcl6 expression. (B) Percentage of Tfh cells (upper panel) or Tfh cell number (lower panel). (C) Representative contour plots of splenic germinal center B cells (GC B; GL-7^{hi} CD95^{hi}), pre-gated on B220^{+}. (D) Percentage of GC B cells (of B220^{+} cells, upper panel) or GC B

cell numbers (lower panel). (E) Cell numbers of various cell types. The bar represent the mean value of each column and statistical significances were calculated by Tukey's multiple comparisons test (B, D) or Student's t-test (E) (*p < 0.05; **p < 0.01; ***p < 0.001). Genotypes are indicated in the figure and data are representative for 12 mice per genotype (A, C). Data were collected in cooperation with Dr. Stephanie Edelmann.

Moreover, an increase in the frequency of germinal center B cells ($B220^+$ $GL\text{-}7^+$ $CD95^+$) was observed (Figure 32 C–D).

However, already in young *Rc3h1/2$^{fl/fl}$; CD4-Cre* mice, total B cell numbers were drastically reduced (Figure 32 E). Hence, marginal zone B cells (MZB; $B220^+$ $CD23^{int}$ $CD21/35^+$) and follicular B cells ($B220^+$ $CD23^{hi}$ $CD21/35^-$) were also decreased in cell numbers (Figure 32 E), accompanied by slightly increased neutrophil numbers. Eosinophils and macrophages were not significantly affected by Roquin-1/2 deficiency (Figure 32 E).

Despite the reduction in total B cells, the frequency and number of germinal center B cells was significantly increased (Figure 32 D). *Rc3h1/2*-deficient mice therefore reproduce one of the most important phenotypes of the *Rc3h1$^{san/san}$* mouse with elevated Tfh and GC B cell numbers. Surprisingly, however, no anti-nuclear antibodies (ANAs) could be detected in the serum of young (6 weeks) and old (>6 months) mice.

8.2.9 The spleen architecture in *Rc3h1/2*-deficient mice is massively disrupted

Analyzing spleen sections of *Rc3h1/2*-deficient mice revealed that the splenic architecture was massively disturbed (Figure 33 A). Only few $CD4^+$ T cells appeared to localize in a T cell zone of residual follicular structures, while $CD8^+$ T cells were distributed randomly. The reduction in B cell numbers became obvious and only few B cells could be found to support a follicle-like structure. Metallophilic macrophages ($MOMA\text{-}1^+$) no longer surrounded the follicle with a marginal zone and appeared dispersed (Figure 33 A). Furthermore, there was a strong reduction of white pulp, characterized by areas lacking $F4/80^+$ cells (Figure 33 B–C). Such severe alteration might be caused by defective interaction and signaling of lymphocytes with accessory cells in the spleen. Those cells influence lymphocyte differentiation as well as tissue organization [161]. $ER\text{-}TR7^+$ reticular fibroblasts, representing T cell supporting stroma cells, appeared more dispersed in *Rc3h1/2*-deficient cells than in wild-type cells (Figure 33 D). Follicular dendritic cells ($FDC\text{-}M1^+$) on the other side, seemed slightly reduced in number, but were still able to form a central network (Figure 33 E).

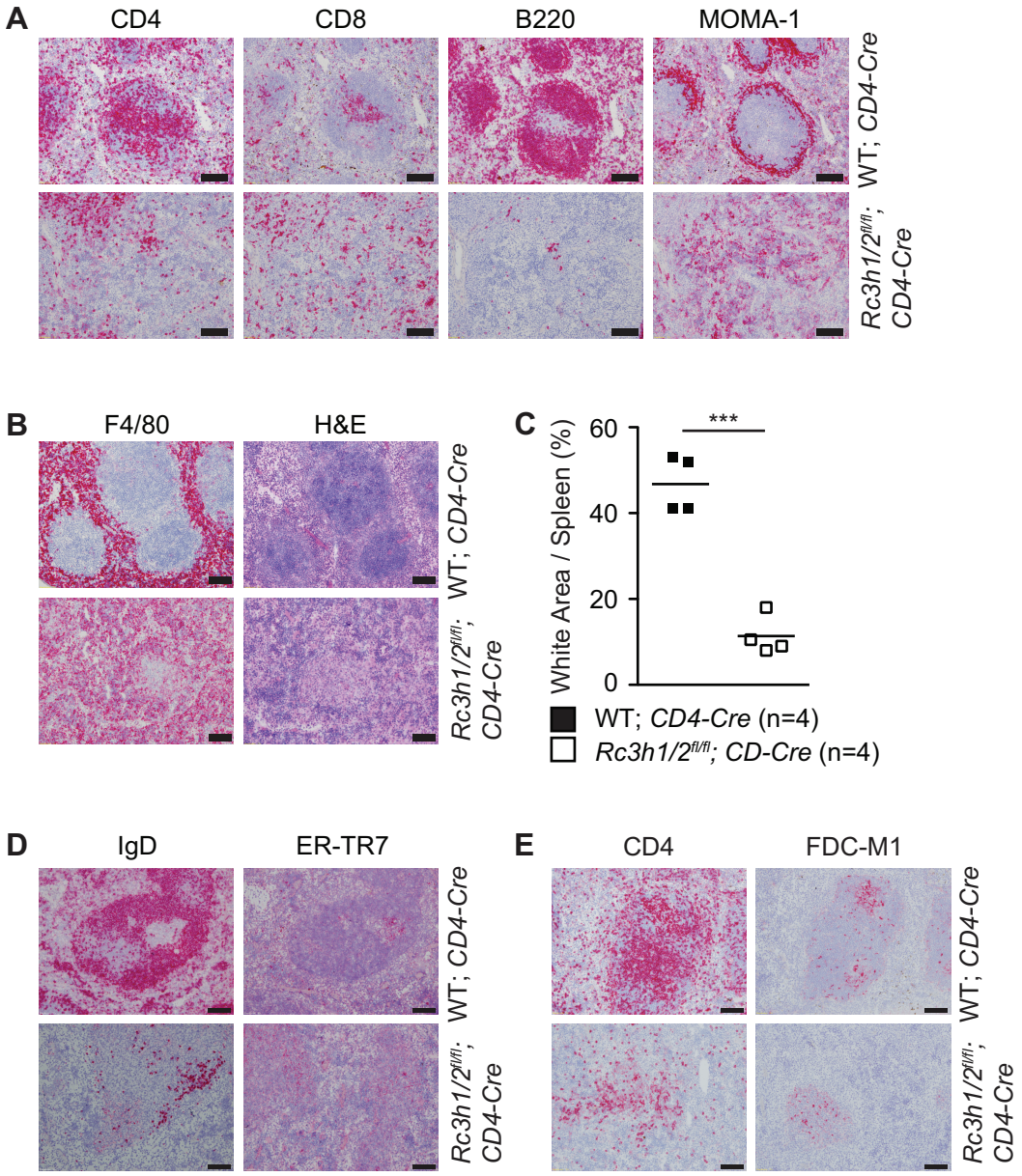

Figure 33: Roquin-1/2 deficiency disrupts the splenic architecture. Consecutive cryo-sections from spleens, stained for CD4, CD8, B220 and MOMA-1 (A), for F4/80 and H&E (B), for IgD and ER-TR7 (D) and for CD4 and FDC-M1 (E) in adult mice. The black bar represents 100 µm. (C) Quantification of white/red pulp in the spleen. The bar represents the mean value of each column and statistical significances were calculated by Student's t-test (*p < 0.001). Genotypes are indicated in the figure and data are representative for more than three different experiments. Cryo-sections and stainings were performed by Prof. Dr. Mathias Heikenwälder and Jessica Zöller, Institute for Virology, Technische Universität München/Helmholtz Zentrum München.**

In three-week-old mice, follicles start to develop. In such young *Rc3h1/2*-deficient mice, these structures appeared less disturbed than in older animals. However, intact follicular structures were already strongly reduced in young *Rc3h1/2*-deficient mice (Figure 34 A–C).

Consistently, B220$^+$, CD4$^+$ and CD8$^+$ cells did no longer form T cell or B cell zones and appeared dispersed. Furthermore, accessory cells such as ER-TR7$^+$ reticular fibroblast and FDC-M1$^+$ follicular dendritic cells as well as MOMA-1$^+$ macrophages were scattered and delocalized (Figure 34 D). Together these data suggest that in *Rc3h1/2$^{fl/fl}$; CD4-Cre* mice, the splenic architecture is likely to be too disturbed to support auto-antibody production.

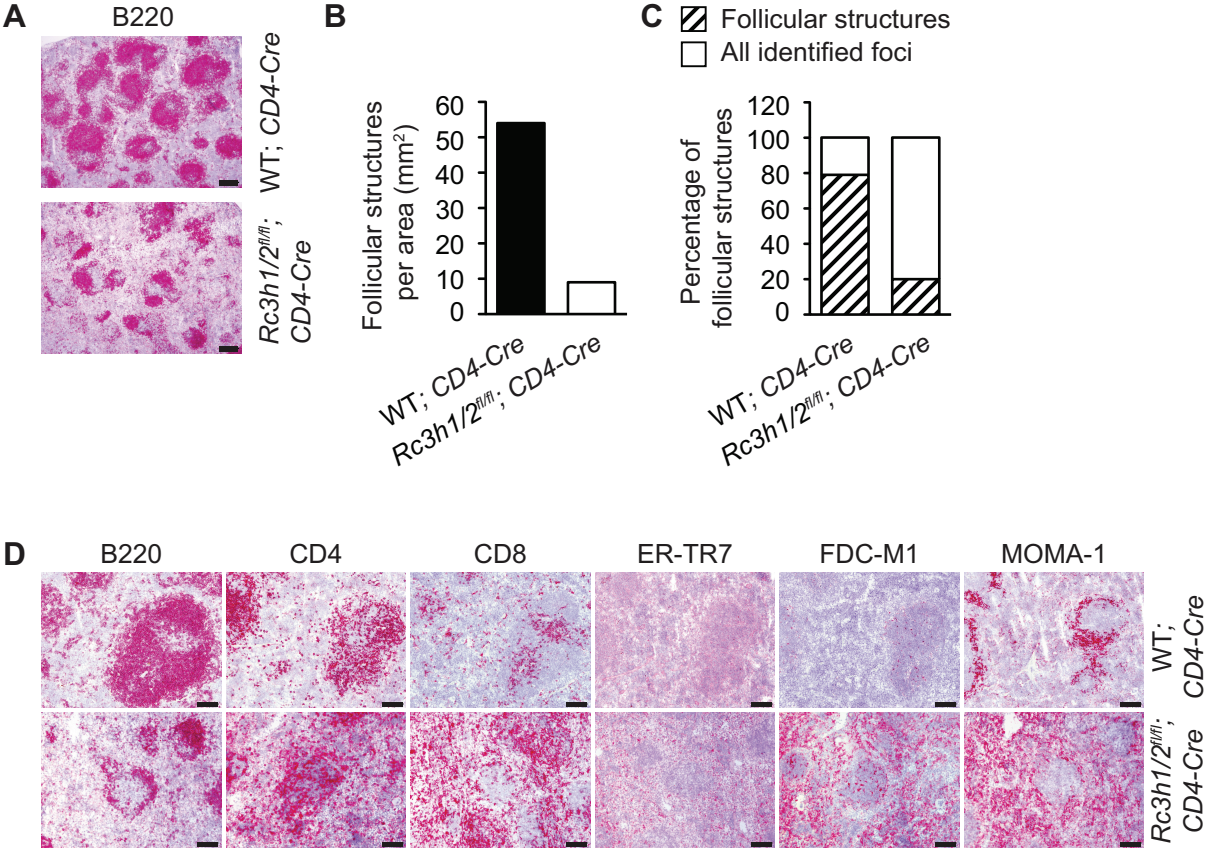

Figure 34: Loss of Roquin-1 and Roquin-2 impairs follicular structure formation in the spleen. (A) Overview of B220$^+$ follicles in the spleen (bar = 200 µm). (B) Number of follicular structures identified by a clear B and T cell and marginal zone. (C) Percentage of follicular structures compared to all visible foci. (D) Consecutive cryo-sections stained for B220, CD4, CD8, ER-TR7, FDC-M1 and MOMA-1 (bar = 100 µm). All data show the analysis of an only 3-week old mouse and genotypes are indicated in the figure. Cryo-sections and stainings were performed by Prof. Dr. Mathias Heikenwälder and Jessica Zöller, Institute for Virology, Technische Universität München/Helmholtz Zentrum München.

8.2.10 Roquin-1 and Roquin-2 control the transition point between Th1 and Tfh cell differentiation

Next, an adoptive transfer model was used to address whether *Rc3h1/2*-deficient cells could spontaneously support Tfh and GC B cell development in an intact spleen. For this, a system

was developed in which CD4$^+$ T cells from *Rc3h1/2$^{fl/fl}$* mice were treated with Cre-recombinase *in vitro*, leading to acute deletion of both proteins.

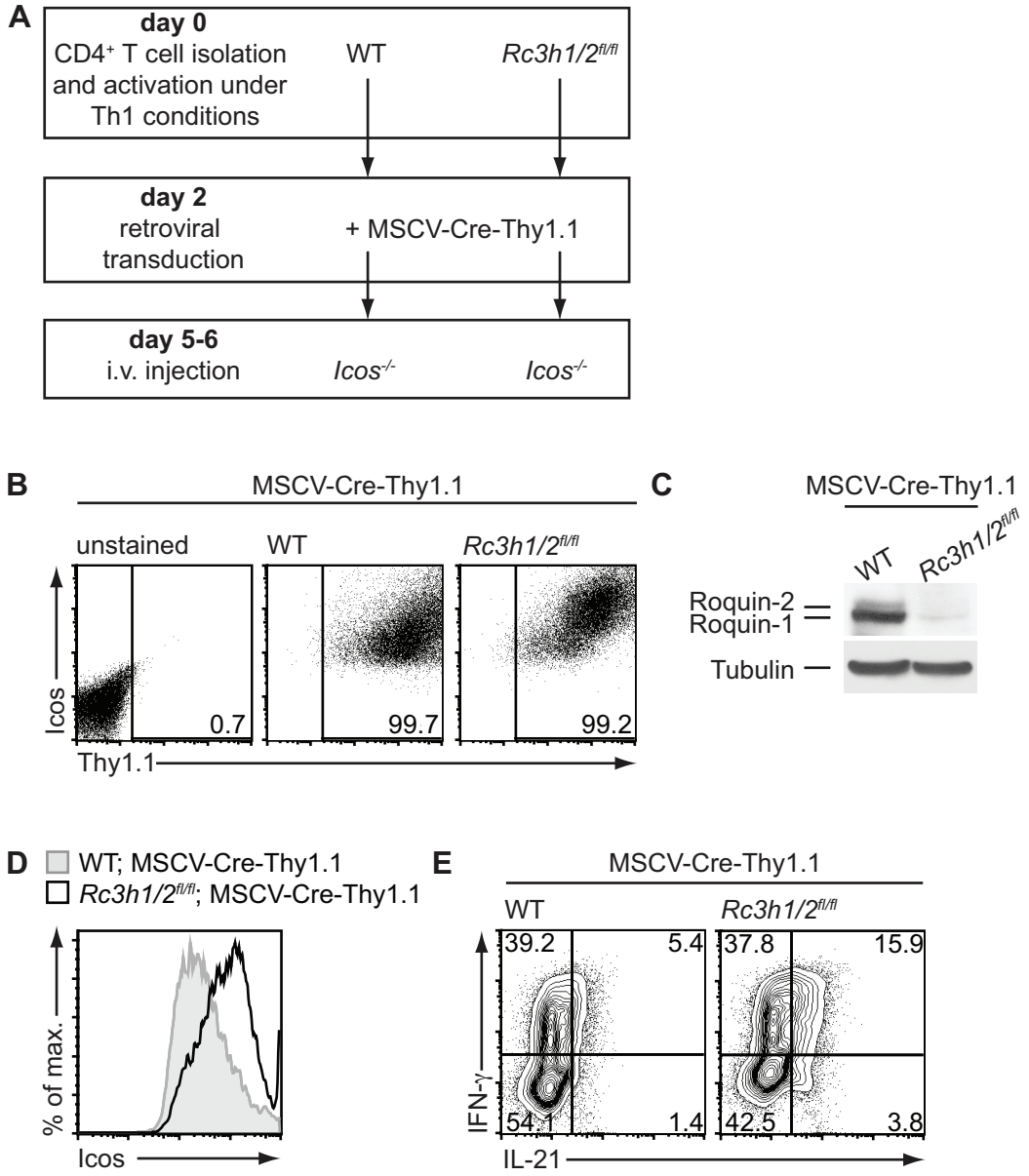

Figure 35: *In vitro* system for the deletion of Roquin-1 and Roquin-2. (A) Experimental outline displaying CD4$^+$ T cell isolation, MSCV-Cre-Thy1.1-transduction and adoptive transfer of wild-type or *Rc3h1/2$^{fl/fl}$* cells into *Icos$^{-/-}$* mice. Expression of Cre (detected as Thy1.1) (B) or Icos (D) on the day of transfer. (C) Protein levels of Roquin-1/2 in Cre-transduced CD4$^+$ T cells. (E) IFN-γ and IL-21 production of PMA and ionomycin re-stimulated cells after MSCV-Cre-Thy1.1-transduction, analyzed at the day of the transfer. Genotypes are indicated in the figure and data are representative for five (B), six (C), four (D) and two (E) independent experiments. The *in vitro* system was developed by Dr. Stephanie Edelmann and evaluated in cooperation.

The recently described transitional stage between Th1 and Tfh cells [108] was motivation to expand the cells for transfer under Th1 differentiation conditions for 5–6 days. Wild-type or *Rc3h1/2*-deficient Th1 cells were transferred into *Icos*-deficient recipient mice to investigate the development of Tfh cells in the absence of endogenous Tfh cells in this niche (Figure 35 A), because *Icos*$^{-/-}$ mice are almost devoid of Tfh cells [96]. Functional deletion of Roquin-1 and Roquin-2 was demonstrated by staining for Thy1.1 expression, as a marker for Cre-recombinase (Figure 35 B), and was shown by Western blotting (Figure 35 C). Consistently, Icos levels were elevated in cells after acute deletion of Roquin-1 and Roquin-2 compared to equally treated wild-type cells (Figure 35 D). In addition, there were more IL-21 single- and IL-21/IFN-γ double-producers after re-stimulation with PMA and ionomycin at the day of the transfer (Figure 35 E). This might indicate that the *Rc3h1/2*-deficient cells already adopt Tfh cell characteristics, because IL-21 is expressed by Tfh cells and important for their function. However, it is important to note that IL-21 expression is not distinctive for Tfh cells, as other cells such as Th17 cells can also express IL-21 [94]. The increased IL-21 expression after deletion of Roquin-1/2 could also be induced via Icos up-regulation and its activation of the transcription factor c-Maf [30].

Six, seven and eight days after transfer, the mice were analyzed for spontaneous Tfh and GC B cell development. Indeed, only Th1 cells deficient for Roquin-1 and Roquin-2 ($CD4^+$ $Thy1.1^+$) gave rise to large numbers of follicular helper T cells, which were reduced to wild-type levels in the course of the next two days (Figure 36 A–B). The transferred double-deficient cells proliferated heavily (Figure 36 C). We assume that these highly activated cells died, since the transferred cells were no longer detected after eight days, as seen for total numbers of Tfh cells (Figure 36 B). Notably, the transferred cells were also not detected in other organs like lung, liver or kidney (data not shown). Despite of the rapid disappearance of the transferred cells, the *Rc3h1/2*-deficient Tfh cells functionally initiated the development of endogenous germinal center B cells, which accumulated from day 6 to day 8 (Figure 36 D–E). These effects could not be observed after transfer of equally treated wild-type cells.

These data demonstrate that Roquin-1 and Roquin-2 directly control the differentiation of Tfh cells. Consequently, loss of Roquin-1/2 proteins led to spontaneous accumulation of Tfh cells in *Rc3h1/2*$^{fl/fl}$*; CD4-Cre* mice (Figure 32). Roquin-1/2 might even control a transition point between Th1 and Tfh cells, as demonstrated by adoptive transfer (Figure 36).

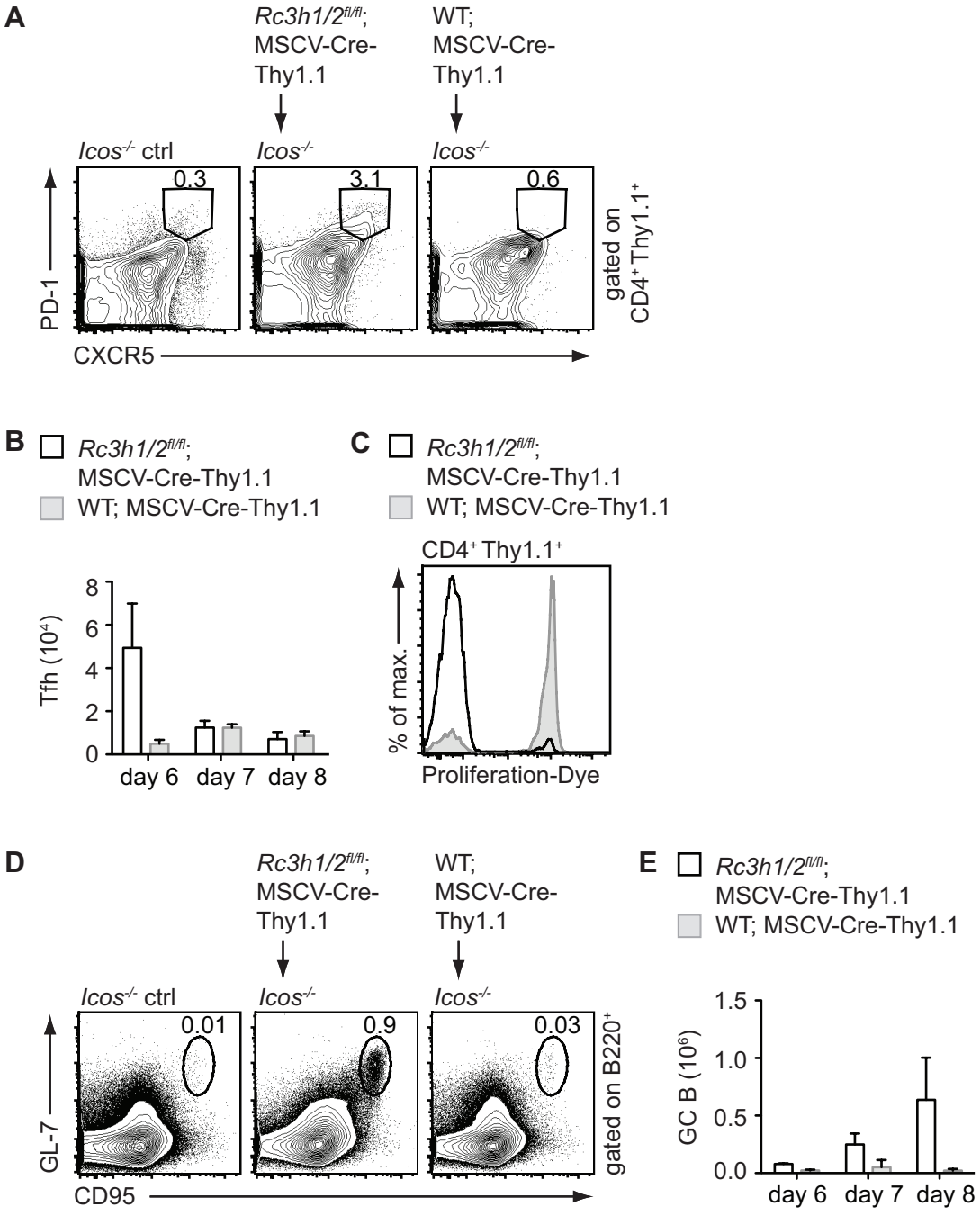

Figure 36: Roquin-1 and Roquin-2 control the differentiation from Th1 to Tfh cells. (A–B) Frequencies (A) and cell numbers (B) of Tfh cells (CD4$^+$ Thy1.1$^+$) at day 6 (A) or day 6, 7 and 8 (B) after transfer of MSCV-Cre-Thy1.1-transduced wild-type or *Rc3h1/2$^{fl/fl}$* cells (Th1-differentiated) into *Icos$^{-/-}$* mice. (C) Proliferation of cells (CD4$^+$ Thy1.1$^+$) at day 6 after transfer. Frequency (D) or cell numbers (E) of GC B cells (B220$^+$) at day 8 (D) or day 6, 7 and 8 (E) after transfer. Genotypes are indicated in the figure and data are representative for five experiments with two (A–B, D–E) and three (C) mice per group. Transfer experiments were established by Stephanie Edelmann and conducted in cooperation.

Plasticity among helper T cell subsets is generally accepted. Among those, the Tfh cell population seems to be one of the most flexible Th cell populations, by displaying features which overlap with other Th cell subsets [162]. Furthermore, Lu et al. propose that several T helper subsets still maintain the potential to display Tfh cell characteristics [163].

Therefore, naive $CD4^+$ T cells were transferred into *CD45.1; CD45.2* wild-type mice to investigate their potential to differentiate into Tfh cells without being previously activated. For the transfer, $CD4^+$ T cells from wild-type; *CD4-Cre* or *Rc3h1/2$^{fl/fl}$; CD4-Cre* mice were purified using magnetic beads and subsequently FACS sorted for $CD4^+$ $CD25^-$ $CD62L^+$ $CD44^-$ T cells (Figure 37 A, upper panel). Eight days after transfer, the mice were analyzed for the development of Tfh cells from transferred $CD45.2^+$ cells. Interestingly, although transferred with a naive phenotype, *Rc3h1/2*-deficient cells were highly activated. Almost 90% of the transferred *Rc3h1/2$^{fl/fl}$; CD4-Cre* cells lost their naive state and expressed the activation marker CD44. Conversely, 90% of transferred wild-type cells stayed in the naive state (Figure 37 A, lower panel). Beside the potential of being highly activated, *Rc3h1/2*-deficient cells also spontaneously differentiated into $CXCR5^{hi}$ PD-1^{hi} Tfh cells, while transferred wild-type cells did not up-regulate these markers (Figure 37 B). This transfer experiment further corroborates the finding that Roquin-1 and Roquin-2 control the differentiation of Tfh cells. Roquin-1 and Roquin-2 seem to play a suppressing role in this differentiation program, which seems to be switched on as a default program if Roquin-1 and Roquin-2 are missing. These proteins might therefore be crucial in preventing germinal center-derived autoimmune diseases and potentially lymphoid cancers by repressing certain co-stimulatory molecules.

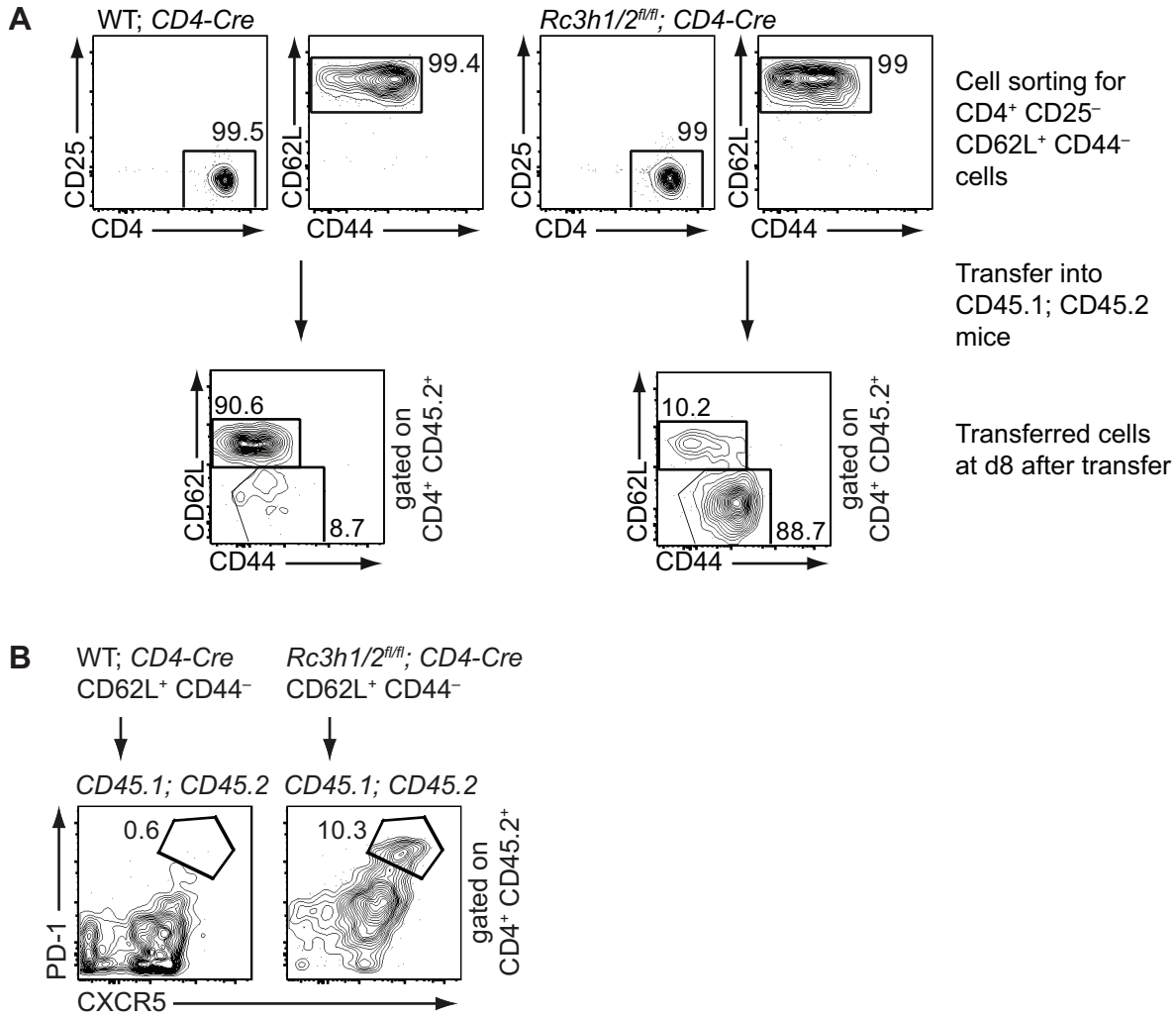

Figure 37: Naive CD4$^+$ T cells from *Rc3h1/2*-deficient mice spontaneously become Tfh cells. For transfer experiments, naive CD4$^+$ T cells from wild-type; *CD4-Cre* or *Rc3h1/2$^{fl/fl}$; CD4-Cre* mice were sorted for CD4$^+$ CD25$^–$ CD62L$^+$ and CD44$^–$ (A, upper panel) and were i.v. injected into CD45.1$^+$ CD45.2$^+$ expressing recipient mice. Eight days after injection the transferred cells were analyzed for the expression of CD62L and CD44 markers (A, lower panel) or the spontaneous conversion into Tfh cells (B).

8.2.11 Roquin-1/2 reciprocally influence Th17 and Treg differentiation

The transfer experiments in section 8.2.10 clearly demonstrated that Roquin-1 and Roquin-2 play a crucial role in Tfh cell differentiation. Therefore, their role in other differentiation programs was investigated. Wild-type or *Rc3h1/2*-deficient CD4$^+$ T cells were activated *in vitro* under Th0, Th1, Th2, Th17 and Treg polarizing conditions. As *Rc3h1/2*-deficient CD4$^+$ T cells were highly activated *ex vivo*, naive CD4$^+$ T cells (CD4$^+$ CD25$^–$ CD62L$^+$ CD44$^–$) were purified as described in section 8.2.10, to avoid any bias. Activating naive T cells with anti-CD3 and anti-CD28 under Th0 conditions was not sufficient to induce IFN-γ or IL-4 production (Figure 38 A, upper panel). Furthermore, *Rc3h1/2*-deficient cells did not produce

significantly more IFN-γ than wild-type cells under Th1 conditions as judged by the MFI of IFN-γ in these cells and there were also similar frequencies of cells expressing IFN-γ (Figure 38 A, middle panel). Furthermore, IL-4 production under Th2-skewing conditions was not altered (Figure 38 A, lower panel). Interestingly, loss of Roquin-1 and Roquin-2 under Th17-conditions, led to a significant increase in IL-17-producing cells (Figure 38 B, upper panel), while Treg cell differentiation marked by Foxp3 expression was strongly reduced (Figure 38 B, lower panel). This is consistent with the notion that Th17 and Treg cells originate from reciprocal differentiation programs [86,87]. Roquin-1 and Roquin-2 were therefore not only involved in the development of Tfh cells, but probably also in navigating Th17/Treg decisions.

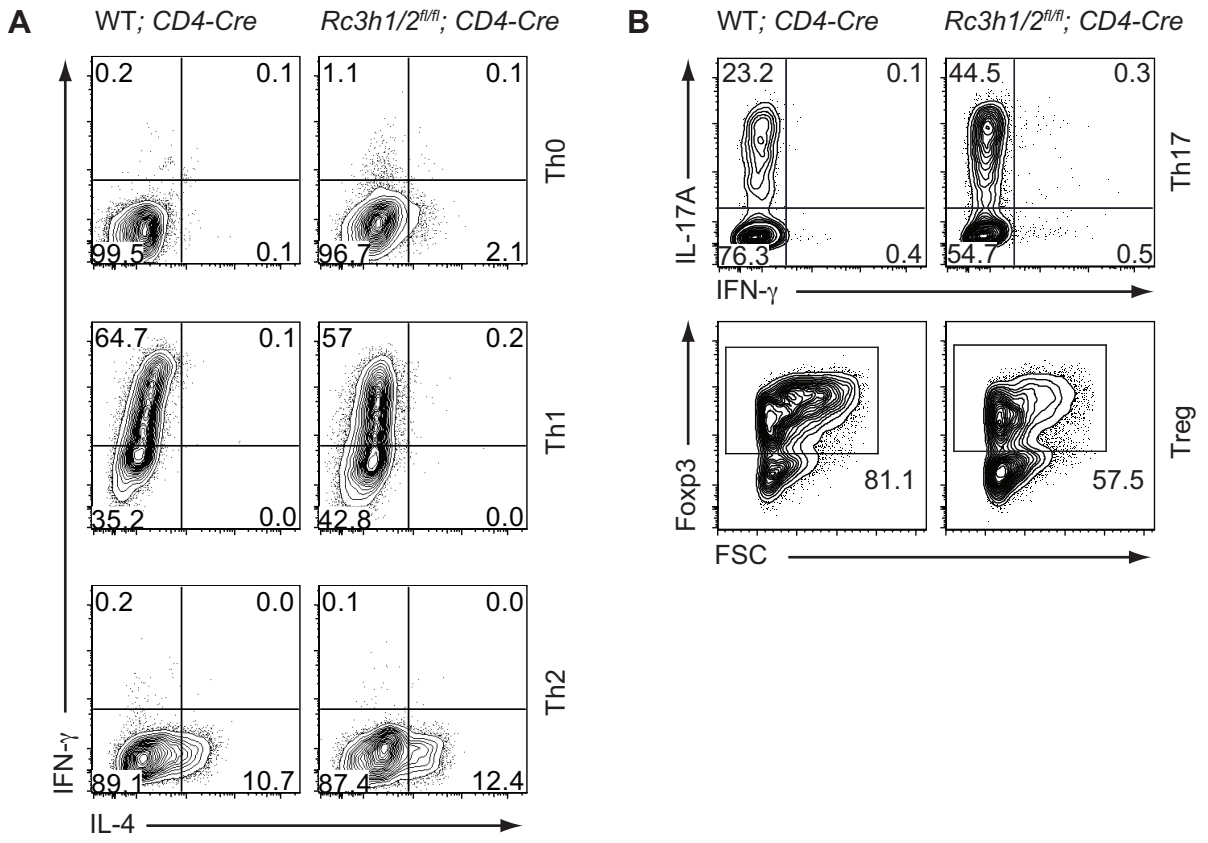

Figure 38: Loss of Roquin-1 and Roquin-2 reciprocally influences Th17 and Treg differentiation. For differentiation experiments, CD4$^+$ T cells from wild-type; *CD4-Cre* or *Rc3h1/2$^{fl/fl}$; CD4-Cre* mice were enriched with CD4$^+$ dynabeads and naive T cells (CD4$^+$ CD25$^-$ CD62L$^+$ CD44$^-$) were sorted on a FACS AriaIII Cell Sorter. Cells were stimulated with anti-CD3/anti-CD28 antibodies, coupled to magnetic beads, under Th0, Th1, Th2 (A), Th17 or Treg (B) differentiation conditions (Table 19). Contour plots are representative for four independent experiments. Experiments were performed in cooperation with Sebastian Warth, who accomplished the T cell differentiation after cells had been isolated and sorted.

Interestingly, IFN-γ had been proposed as a target of Roquin-1, only on the basis though of increased Ifng mRNA half-life in T cells from san/san mice [157]. However, by evaluating IFN-γ protein levels in the differentiation experiments above (Figure 38), we cannot confirm IFN-γ as a direct target of Roquin-1/2 proteins. Roquin-1/2 deficiency did neither significantly enhance the MFI of IFN-γ nor the number of IFN-γ-producing cells under Th1 skewing conditions. Nevertheless, IFN-γ certainly plays an important role in the disease progression of san/san mice. Prolonged half-life of IFN-γ mRNA in *Rc3h1*$^{san/san}$ mice led to the massive accumulation of short-lived effector CD8$^+$ cells (SLECs) in these mice. This phenotype was attenuated by crossing the san/san mice to IFN-γR knockouts [157].

We therefore speculated that IFN-γ might be more deregulated in CD8$^+$ than in CD4$^+$ cells. To evaluate IFN-γ expression by CD4$^+$ and CD8$^+$ T cells, total splenocytes were stimulated with antiCD3/antiCD28 for five hours. Interestingly, CD4$^+$ cells from *Rc3h1/2*$^{fl/fl}$*; CD4-Cre* mice exhibited only marginally enhanced IFN-γ expression, while CD8$^+$ T cells produced enormous amounts of IFN-γ (Figure 39). Notably, by stimulating total splenocytes, the initial differences in the activation status between *Rc3h1/2*$^{fl/fl}$*; CD4-Cre* and wild-type cells as well as CD4$^+$ and CD8$^+$ T cells have to be taken into account. CD8$^+$ T cells from double-deficient mice were more activated than CD4$^+$ T cells and both T cell lineages were more activated compared to wild-type cells (Figure 29). This might explain why CD8$^+$ T cells from *Rc3h1/2*$^{fl/fl}$*; CD4-Cre* mice produced such excessive amounts of IFN-γ. Nevertheless, it is likely that the elevated IFN-γ levels could indeed have a positive feedback effect, by driving the accumulation of effector CD8$^+$ T cells in *Rc3h1/2*$^{fl/fl}$*; CD4-Cre* mice similar to *Rc3h1*$^{san/san}$ mice. IFN-γ might also contribute to other phenotypes in *Rc3h1/2*$^{fl/fl}$*; CD4-Cre* mice such as the disrupted splenic architecture. However, IFN-γ is most probably not a direct target of Roquin-1/2 proteins, as implied by the differentiation experiment above (Figure 38). Enhanced IFN-γ expression could as well be caused by increased co-stimulation of effector cells, which can indeed stabilize the mRNA of cytokines such as IFN-γ [164]. Therefore, the exact mechanism of IFN-γ deregulation in *Rc3h1*$^{san/san}$ and *Rc3h1/2*$^{fl/fl}$*; CD4-Cre* mice remains to be specified.

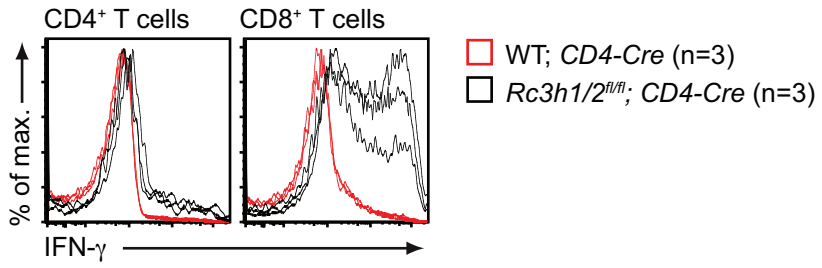

Figure 39: Loss of Roquin-1/2 causes elevated IFN-γ levels in CD8$^+$ T cells. Total splenocytes from wild-type; *CD4-Cre* or *Rc3h1/2$^{fl/fl}$; CD4-Cre* mice were stimulated with antiCD3 and antiCD28 for 5 h adding Brefeldin A for 2 h. Cells were stained for IFN-γ cytokine expression in CD4$^+$ (left panel) or CD8$^+$ (right panel) T cells.

8.2.12 The NF-κB pathway is activated in *Rc3h1/2*-deficient cells

Th17 and Tfh cell differentiation share Irf4 as an essential transcription factor [90,165], suggesting that loss of Roquin-1/2 could induce Tfh and Th17 cell differentiation via increased Irf4 signaling. In addition to Irf4, also up-regulation of Bcl6 could explain that *Rc3h1$^{san/san}$* and *Rc3h1/2$^{fl/fl}$, CD4-Cre* mice developed spontaneous Tfh and germinal center B cells ([39] and Figure 32, respectively). Therefore, the expression of the Tfh cell transcription factors Bcl6 [68-70] and Irf4 [103,104] was investigated. The expression levels of Bcl6 were not markedly altered in *Rc3h1/2*-deficient Tfh cells (Figure 32 A, right). However, analyzing Irf4 expression levels after acute deletion of Roquin-1 and Roquin-2 in Th1 cells and in CD4$^+$ T cells from *Rc3h1/2$^{fl/fl}$; CD4-Cre* mice revealed significantly increased Irf4 protein amounts (Figure 40 A–D).

As Irf4 is a down-stream transcriptional target of NF-κB, activation of the canonical and alternative NF-κB pathway was investigated. The canonical pathway did not seem to be strongly affected. However, there was a slight increase in p65 and IκBα phosphorylation (Figure 40 B), while IκBα itself was not degraded. On the contrary, the alternative NF-κB pathway was highly activated. This became apparent by increased expression of p100 and p52 as well as enhanced processing of p100 to p52 in Th1-cultured cell as well as *ex vivo* isolated CD4$^+$ T cells from *Rc3h1/2$^{fl/fl}$; CD4-Cre* mice (Figure 40 C–D). Functionally active nuclear p52 was detected in cell fractionation experiments (Figure 40 E).

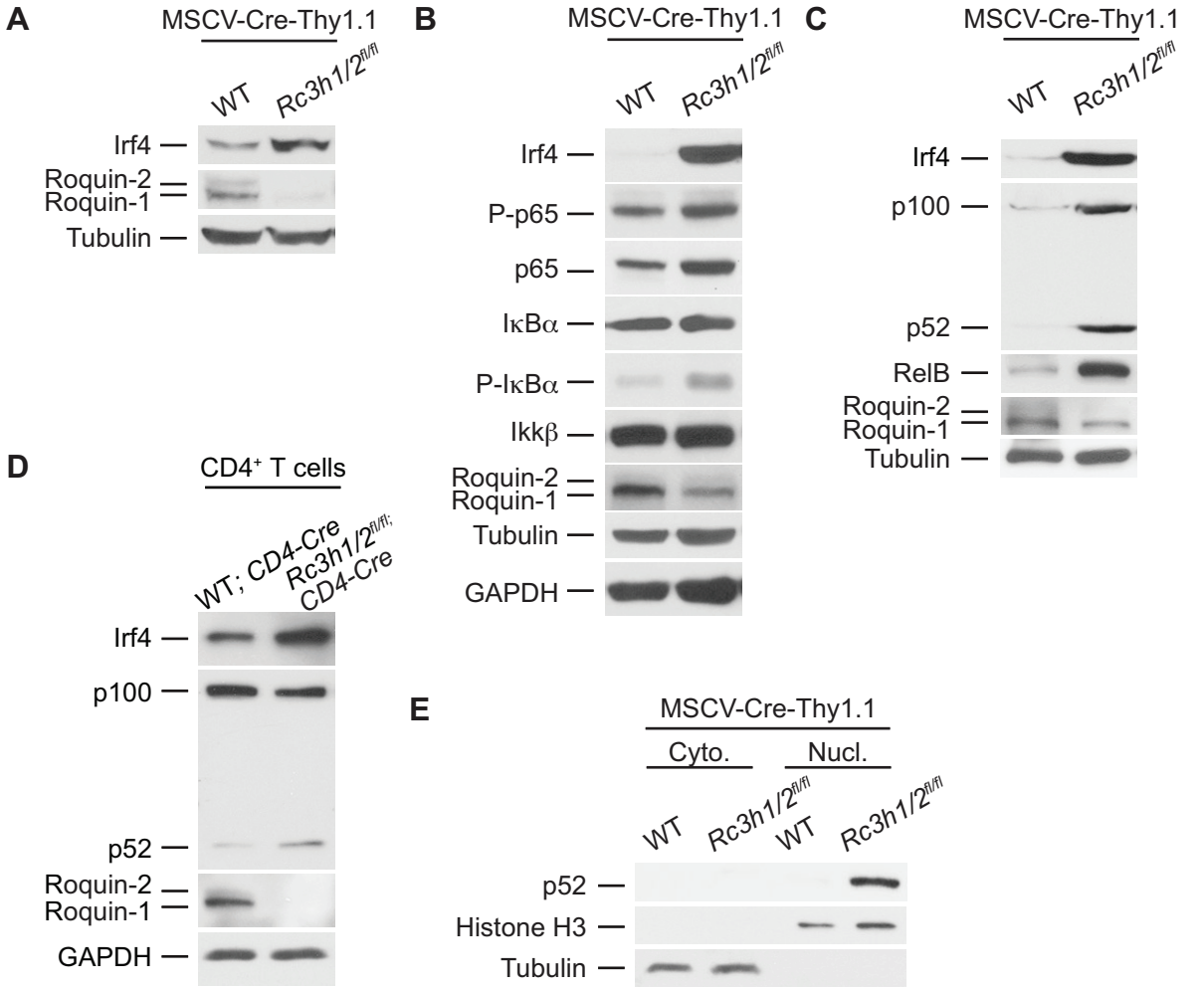

Figure 40: Roquin-1/2 deletion up-regulates Irf4 and leads to activation of the NF-κB pathway. Western blot analysis of protein lysates from wild-type or *Rc3h1/2*$^{fl/fl}$ CD4$^+$ T cells after Cre-transduction, showing Irf4 levels (A) and factors involved in the canonical (B) or alternative NF-κB pathway (C), each representing an independent experiment. (D) Western blot analysis of purified CD4$^+$ T cells, showing factors of the alternative NF-κB pathway. (E) Western blot analysis of cytoplasmic and nuclear extracts from wild-type or *Rc3h1/2*$^{fl/fl}$ CD4$^+$ T cells after Cre-transduction. Data are representative for four (D) and three (E) experiments. (A–C) Western blotting was accomplished by Claudia Lohs.

8.2.13 Ox40 activates the NF-κB pathway and is a novel target of Roquin-1 and -2

Activation of the NF-κB pathway could be caused by Roquin-1/2 targets, which were de-repressed in the knockout situation. Therefore, different mRNAs were tested by quantitative PCR, which were involved in the activation of NF-κB. In three biological replicates, no significant increase could be seen for *Ikkα*, *Ikkβ*, *Ikkγ*, *NIK*, *Ciap1*, *Ciap2*, *Traf2*, *Traf3* and *Tradd* gene expression. Interestingly, *Icos*, *RelB*, *Irf4* and *Ox40* mRNA levels were elevated (Figure 41).

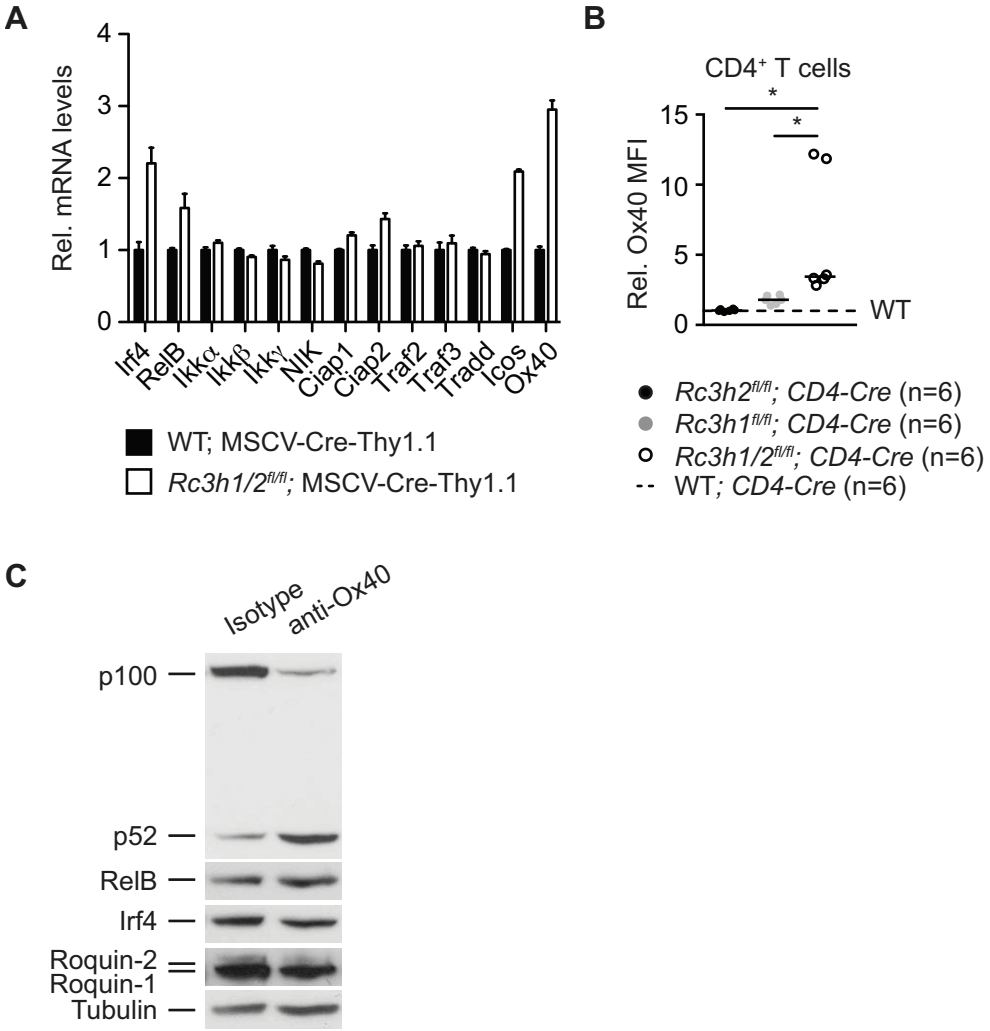

Figure 41: Loss of Roquin-1 and Roquin-2 de-represses Ox40. (A) Quantitative PCR analysis of factors involved in NF-κB signaling. Data are representative for three biological replicates from wild-type or *Rc3h1/2*$^{fl/fl}$ CD4$^+$ T cells after Cre-transduction. (B) Relative median fluorescence intensity (MFI) of Ox40 in CD4$^+$ T cells from knockout mice, all normalized to an equal number of wild-type; *CD4-Cre* mice. (C) Western blot of Th1-differentiated T cell lysates from C57BL/6 mice, treated with 10 µg/ml isotype control antibody or anti-Ox40 (OX86) for three days, showing factors of the alternative NF-κB pathway. Genotypes are indicated in the figure and data are representative for three (C) experiments. Bars represent the median value of each column and statistical significances were calculated by Tukey' multiple comparisons test (*p < 0.05). (A) qPCR was performed by Claudia Lohs.

Ox40 was included as a candidate gene, because it was shown to activate the NF-κB pathway [166]. Furthermore, as described in section 8.1.5 and 8.1.6, array approaches identified Ox40 as a promising new target of Roquin-1. Consequently, Ox40 protein levels were 2-fold increased in CD4$^+$ T cells from *Rc3h1*$^{fl/fl}$*; CD4-Cre* mice, and even higher increased in *Rc3h1/2*-deficient CD4$^+$ T cells compared to wild-type or *Rc3h2*$^{fl/fl}$*; CD4-Cre* CD4$^+$ T cells

(Figure 41 B). Furthermore, cultivating Th1 cells in the presence of an agonistic anti-Ox40 antibody (Ox86) was sufficient to activate the alternative NF-κB pathway with increased processing of p100 to p52. However, the stimulation was not effective to up-regulate Irf4 expression compared to the isotype control (Figure 41 C). In these experiments, Irf4 was expressed after 1 h, 5 h, 48 h and 72 h of activation and completely vanished after six days. The presence of the anti-Ox40 antibody, though, had no influence on Irf4 expression levels. We nevertheless hypothesize that Ox40 co-stimulation in combination with additional signals could increase Irf4 expression.

Moderately elevated Ox40 levels in *Rc3h1*$^{fl/fl}$*; CD4-Cre* mice compared to significantly increased Ox40 expression in *Rc3h1/2*$^{fl/fl}$*; CD4-Cre* mice were reminiscent of the extent of Icos deregulation in these mice (Figure 30). Furthermore, Roquin-1 was shown to directly bind to Ox40 mRNA (Figure 19). Therefore we tested redundant functions of Roquin-2 in respect to this novel target of Roquin-1. Indeed, Roquin-2 (aa 1–438) could equally well bind to full-length Ox40 mRNA (Figure 42 A). Furthermore, direct repression of Ox40 was investigated *in vitro* by transduction of CAR-transgenic CD4$^+$ T cells deficient for Roquin-1 with adenovirus expressing Roquin-1 and Roquin-2 proteins. Roquin-1 wild-type and both isoforms of Roquin-2 (aa 1–1125 and 1–1187) down-regulated Ox40 to the same extent (Figure 42 B), whereas the inactive form of Roquin-1 (aa 1–509) could not repress Ox40. These data support the conclusion that Ox40 is a novel target of Roquin-1 and Roquin-2, which was de-repressed in *Rc3h1*$^{fl/fl}$*; CD4-Cre* and *Rc3h1/2*$^{fl/fl}$*; CD4-Cre* mice. Furthermore, both proteins could independently bind to the Ox40 mRNA and repress Ox40 expression *in vitro*.

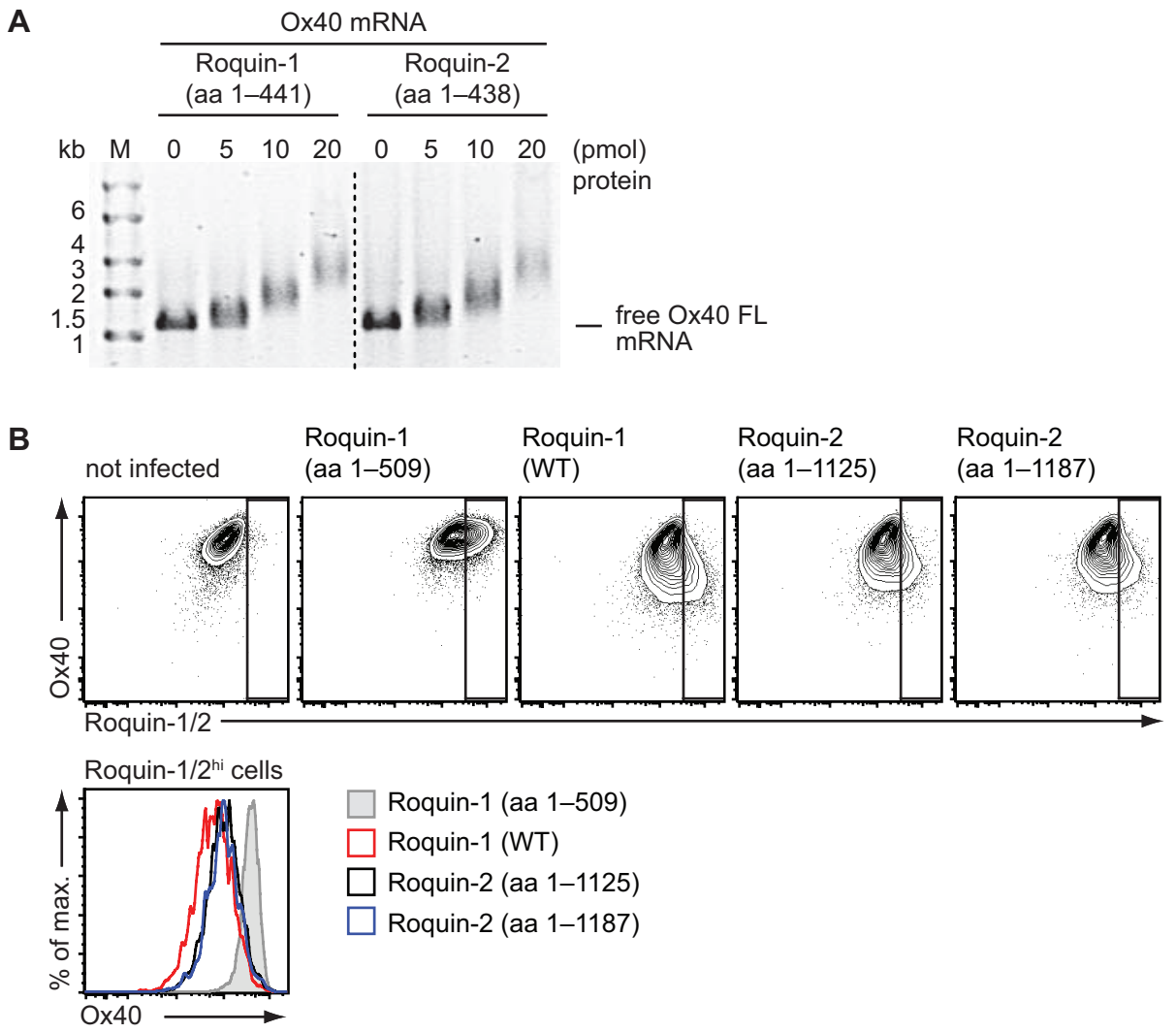

Figure 42: Roquin-1 and Roquin-2 redundantly control Ox40 expression. (A) EMSA with 1 pmol Ox40 full-length mRNA and 0–20 pmol of recombinant Roquin-1 (aa 1–441) or Roquin-2 (aa 1–438). (B) Ox40 levels after adenoviral transduction of CD4$^+$ T cells from *Rc3h1$^{fl/fl}$; CAG-CAR$^{stop\text{-}fl}$; CD4-Cre* mice with an inactive Roquin-1 (aa 1–509), Roquin-1 wild-type (WT) or two isoforms of Roquin-2 (aa 1–1125 or aa 1–1187), with histogram overlay of Roquin-1/2^{hi} cells (below). All plots in (A) are pre-gated on CAR$^+$ cells. Data are representative for two (A) and three (B) experiments. (A) EMSA was performed by Gitta Heinz.

8.2.14 Loss of Roquin-1/2 drives Tfh cell differentiation independently of Icos

Having established Ox40 as a new target of Roquin-1 and Roquin-2, we hypothesized that the de-regulation of both co-stimulatory receptors might contribute to the phenotypes observed in *Rc3h1/2$^{fl/fl}$; CD4-Cre* mice. To assess the role of Icos in these animals, triple knockout (TKO) mice were generated, which were deficient for Roquin-1 and Roquin-2 in the T cell compartment and overall deficient for Icos (*Rc3h1/2$^{fl/fl}$; CD4-Cre; Icos$^{-/-}$*). Icos expression

was reduced in *Rc3h1/2$^{fl/fl}$; CD4-Cre* mice heterozygous for Icos and was indeed absent in *Rc3h1/2$^{fl/fl}$; CD4-Cre; Icos$^{-/-}$* mice (Figure 43 A). Ox40 levels were still up-regulated in these mice, although Icos ablation led to a slight reduction in Ox40 overexpression levels (Figure 43 B).

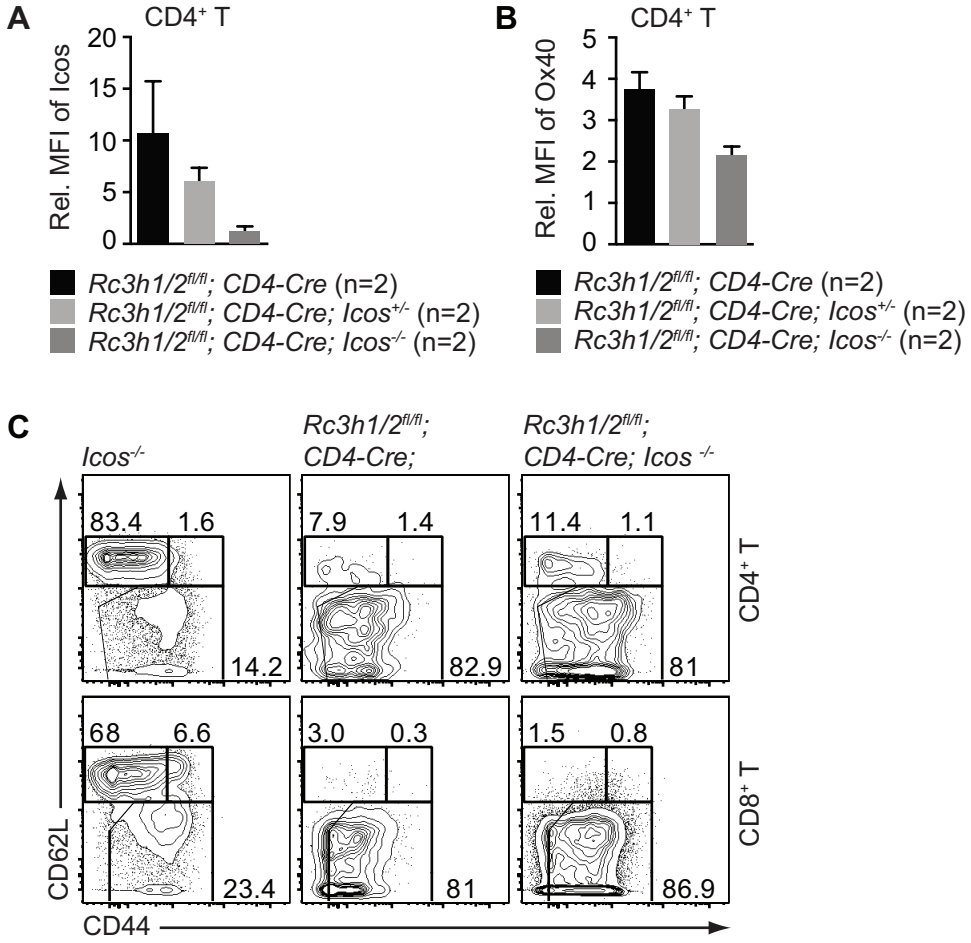

Figure 43: The absence of Icos in *Rc3h1/2$^{fl/fl}$; CD4-Cre* mice does not revert the effector-like phenotype of the double knockout. (A–B) Mean value of the relative median fluorescence intensity of Icos (A) or Ox40 (B) in CD4$^+$ T cells from knockout mice, all normalized to an equal number of *Icos$^{-/-}$* mice. (C) Representative contour plots of CD4$^+$ (upper panel) or CD8$^+$ (lower panel) splenocytes expressing the markers CD62L and CD44. Genotypes are indicated in the figure and data are representative for 4 (C) mice per genotype.

We then analyzed the most important phenotypes of the *Rc3h1/2$^{fl/fl}$; CD4-Cre* mice in the Icos TKOs. Surprisingly, loss of Icos did not alter the massive increase of effector-like CD4$^+$ and CD8$^+$ T cells in the double knockout situation (Figure 43 C), implying that other signals than Icos, such as Ox40 for example, play a dominant role in the activation of T cells from *Rc3h1/2$^{fl/fl}$; CD4-Cre* mice. Furthermore, Icos TKOs were still able to spontaneously form

Tfh cells (Figure 44 A), although Icos was thought to be crucial in Tfh cell differentiation [96]. All four mice analyzed exhibited clearly increased frequencies of Tfh cells compared to wild-type or *Icos*$^{-/-}$ animals. Examining B cells in these mice revealed markedly reduced B220^{+} B cells (Figure 44 B). Two mice appeared unhealthy and were completely devoid of B cells. Consequently they did not develop GC B cells, while in the other two mice only the older one (17 weeks) exhibited spontaneous GC B cell development, while the younger one (12 weeks) did not (Figure 44 C).

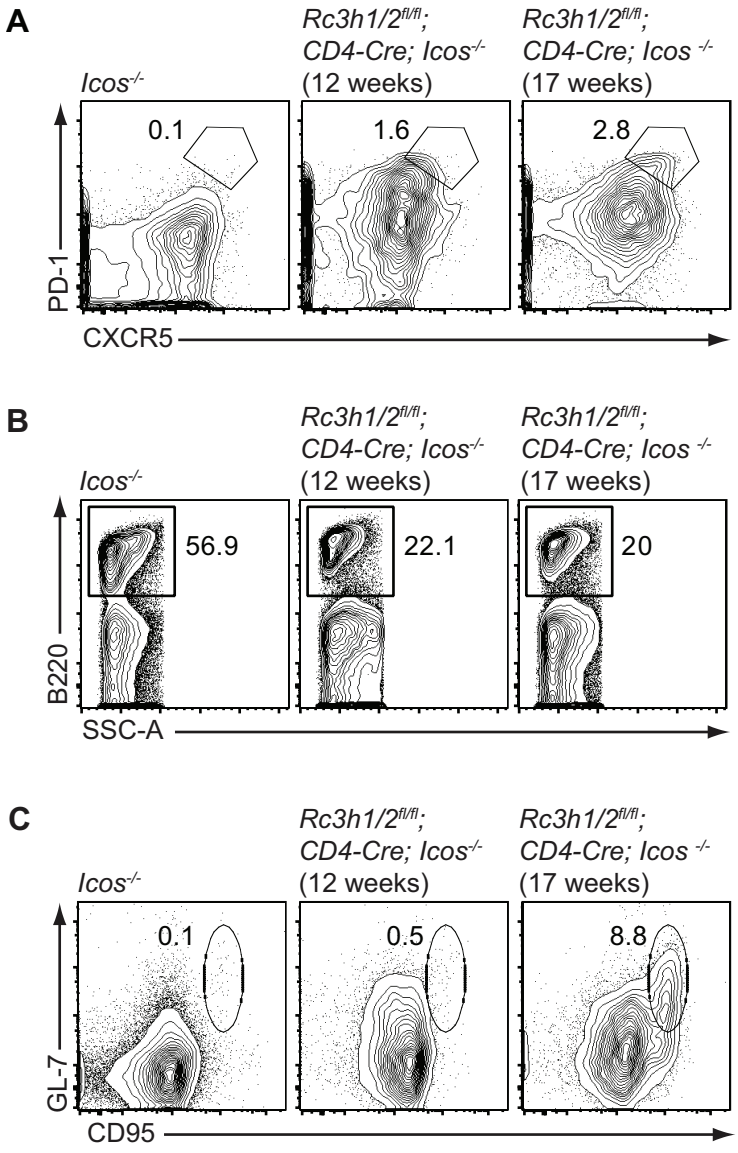

Figure 44: Loss of Roquin-1/2 proteins causes spontaneous Tfh and GC B cell formation even in the absence of Icos. (A–C) Representative contour plots of splenic Tfh cells (PD-1^{hi} CXCR5^{hi}), pre-gated on CD4^{+} (A), of B220^{+} cells (B) and of germinal center B cells (GL-7^{hi} CD95^{hi}), pre-gated on B220^{+} (C). All genotypes are indicated in the figures. Data are representative for four (A) and two of four mice, which still contained B220^{+} cells (B–C, also see section 8.2.14) mice.

Thus, combined loss of Roquin-1 and Roquin-2 seemed to override the need for Icos co-stimulation in the generation of Tfh cells and probably also GC B cells.

Remarkably, spleen sections from two mice analyzed revealed close to normal splenic architecture with follicle-like structures and marginal zones. Furthermore, the network of follicular dendritic cells (FDC-M1^{+}) clearly spanned across the follicle structures (Figure 45 A). Loss of Icos signaling obviously normalized the development of the splenic architecture.

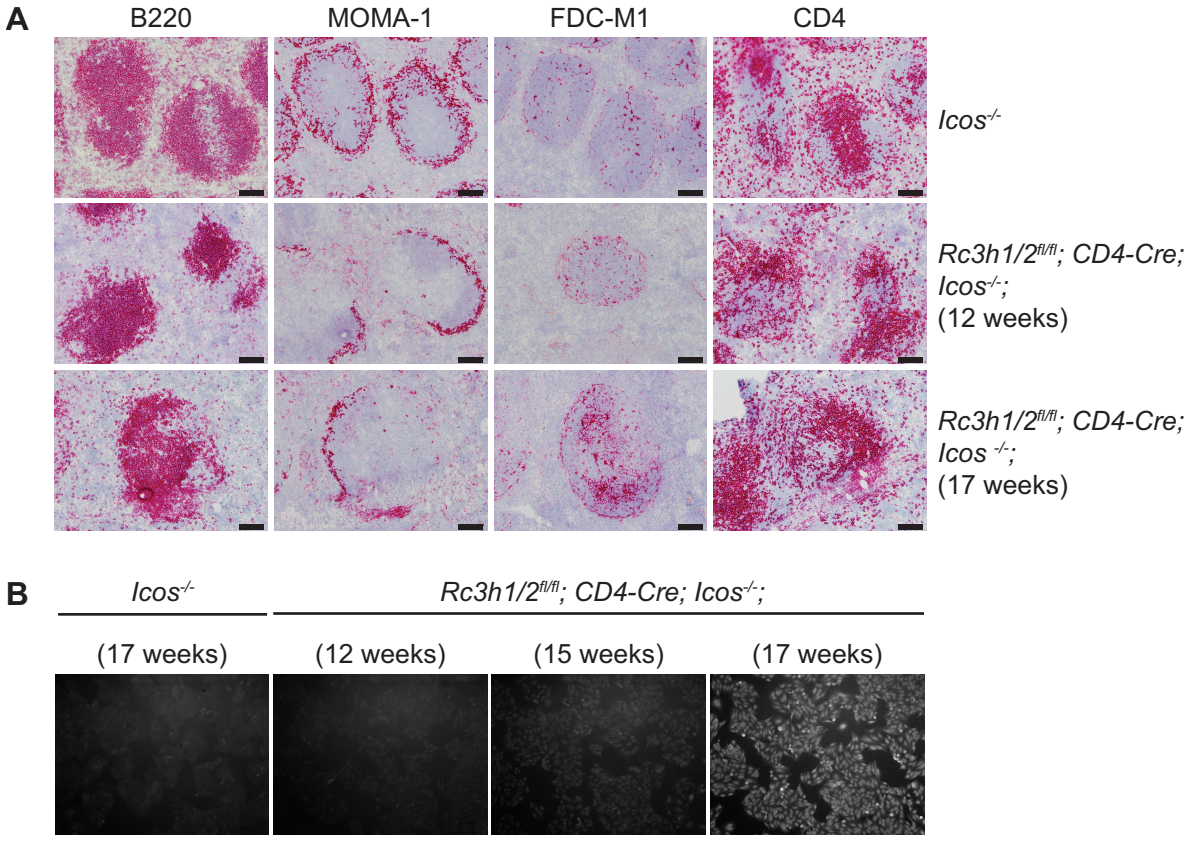

Figure 45: Rescue of splenic architecture supports auto-antibody formation in Icos TKOs. (A) Consecutive cryo-sections from spleens, stained for B220, MOMA-1, FDC-M1 and CD4. The black bar represents 100 µm. Cryo-sections and staining were performed by Prof. Dr. Mathias Heikenwälder and Jessica Zöller, Institute for Virology, Technische Universität München/Helmholtz Zentrum München. (B) Indirect immunofluorescence for antinuclear antibodies (HEp-2). Each panel represents one animal with the indicated phenotype.

As described in section 8.2.9, loss of Roquin-1/2 in T cells led to a complete destruction of the splenic architecture, impeding auto-antibody formation. The intact follicle structure in the Icos TKO and enhanced Tfh cell frequency might actually support auto-antibody formation. Indeed, auto-antibodies (ANAs) were detected in serum from a 17 weeks old male mouse.

Although only few animals were analyzed so far, ANAs appeared to be formed with age, as auto-antibodies started to occur in a male mouse at 15 weeks of age (Figure 45 B). Comparing these data with the frequency of Tfh and GC B cells in the respective animal revealed that only the older mouse (17 weeks) had auto-antibodies and GC B cells. The younger mouse (11 weeks) did not spontaneously develop GC B cells, while the 15 weeks old mouse was not analyzed for GC B cells. We therefore assume that spontaneous GC B cell development as well as the occurrence of ANAs could manifest with age in these Icos TKOs. We furthermore speculate that Ox40 expression, which was still elevated in Icos TKOs, might even be able to substitute for Icos deficiency in Tfh cell and germinal center formation. Considering a recent publication, which demonstrated that the level of PIP_3 generated by PI3K controlled the magnitude of the germinal center reaction [167], it would be interesting to address the possibility that Ox40 signaled via PI3K to influence the germinal center reaction.

Taken together, these data demonstrated that loss of Roquin-1 and Roquin-2 caused spontaneous Tfh and GC B cell development even in the complete absence of Icos, which subsequently led to the formation of auto-antibodies in an almost intact splenic environment. Loss of Icos signaling on the one hand reversed the disruption of the splenic architecture, which could allow for the development of auto-antibodies in intact follicle structures. A recent study, however, demonstrated that ablation of Icos in san/san mice, which had intact spleens and spontaneous germinal centers, did not prevent ANA development, but even led to the occurrence of homogenous anti-nuclear antibodies in *Rc3h1*$^{san/san}$ mice [159]. Loss of Icos signaling thus seems to correlate with the development of auto-antibodies in the absence of functional Roquin proteins in *Rc3h1*$^{san/san}$ and *Rc3h1/2*$^{fl/fl}$*; CD4-Cre* mice.

8.2.15 Reducing IFN-γ levels in *Rc3h1/2*-deficient mice rescues splenic architecture but not effector-like phenotype

Very recently it had been described that loss of IFN-γ signaling reversed the phenotype of short-lived effector $CD8^+$ T cells, characterized by a $CD62L^{lo}$ $KLRG1^{hi}$ phenotype [157]. Crossing *Rc3h1*$^{san/san}$ mice to IFN-γR knockout mice reduced SLEC numbers to wild-type levels and total $CD44^{hi}$ $CD8^+$ T cells declined to only 3-fold above wild-type levels compared to 9-fold in the *Rc3h1*$^{san/san}$ mice. Therefore, *Rc3h1/2*$^{fl/fl}$*; CD4-Cre, IFN-γ*$^{-/-}$ mice (IFN-γ TKO) were generated to assess the effect of IFN-γ signaling on the double knockout phenotype.

Total splenocytes from *IFN-γ*-deficient mice with or without additional deletion of *Rc3h1/2* genes, did not produce IFN-γ after 5 h of PMA and ionomycin stimulation (Figure 46 A). Surprisingly however, the effector-like phenotype of *Rc3h1/2*-deficient mice was not reversed or reduced as in the san/san mouse upon loss of IFN-γ signaling. In contrast, even more $CD4^+$ T cells seemed to adopt a $CD44^{hi}$ $CD62L^{lo}$ phenotype in the few IFN-γ TKOs analyzed, compared to *Rc3h1/2*-deficient mice (Figure 46 B, compare to Figure 29 A).

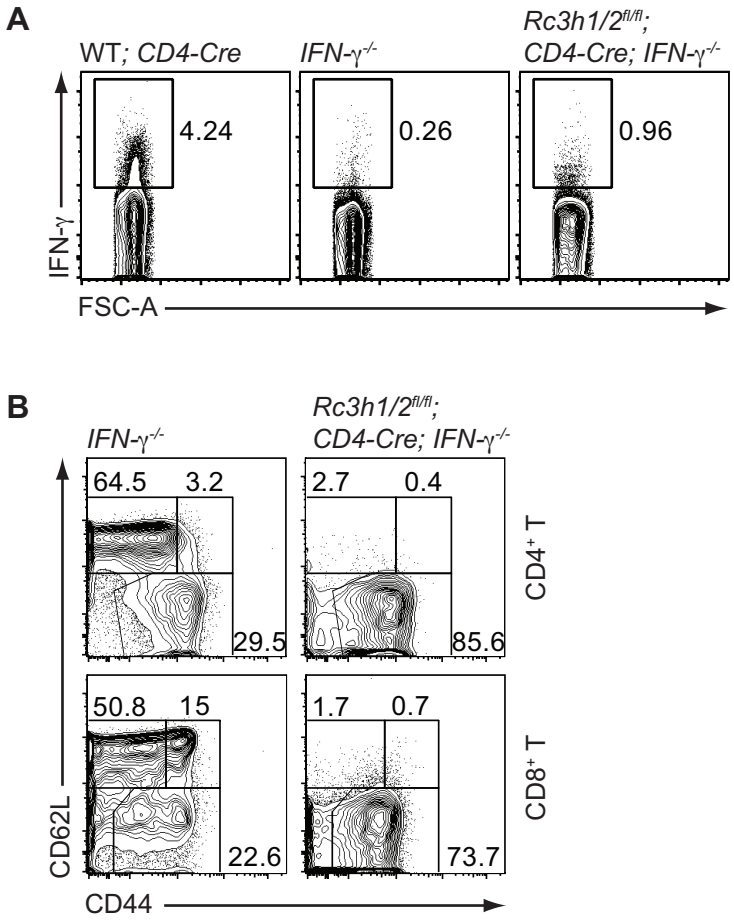

Figure 46: IFN-γ is not responsible for the effector-like T cell phenotype caused by loss of Roquin-1/2. (A) Representative contour plots showing IFN-γ production after stimulation of total splenocytes for 5 h with PMA and ionomycin. (B) Representative contour plots from $CD4^+$ (upper panel) or $CD8^+$ (lower panel) splenocytes, showing naive ($CD62L^{hi}$ $CD44^{lo}$), effector-like ($CD62L^{lo}$ $CD44^{hi}$) or memory-like ($CD62L^{hi}$ $CD44^{hi}$) T cells. Genotypes are indicated in the figure and data are representative for two (A), three (B, control) and four (B, IFN-γ TKO) individual mice per genotype.

Although IFN-γ played a more dominant role in the development of effector T cells in the san/san mouse compared to Icos signaling [157,159], the ablation of neither IFN-γ nor Icos was able to rescue the activation phenotype in *Rc3h1/2$^{fl/fl}$; CD4-Cre* mice. This suggests that other factors are causing this aberrant T cell activation in *Rc3h1/2$^{fl/fl}$; CD4-Cre* mice. However, loss of Roquin-1 and Roquin-2 might also reduce the activation threshold of $CD4^+$ and $CD8^+$ T cells rendering them sensitive to even low stimuli, which might lead to constant activation.

Similar to the Icos TKOs, all IFN-γ TKOs showed enhanced frequencies of Tfh cells without immunization. Two of four animals were able to spontaneously generate GC B cells (Figure 47 A–B). However, the ability to induce GC B cells did not correlate with age. Consecutive cryo-sections of spleens from IFN-γ TKOs were then analyzed to compare the degree of destruction in spleens of *Rc3h1/2*-deficient mice. Interestingly, also reducing IFN-γ signaling was sufficient to largely rescue the splenic architecture (Figure 47 C). In some but not all animals, $B220^+$ cells formed a clear B cell zone, surrounded by metallophilic macrophages (MOMA-1^+). The B cells, however, did not fully localize in the marginal zone. Furthermore, IFN-γ TKOs clearly developed ANAs, correlating with the rescue in the splenic architecture, as could similarly be seen in Icos TKOs. In contrast to Icos TKOs, however, all IFN-γ TKOs developed auto-antibodies with an age of only 11 weeks (Figure 47 D).
Although these investigations included only few mice of the respective genotypes, the phenotypes of the analyzed individuals indicated that loss of IFN-γ was sufficient to rescue the follicular organization in the spleen of IFN-γ TKOs. In an almost intact splenic environment, loss of Roquin-1 and Roquin-2 indeed caused auto-antibody formation by increasing Tfh and GC B cells. However, reducing IFN-γ signaling did not reverse other double knockout phenotypes such as increased numbers of effector-like T cells ($CD62L^{lo}$ $CD44^{hi}$) and reduced numbers of naive T cells ($CD62L^{hi}$ $CD44^{lo}$) (Figure 29). Although IFN-γ and Icos signaling (section 8.2.14) contributed to several phenotypes, which developed due to loss of Roquin protein function, the molecular origin of these phenotypes is probably caused by a complex interaction of several deregulated signaling pathways.

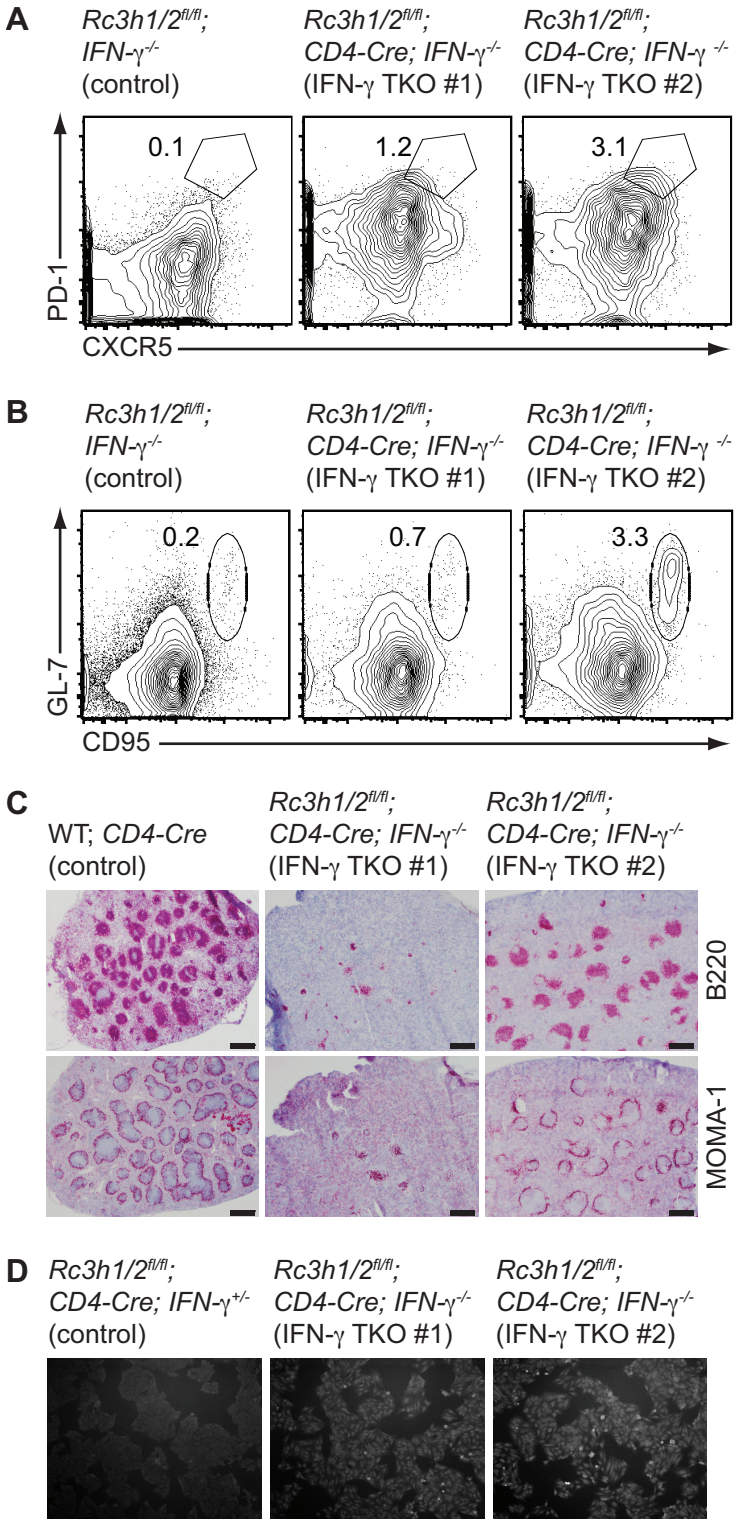

Figure 47: Rescue of splenic architecture supports auto-antibody formation in IFN-γ TKOs. (A–B) Representative contour plots of splenic Tfh cells (PD-1^{hi} CXCR5^{hi}), pre-gated on CD4^{+} (A) and of splenic germinal center B cells (GL-7^{hi} CD95^{hi}), pre-gated on B220^{+} (B). (C) Consecutive cryo-sections from spleens, stained for B220 and MOMA-1. The black bar represents 500 µm. Cryo-sections and stains were performed by Prof. Dr. Mathias Heikenwälder and Jessica Zöller, Institute for Virology, Technische Universität München/Helmholtz Zentrum München. (D) Indirect immunofluorescence for antinuclear antibodies (HEp-2). Each panel represents one animal with the indicated phenotype.

9 Discussion

In this research project, the roles of Roquin-1 and Roquin-2 were investigated *in vitro* and *in vivo*. An important finding was the discovery of a *cis*-element in the 3'UTR of ICOS mRNA for effective Roquin-1 and Roquin-2 protein binding. Furthermore, the work addressed the functions of Roquin-1 and Roquin-2 *in vivo* by investigating loss of function in mice with conditional deletions. These studies revealed functional redundancy of Roquin-1 and -2 in the control of the co-stimulatory molecules Icos and Ox40, the latter one being a novel mRNA target of both proteins. Combined deletion of Roquin-1/2 proteins augmented Ox40 co-stimulation through the alternative NF-κB pathway and increased Irf4 transcription factor levels. This work further demonstrated a crucial role for Roquin-1 and Roquin-2 proteins in the prevention of autoimmunity and the maintenance of tolerance by impeding inappropriate T cell activation and Tfh cell differentiation.

9.1 The RNA-binding of Roquin-1 and Roquin-2

As described in the introduction (section 5.2.1) RNA-binding proteins recognize specific *cis*-elements mostly in the 3'UTR of their target mRNAs and interact with the mRNA via special RNA-binding domains such as zinc fingers. Recently, the newly defined ROQ domain in Roquin-1 had been proposed to be involved in RNA binding. Although immunoprecipitation experiments showed that the ROQ domain was important in the interaction of Roquin-1 with ICOS mRNA [149], the results could not exclude an indirect contribution such as the binding via cellular co-factors. Furthermore, the nature of the recognition motif for protein–RNA interaction remains to be identified. This research work therefore addressed the role of the ROQ domain in direct protein–RNA interaction, which is discussed below. Furthermore, the search for recognition elements in the ICOS mRNA revealed remarkable insights into the structure- and sequence-requirements for protein–RNA interaction, as described in the following sections.

9.1.1 Roquin-1 recognizes a *cis*-element in the 3'UTR of ICOS mRNA

The repression of ICOS mRNA by Roquin-1 and -2 proteins depends on the presence of the 3'UTR, as ICOS CDS alone does not respond to Roquin-1 regulation [149]. Scanning the 3'UTR for conserved protein-binding sites, however, did not reveal recognition motifs such as AREs,

albeit six regions in the 3'UTR of ICOS were highly conserved between mouse and human [119]. Therefore, previous studies tested the response of three larger regions of the 3'UTR in the context of a reporter construct to Roquin-1 overexpression. The last part of the 3'UTR, containing a putative miR-101 binding site, was well repressed by Roquin-1. However, a shortened 47-nt sequence containing this miR-101 binding site was only moderately repressed by Roquin-1. Mutating the miR-101 binding site led to a non-significant residual repression [119]. Due to this correlation, a mechanism was suggested, in which Roquin-1 repressed ICOS mRNA by interacting with miR-101 to induce mRNA decay. However, subsequent studies in cells, which were devoid of mature miRNAs and therefore impaired in miRNA-mediated gene silencing, clearly demonstrated that Roquin-1-mediated repression of ICOS mRNA functions independently of the miRNA pathway [149]. We therefore assumed that direct Roquin-1 protein interaction with the ICOS mRNA might be the first step in the targeting and regulation of ICOS. Indeed, I could demonstrate in EMSAs that recombinant Roquin-1 protein directly binds to *in vitro* transcribed ICOS mRNA, exhibiting a binding preference for the ICOS 3'UTR (Figure 7). Furthermore, I showed that Roquin-1 binds to an element of so far unknown sequence or structure, located between 100 and 200 nucleotides downstream of the stop codon in the ICOS 3'UTR (Figure 11 and Figure 12). Interestingly, we noticed that Roquin-1 had a general affinity for mRNA, as indicated by the disappearance of free ICOS CDS mRNA at very high protein concentrations (Figure 7). Such a behavior could be explained by a bimodal binding kinetic, in which Roquin-1 generally binds to mRNA with a low binding affinity, but has higher affinity for its responsive *cis*-element within a target mRNA. In addition, specific binding seemed to occur in a cooperative manner by sequential binding and shifting of the mRNA with increasing protein concentrations. This raises the possibility that Roquin-1 has more than one binding site in the ICOS 3'UTR, which is also in line with previous studies, mapping a Roquin-1 binding site at the 3'end of the UTR, adjacent to the miR-101 binding site [155]. It might be deceptive to focus on the 47-nt sequence, containing the miR-101 binding site, while ICOS repression did not depend on the miRNA pathway. Nevertheless, the last part of the 3'UTR containing the 47-nt element as well as the element mapped in the present work (Figure 12) could both be independently bound and be regulated by Roquin-1 [119,149,155]. The fact that the 47-nt element on its own was much less repressed than the larger region containing the 47-nt element implies that additional co-factors might recognize sites, which are not present in these 47 nts. Indeed, some cell lines are unable to support Roquin-1-mediated ICOS repression in overexpression experiments, indicating a need for co-factors, which are not present in these

cell lines (unpublished observation). It is therefore very likely that Roquin-1 requires additional factors *in vivo*, which bind to further *cis*-elements in the 3'UTR of ICOS and contribute to efficient ICOS repression.

Importantly, I could find that Roquin-1 binding to the ICOS mRNA containing a *cis*-element did not depend on the length of the transcript (Figure 7 and Figure 11). While sequences of the 3'UTR, which were mapped for binding, confer a basal level of repression, the efficiency of repression increased upon extending the 3'UTR further [149]. On the one hand, this could reflect the need for co-factor binding, which essentially contributes to ICOS repression. On the other hand, the presence of several *cis*-elements in the extensively long 3'UTR of the ICOS mRNA seems physiologically reasonable, given that cooperation of a number of *cis*-elements together determine the rate of mRNA decay [123]. ICOS is a factor especially needed upon activation of T cells and proliferating cells express mRNAs with shortened 3'UTRs [129]. The expression of short 3'UTR devoid of any *cis*-elements seems to be a suitable mechanism to avoid repression, in a setting of acute T cell activation when there is need for ICOS signaling. In resting cells, Roquin-1 might be able to fully repress ICOS by cooperating with other *trans*-acting factors or by occupying several binding motifs to induce effective mRNA decay.

9.1.2 Characterizing the *cis*-element in the ICOS 3'UTR further

Despite localizing a crucial Roquin-1 recognition element to 100 nucleotides in the ICOS 3'UTR (Figure 12), we still do not know the sequence or structure characteristics of this element. Identifying the exact *cis*-element is important for the understanding of the protein–RNA interaction and will facilitate the identification and characterization of new targets, specified by the presence of the Roquin-1 *cis*-element. Therefore, a new research project has been started by a colleague to address these open questions and to further examine the characteristics of the *cis*-element by crosslinking Roquin-1 to the mRNA *in vitro* and in cells. Moreover, it is important to functionally test the minimal response element. It is necessary therefor to inhibit functional responses by mutating essential nucleotides. However, the binding may not only involve a certain sequence but also structure determinants, hampering the mutagenesis approach.

Computational tools cannot reliably predict potential secondary structures larger than 100 nts. Therefore we applied SHAPE [153] for obtaining the preferred secondary structure of 100-nt fragments of the ICOS mRNA, to set the molecular basis for future mutagenesis studies. We focused on three fragments of the ICOS mRNA, including the 100-nt binding element

(700–800) mapped in EMSAs (Figure 12) and two 100-nt long sequences 5' (600–700) and 3' (800–900) to the mapped element. Interestingly, all computational predictions were slightly different from the structures revealed by SHAPE, except for one of the suggested foldings for the 700–800 *cis*-element, which was identical to the SHAPE result. Furthermore, only the 700–800 *cis*-element exhibited a two-finger-like structure with a shorter (15 nts) and a longer (39 nts) hairpin, while the other fragments folded in long or bulgy structures (Figure 14). Together these still preliminary data strongly suggest that the two-finger-like configuration of the 700–800 *cis*-element might constitute a novel structural *cis*-element for protein recognition and binding.

9.1.3 The ROQ domain is a new RNA-binding domain

In this research work, I could demonstrate that the amino-terminus of Roquin-1, comprising RING finger, ROQ domain and zinc finger, can directly bind to its mRNA target (section 8.1). As will be discussed below, the zinc finger does not play an essential role in RNA binding and immunoprecipitation experiments did not reveal an important role for the RING finger in RNA binding [149]. I therefore conclude that the ROQ domain is a novel RNA binding domain, indispensable for the binding and subsequent repression of Roquin-1 mRNA targets. Nevertheless, the RING and zinc fingers may help in ICOS mRNA binding or regulation.

Deletion of the zinc finger in Roquin-1 led to a marked decrease in protein–RNA interaction in overexpression studies, while point mutations in the zinc finger cause only a mild negative effect on ICOS mRNA repression [150]. *In vitro*, the mutation of the zinc finger did not significantly affect the binding affinity in EMSA experiments (Figure 8 B). We therefore assume that the zinc finger can contribute to RNA-binding, but is not essential. Such zinc finger modules normally act in tandem to exert RNA-binding activity. The presence of only one zinc finger in Roquin-1 and Roquin-2 might therefore exert slightly different functions. It might help to bind multiple Roquin-1 protein molecules to the same ICOS mRNA. A modular structure with more than one RNA-binding domains is common to many RNA-binding proteins [168]. Such modules enable the protein to bind to its target mRNA with higher affinity, thereby increasing the specificity for a substrate among an enormous diversity of mRNAs [168]. Although the zinc finger mutations in Roquin-1 did not alter the RNA binding affinity *in vitro* (Figure 8 B), it might specify the function of Roquin-1 *in vivo*.

Roquin-1 and Roquin-2 also contain a RING finger 3' to the ROQ domain and the zinc finger. The molecular function of the RING finger had been investigated, however, the exact role of

the RING finger has not been defined yet. Auto-ubiquitination could not be observed, which indicates that the RING finger might not exert E3 ligase activity on Roquin-1 itself [150]. Still, deletion of the RING finger in Roquin-1 clearly reduced ICOS protein repression [149]. One possibility, which has not been addressed so far, is the involvement of the RING finger in RNA-degradation. Only recently, the turnover of AU-rich cytokine mRNAs had been linked to ubiquitination. The impairment of protein ubiquitination inhibited ARE-mediated decay [169]. Moreover, a new ubiquitin ligase (MEX-3C) was shown to directly bind the HLA-A2 mRNA and to post-transcriptionally regulate the mRNA stability, while it also repressed HLA-A2 protein expression [170]. This suggests that mRNA decay and down-regulation of target proteins are two processes that are linked.

Finally, NMR (Nuclear magnetic resonance) or crystal structures of Roquin-1 would further elucidate the relation and functional dependence of the single protein domains to each other.

9.2 Roquin-1 and Roquin-2 serve redundant functions

Recent work has contributed a lot to the understanding of Roquin-1 function in the immune system. The functions of its paralog Roquin-2, however, were largely unknown. Roquin-2 is typically expressed at lower levels than Roquin-1 in different tissues and importantly in T cells (Figure 20 and Figure 25), and Roquin-2 was therefore assumed to play a minor role in T cell homeostasis. However, this work demonstrates a critical importance of Roquin-2 as an evolutionary safeguard against autoimmunity, compensating Roquin-1 function in post-transcriptional gene regulation.

9.2.1 Redundancy and lateral inhibition of Roquin-1 and Roquin-2

The severe lupus-like autoimmune phenotype in *Rc3h1*$^{san/san}$ mice [39] conflicts with the normal immune system of *Rc3h2*$^{fl/fl}$*; CD4-Cre* mice (section 8.2.4) and the relatively mild immune phenotypes of Roquin-1 deficiency in T, B and hematopoietic cells [120]. We therefore speculated that the highly conserved Roquin-2 paralog substitutes for loss of Roquin-1 in *Rc3h1*$^{fl/fl}$*; CD4-Cre* mice, while the presence of Roquin-1^{san} protein might hinder Roquin-2 in rescuing autoimmune phenotypes.

Indeed, I could show *in vitro* that Roquin-2 is fully capable of and equally efficient in performing key functions of Roquin-1. Roquin-2 could bind to ICOS and Ox40 mRNA independently of Roquin-1 (Figure 16 and Figure 42) and exhibited the same preference for binding to the 3'UTR of ICOS mRNA (Figure 16). Direct RNA binding may be the first step

in Roquin-1-dependent ICOS mRNA repression. Roquin-1 further interacts with members of the decapping machinery such as Edc4 to induce ICOS mRNA decay [149]. Likewise, Roquin-2 was able to directly interact with Edc4 independently of Roquin-1, as shown by immunoprecipitation experiments in MEF cells deficient for *Rc3h1*, *Rc3h2* or both genes (Figure 31). Furthermore, both paralogs co-localized to P bodies, as shown by overexpression in A549 cells ([150] and Figure 21). Finally, overexpression of both proteins in primary $CD4^+$ T cells demonstrated that both proteins could equally well down-regulate ICOS or Ox40 expression levels (Figure 31 and Figure 42). Thus, Roquin-2 resembles Roquin-1 in direct target mRNA binding, localization and interaction with the decapping factor Edc4 to repress target gene expression.

However, functional compensation of Roquin-2 cannot completely explain the phenotypes observed in the different mouse models. We therefore propose a model that includes an inhibitory regulation of Roquin-1/2 proteins to explain the observed compensation of partial loss-of-function in some mouse models (Figure 48). This inhibitory effect is apparent when comparing the levels of the post-transcriptional target Icos on T cells from *Rc3h1*$^{fl/fl}$*; CD4-Cre* mice, *Rc3h2*$^{fl/fl}$*; CD4-Cre* mice, *Rc3h1/2*$^{fl/fl}$*; CD4-Cre* mice or *Rc3h1*$^{san/san}$ mice. Notably, the protein levels of Roquin-1, Roquin-1^{san} or Roquin-2 were not altered in T cells from mice with the different genotypes (Figure 29, [157] and Figure 25, respectively) and Roquin-1 as well as Roquin-1^{san} proteins were five times more abundant than Roquin-2 (section 8.2.4 and [157]).

The removal of Roquin-2 protein had no effect on Icos expression. Surprisingly however, the ablation of *Rc3h1* caused only a moderate up-regulation of Icos, although it removed five times more Roquin protein. Combined loss of Roquin-1/2 on the other hand greatly enhanced Icos expression levels. This indicates that in wild-type cells Roquin-2 does not contribute to Roquin-1/2 function. Instead its function appears either inhibited or the protein cannot compete with the much greater amount of Roquin-1 protein. However, in *Rc3h1*-deficient cells, Roquin-2 displays an increased activity, as it is not inhibited anymore. It is now able to compensate for most of the Roquin-1 loss-of-function and thereby prevents major phenotypes of autoimmunity. Interestingly, in T cells from *Rc3h1*$^{san/san}$ mice, Icos was expressed at higher levels compared to T cells from *Rc3h1*$^{fl/fl}$*; CD4-Cre* mice but at lower levels compared to T cells from *Rc3h1/2*$^{fl/fl}$*; CD4-Cre* mice (as judged from [39]). This effect can be explained with the Roquin-1^{san} protein retaining the inhibitory regulation of Roquin-2 function at a similar or reduced extent. At the same time, the Roquin-1^{san} protein loses most of its activity in post-transcriptional gene regulation, as exemplified by the high levels of Icos. Therefore, Roquin-2

protein cannot complement the hypomorphic function of the Roquin-1^{san} protein [39,119], which is still present at five-fold levels compared to Roquin-2. The nature of the inhibitory effect is currently unclear, but a competitive, dominant negative or negative feedback mechanism would be possible.

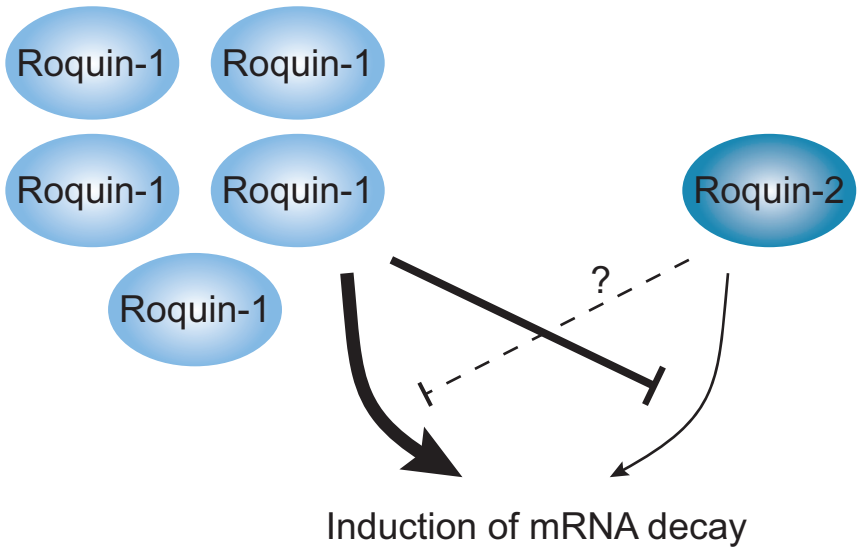

Figure 48: Roquin-1 impairs Roquin-2 function. This conclusion is based on the analyses of mice deficient for Roquin-1 [120], Roquin-2 or both proteins (section 8.2.4 and 8.2.6) as well as *Roquin-1$^{san/san}$* mice [39]. The conservation of both proteins implies that Roquin-2 could also impair Roquin-1 function, but to a minor extent, because of low Roquin-2 protein expression levels. Consequently, Roquin-2 can only exert its function in the absence of Roquin-1 constituting an important safety mechanism in the prevention of autoimmunity.

9.2.2 Evolutionary role of *Rc3h1* gene duplication

Low Roquin-2 expression levels in peripheral T cells were sufficient to suppress those alterations in *Rc3h1$^{fl/fl}$; CD4-Cre* mice that developed in *Rc3h1$^{san/san}$* or *Rc3h1/2$^{fl/fl}$; CD4-Cre* mice. These include that T cells become excessively activated and that CD4^{+} T cells are driven towards a Tfh cell phenotype, causing ANA formation in san/san mice even in the absence of immunization. This indicates that the *Rc3h1/Rc3h2* gene duplication ensures tight control of T cell activation and Tfh cell differentiation to prevent autoimmunity.

However, full redundancy is presumably unstable in evolution due to the lack of selective pressure. Novak et al. therefore have established several assumptions under which genetic redundancy can persist in evolution [171]. In the light of functional redundancy of Roquin-1 and Roquin-2 as well as lower expression levels of Roquin-2 compared to Roquin-1 the

evolutionary advantage of gene duplication may not involve diversification of both proteins in the immune system, but rather improve adaptation of protein expression levels. In this scenario, Roquin-2 can only persist in evolution, if the mutation rate is lower in Roquin-2 than in Roquin-1. We have detected a non-redundant role of Roquin-2 though: complete lack of Roquin-2 causes postnatal death in mice (section 8.2.3). Therefore, selective pressure is high to maintain Roquin-2. In regard to Roquin-2-function this could imply that Roquin-2 does exert – so far unknown – essential molecular functions outside the immune system, which ensures evolutionary stability. Functional diversification might have occurred in the carboxy-terminal region, which is less conserved between Roquin-1 and Roquin-2 (Figure 15). In addition, Roquin-2 comprises functions in the immune system redundant to Roquin-1. Here, Roquin-2 plays a minor role in healthy mice. However, in the case of loss of Roquin-1-function (*Rc3h1*$^{fl/fl}$*; CD4-Cre*), Roquin-2 can substitute for Roquin-1 and prevent the onset of autoimmunity.

9.3 Role of Roquin-1 and Roquin-2 in autoimmune disease

Autoimmune diseases can be classified into organ-specific and systemic diseases. Systemic diseases such as SLE often display multiple characteristics and are initiated by many different triggers. Due to these diverse phenotypes, it was generally assumed that SLE might never be caused by just one single genetic mutation [117]. The san/san mouse is an outstanding counter-example and ascribes enormous importance to Roquin-1 and Roquin-2 in the control of autoimmune disease by directing T helper cell differentiation.

9.3.1 Do Roquin-1 and Roquin-2 intrinsically control Tfh cell differentiation?

We found that combined loss of Roquin-1 and Roquin-2 in T cells led to the spontaneous formation of Tfh and GC B cells (Figure 32). The increase of germinal center B cells in *Rc3h1/2*$^{fl/fl}$*; CD4-Cre* mice is induced via cell-extrinsic mechanisms such as cytokines or increased co-stimulation by Tfh cells, since we investigated T cell-specific loss of function. Likewise, also the development of GC B cells in san/san mice was mostly due to cell-extrinsic mechanisms, although the san-mutation is not restricted to T cells [118]. In contrast, Tfh cells in *Rc3h1*$^{san/san}$ mice accumulated in a T cell intrinsic manner [111].

Nakayamada et al. recently described a transitional stage between Th1 and Tfh cells [108]. As plasticity of T helper cell subsets seems to be an important feature in immune responses, we wanted to investigate the role of Roquin-1 and Roquin-2 in controlling the cellular transition

point between Th1 and Tfh cells. Adoptive transfer experiments showed that Th1 cells lacking Roquin-1/2 proteins proliferated heavily and were indeed able to convert into Tfh cells, while wild-type Th1 cells could not (Figure 36). Furthermore, these pre-activated T cells deficient for Roquin-1/2 were actually potent to induce a concomitant increase in GC B cells (Figure 36). However, previous publications have shown that *in vitro* cultured cells in a variety of conditions could adopt Tfh cell differentiation after immunization [163]. Thus, it remains to be investigated, if loss of Roquin-1/2 proteins also drives cells from other T helper cell subsets into a Tfh cell phenotype.

Importantly, the spontaneous differentiation into Tfh cells did not require *ex vivo* T cell activation, since it was also observed after adoptive transfer of sorted naive $CD4^+$ T cells from *Rc3h1/2$^{fl/fl}$; CD4-Cre* mice (Figure 37). Interestingly, almost all transferred naive cells deficient for *Rc3h1/2* up-regulated the activation marker CD44, while transferred wild-type cells stayed predominantly naive ($CD62L^+$). This indicates that loss of both Roquin-1 and Roquin-2 led to an enormous reduction of the activation threshold of these T cells, notably in the absence of antigen.

Collectively, these data suggest a model in which the combined loss of Roquin-1/2 proteins or the impaired function of Roquin-1^{san} protein triggers Tfh cell differentiation. Within this differentiation a de-repression of several known and unknown Roquin-1/2 targets may functionally cooperate. We envision a concept of inappropriate co-stimulation at the naive T cell stage, via the increased expression of Icos and Ox40 due to loss-of-function of Roquin proteins, which initiate the Tfh cell differentiation. These two co-stimulatory receptors normally expand activated T cells and control the size of the effector T cell pool. Inappropriate co-stimulation may therefore select those T cells for effector T cell differentiation that receive increased TCR-signals due to a certain degree of self-reactivity. The cooperation of the self-reactive TCR and inappropriate co-stimulation signals may then lead to aberrant T cell activation and subsequent Tfh cell differentiation.

9.3.2 How can increased co-stimulation drive Tfh cell commitment?

To identify the molecular cause for the spontaneous development of follicular helper T cells in *Rc3h1/2$^{fl/fl}$; CD4-Cre* mice, we examined the expression of Bcl6 and Irf4, two critical transcription factors involved in Tfh cell differentiation [69-71,105]. While the expression of Bcl6 is not considerably affected in the double knockout situation (Figure 32), Irf4 levels were markedly elevated in cells deficient for Roquin-1/2 proteins (Figure 40). Increased Irf4

activity may augment Tfh cell numbers, since *Irf4*-deficient T cells are greatly impaired in this differentiation program [104,105].

Irf4, however, is not only involved in Tfh cell differentiation but also drives Th17 cell commitment [90,104,105]. The observed increased Tfh and Th17 differentiation in *Rc3h1/2*-deficient cells is therefore a likely consequence from the up-regulation of Irf4 protein levels (Figure 38). It is furthermore described that the Th17 cell differentiation program reciprocally influences Treg differentiation [86,87] and that Irf4 might even be involved in the conversion of Treg cell into Tfh cells [66]. Irf4 can also directly bind to the promoter of Icos and induce its expression [91], which could additionally explain the exceedingly high Icos levels in *Rc3h1/2*-deficient T cells. Interestingly, the Irf4-binding protein Def6 was shown to negatively regulate Irf4 [172] and deficiency of Def6 correlated with systemic lupus-like autoimmunity, characterized amongst others by the accumulation of effector T cells [173]. In *Def6*-deficient mice these activated T cells are impaired to undergo apoptosis, which would be crucial to maintain T cell homeostasis.

Importantly, Irf4 is a target of NF-κB signaling [55] and we could demonstrate spontaneous activation of the NF-κB pathway in *Rc3h1/2$^{fl/fl}$; CD4-Cre* mice (Figure 40). Loss of Roquin-1/2 proteins especially induced the alternative NF-κB pathway (Figure 40 C–D), presumably via de-repressed levels of the novel mRNA target Ox40. Ox40 was potent to induce p100 to p52 processing but not an increase in Irf4 expression after stimulation of wild-type cells with an agonistic antibody against Ox40 (Figure 41 C). It is nevertheless likely that Irf4 levels are increased due to Ox40 in combination with other signals in *Rc3h1/2*-deficient cells. At this point it is not clear whether Irf4 is also a direct target of Roquin-1/2 proteins.

In addition, Ox40 has been implicated in a large number of autoimmune and inflammatory diseases like experimental autoimmune encephalomyelitis, arthritis or diabetes [42]. A single dose of an agonistic antibody against Ox40 was even sufficient to break existing tolerance in $CD4^+$ T cells and to restore T cell function [45]. While deletion of Ox40 together with CD30 rescued lethal autoimmunity in Foxp3-deficient mice [174], transgenic mice expressing OX40L on dendritic cells strongly increased the appearance of $CD4^+$ T cells with a $CD62L^{lo}$ phenotype, presumably being Tfh cells, which accumulated in germinal centers after immunization [175]. Another early study linked failure of CXCR5 up-regulation to the compromised function of Ox40 in *CD28*-deficient mice [16]. This study, however, did not address a possible contribution of Icos to the up-regulation of CXCR5 expression that was recently proposed [96].

Ox40 may therefore play a critical role in the development of Tfh cells, especially as both Icos and Ox40 overlap in down-stream signaling [25]. Icos and Ox40 activate the PI3K signaling pathway, while Ox40 additionally induces the NF-κB pathway [166,176,177]. Not only the NF-κB pathway and Irf4 activation are linked to Tfh cell development. Remarkably, it was recently demonstrated that the amount of PIP_3 generated by PI3K in an immune response determined the magnitude of the germinal center reaction [167]. Together these data imply that both Icos and Ox40 co-stimulation can induce Tfh differentiation and effector T cells in *Rc3h1/2*–deficient $CD4^+$ T cells, via redundant and cooperative down-stream signaling.

9.3.3 Which factors cause the splenic disorder in *Rc3h1/2*-deficient mice?

Spontaneous formation of Tfh and GC B cells in san/san mice is accompanied by the development of anti-nuclear antibodies [39]. We show that combined Roquin-1 and Roquin-2 deficiency in T cells led to spontaneous Tfh and GC B cell differentiation, but did not induce anti-nuclear antibodies (section 8.2.8). This can be due to several reasons. On the one hand the observed changes in san/san mice may require the presence of the mutation in cells outside of the T cell compartment. On the other hand, we propose that profound perturbation of the splenic microarchitecture in *Rc3h1/2$^{fl/fl}$; CD4-Cre* mice may no longer permit progression towards a lupus-like disease (Figure 33 and Figure 34). We demonstrated that already in young (3 weeks) mice, follicular structures were greatly diminished and intact follicular structures were hardly detectable (Figure 34). Furthermore, stromal cells such as ER-$TR7^+$ reticular fibroblasts were delocalized across the spleen in young animals and somewhat dispersed in older ones. In addition, the white pulp was strongly reduced in the spleen (Figure 33 B and C). The organization of stromal cells in the white pulp is indeed crucial for T and B cell homing, survival and co-stimulation [178].

However, at this point we do not know which *trans*-acting factor interferes with the follicular organization. We assume that inaccurate co-stimulation accompanied with altered cytokine production by chronically activated T cells may contribute to the splenic disorder, as will also be discussed in the following sections. It is furthermore likely that the decreased numbers of B cells in *Rc3h1/2$^{fl/fl}$; CD4-Cre* mice (Figure 32 E) do not provide sufficient lymphotoxin signals. Lymphotoxin receptor signaling is required for the development and maintenance of the microarchitecture in the white pulp [161]. Testing those factors, which are crucial for the splenic organization, will certainly reveal the molecular cause for the disrupted splenic architecture in *Rc3h1/2$^{fl/fl}$; CD4-Cre* mice.

9.3.4 Can loss of Icos reverse the Roquin-1/2-knockout phenotype?

Deregulated Icos levels and spontaneous formation of Tfh cells are two hallmark phenotypes observed in the san/san mouse. Both Icos and its paralog CD28 are essential for the GC reaction [22,23,96], but are temporally separated in their expression and function (section 5.1.2). While loss of CD28 co-stimulation partially corrected *sanroque*-dependent Tfh cell accumulation, the *sanroque* alleles in *CD28*$^{-/-}$ mice restored Tfh formation upon immunization comparable to wild-type levels. These effects were reverted upon additional ablation of the Icos ligand, and *Rc3h1*$^{san/san}$ mice deficient for both CD28 and Icos ligand no longer mounted a proper GC response upon SRBC (sheep red blood cells) immunizations [118]. This implied that Roquin^{san} broke the compartmentalization of CD28 and Icos signaling and that de-repressed Icos levels contributed to the Tfh-induced pathology of *Rc3h1*$^{san/san}$ mice. However, it is very likely that factors other than Icos critically contributed to the phenotypes of *Rc3h1*$^{san/san}$ mice, since Icos deficiency did not prevent the development of autoimmunity. Recent work demonstrated that complete loss of Icos in *Rc3h1*$^{san/san}$ mice did not rescue but led to the occurrence of whole anti-nuclear antibodies in *Rc3h1*$^{san/san}$ mice [159]. Icos deficiency in *Rc3h1*$^{san/san}$ mice also failed to rescue the expansion of effector-like T cells [159].

Similarly, ablation of Icos in *Rc3h1/2*$^{fl/fl}$*; CD4-Cre* mice did not reverse the activation phenotype of CD4$^+$ and CD8$^+$ T cells (Figure 43). Strikingly, loss of Icos signaling did also not impede the spontaneous development of Tfh cells (Figure 44). This remarkable finding is the first evidence of a possible bypass mechanism to avoid the dependence on Icos signaling for the development of Tfh cells. We speculate that elevated Ox40 levels in the Icos TKO may substitute for loss of Icos. These assumptions are supported by the fact that both Icos and Ox40 signal share the down-stream PI3K signaling pathway [176,177]. As had been mentioned before, the amount of PIP_3 generated by PI3K seemed to be detrimental for the extent of the germinal center response [167] and Ox40 was also shown to be involved in a number of autoimmune diseases [42]. In addition, both Icos and Ox40 are important for the survival of effector T cells [43,179] and constitutive Ox40 triggering through transgenic expression of the Ox40 ligand on T cells leads to massive induction of effector-like CD4$^+$ but not CD8$^+$ T cells [44]. This implies that Ox40 signaling may strongly contribute to the effector like phenotype at least of CD4$^+$ T cells. It would be exciting to investigate loss of Ox40 signaling in the Roquin-1/2 double knockout situation. The results would elucidate the effect of Ox40 especially in regard to the T cell activation phenotype.

9.3.5 What is the role of IFN-γ in *Rc3h1/2*-deficient mice?

In addition to Icos and Ox40 mRNA, Ifng mRNA was recently proposed to be a potential new target of Roquin-1. In *Rc3h1*$^{san/san}$ mice, IFN-γ was shown to enhance short-lived effector CD8$^+$ T cells (SLECs) with increased effector function [157]. However, investigating IFN-γ protein levels in Th1 differentiation experiments, we cannot readily confirm IFN-γ as a direct target of Roquin proteins. Loss of Roquin-1/2 did neither enhance IFN-γ levels nor the number of IFN-γ-producing cells (Figure 38). In addition, the so far presented evidence cannot rule out indirect stabilization of Ifng mRNA in SLECs from san/san mice. Such stabilization of the mRNA of IFN-γ and other cytokines has been reported in the context of Ox40 stimulation [164]. We therefore assume that elevated co-stimulation by receptors such as Ox40 or Icos aberrantly enhances IFN-γ production.

We also assessed the role of IFN-γ in the accumulation of effector and Tfh cells in *Rc3h1/2*$^{fl/fl}$*; CD4-Cre* mice. IFN-γ signaling was not only shown to influence CD8$^+$ effector like properties [157], but was also demonstrated to be involved in the pathogenic accumulation of Tfh cells and spontaneous generation of germinal centers [159]. Surprisingly however, loss of IFN-γ signaling in *Rc3h1/2*$^{fl/fl}$*; CD4-Cre, IFN-γ*$^{-/-}$ mice did neither reverse the accumulation of effector CD4$^+$ and CD8$^+$ T cells nor the spontaneous formation of Tfh cells observed in *Rc3h1/2*-deficient mice (Figure 46 and Figure 47). However, several *sanroque* phenotypes were only partially reversed by the genetic removal of different co-stimulatory receptors or cytokines such as IFN-γ. This points at a cooperation of several factors in the development of the lupus-like autoimmune disease.

Importantly, IFN-γ influences the splenic organization and continuous administration of large amounts of IFN-γ to rats causes severe alterations of the splenic architecture [180]. Indeed, ablation of IFN-γ restored the follicular structure in spleens of IFN-γ TKO mice to a great extent (Figure 47) and consequently all of these animals developed ANAs with the age of only 11 weeks. Furthermore, loss of Icos co-stimulation was also sufficient to normalize the splenic architecture in Icos TKO mice. Therefore, we postulate the model that de-repressed co-stimulation in *Rc3h1/2*$^{fl/fl}$*; CD4-Cre* mice causes a highly activated T cell phenotype with spontaneous formation of Tfh and GC B cells. However, ANAs do not occur due to the disrupted splenic architecture presumably caused by effector cytokines such as IFN-γ, which are overly produced due to enhanced co-stimulation.

9.4 Conclusion

This work revealed direct protein–RNA interaction via the amino-terminal ROQ domain as the first step of the molecular mechanism of mRNA target repression by Roquin family proteins. In addition, functional redundancy was demonstrated for the paralogs Roquin-1 and Roquin-2 in the repression of the known and novel mRNA targets Icos and Ox40. *In vivo* analyses further revealed the crucial functions of Roquin-1 and Roquin-2 in T cell activation and differentiation and consequently in the prevention of autoimmunity.

Most importantly, this work solved a current paradox: The san mutation in Roquin-1 caused a severe autoimmune phenotype, but the complete loss of Roquin-1 did not. Our findings demonstrated compensation of Roquin-1 by Roquin-2, involving a previously unappreciated dominant-negative effect of Roquin-1 on Roquin-2 protein function. Such redundancy is a fundamental concept in evolution, establishing a safety mechanism to prevent fatal diseases such as autoimmunity.

10 References

1. Murphy, K., Travers, P. & Walport, M. *Janeway's immunobiology*. (Garland Science, 2008).
2. Hoffmann, J. A. Phylogenetic Perspectives in Innate Immunity. *Science* **284**, 1313–1318 (1999).
3. Oettinger, M. A., Schatz, D. G., Gorka, C. & Baltimore, D. RAG-1 and RAG-2, adjacent genes that synergistically activate V(D)J recombination. *Science* **248**, 1517–1523 (1990).
4. Schatz, D. G., Oettinger, M. A. & Baltimore, D. The V(D)J recombination activating gene, RAG-1. *Cell* **59**, 1035–1048 (1989).
5. Tonegawa, S. Somatic generation of antibody diversity. *Nature* **302**, 575–581 (1983).
6. Goodnow, C. C., Sprent, J., de St Groth, B. F. & Vinuesa, C. G. Cellular and genetic mechanisms of self tolerance and autoimmunity. *Nat Cell Biol* **435**, 590–597 (2005).
7. Starr, T. K., Jameson, S. C. & Hogquist, K. A. Positive and Negative Selection of T Cells. *Annual Review of Immunology* **21**, 139–176 (2003).
8. Kranz, D. M. Two mechanisms that account for major histocompatibility complex restriction of T cells. *F1000 Biol Rep* **1**, 55 (2009).
9. Hsieh, C.-S., Lee, H.-M. & Lio, C.-W. J. Selection of regulatory T cells in the thymus. *Nature Reviews Immunology* **12**, 157–167 (2012).
10. Bretscher, P. A. A two-step, two-signal model for the primary activation of precursor helper T cells. *Proc. Natl. Acad. Sci. U.S.A.* **96**, 185–190 (1999).
11. Heissmeyer, V., Ansel, K. M. & Rao, A. A plague of autoantibodies. *Nature Publishing Group* **6**, 642–643 (2005).
12. Schwartz, R. H. T Cell Anergy. *Annual Review of Immunology* **21**, 305–334 (2003).
13. Becker, J. C. *et al.* Negative transcriptional regulation in anergic T cells. *Proc. Natl. Acad. Sci. U.S.A.* **92**, 2375–2378 (1995).
14. Wells, A. D., Walsh, M. C., Bluestone, J. A. & Turka, L. A. Signaling through CD28 and CTLA-4 controls two distinct forms of T cell anergy. *J. Clin. Invest.* **108**, 895–904 (2001).
15. Nurieva, R. I., Liu, X. & Dong, C. Yin-Yang of costimulation: crucial controls of immune tolerance and function. *Immunological reviews* **229**, 88–100 (2009).
16. Walker, L. S. *et al.* Compromised OX40 function in CD28-deficient mice is linked with failure to develop CXC chemokine receptor 5-positive CD4 cells and germinal centers. *J Exp Med* **190**, 1115–1122 (1999).
17. McAdam, A. J. *et al.* Mouse inducible costimulatory molecule (ICOS) expression is enhanced by CD28 costimulation and regulates differentiation of CD4+ T cells. *J Immunol* **165**, 5035–5040 (2000).
18. Sharpe, A. H. & Freeman, G. J. The B7–CD28 Superfamily. *Nature Reviews Immunology* **2**, 116–126 (2002).
19. Monks, C. R., Freiberg, B. A., Kupfer, H., Sciaky, N. & Kupfer, A. Three-dimensional segregation of supramolecular activation clusters in T cells. *Nature* **395**, 82–86 (1998).
20. Schwartz, R. H. T cell clonal anergy. *Curr Opin Immunol* **9**, 351–357 (1997).
21. Bachmann, M. F. *et al.* Distinct roles for LFA-1 and CD28 during activation of naive T cells: adhesion versus costimulation. *Immunity* **7**, 549–557 (1997).
22. Shahinian, A. *et al.* Differential T cell costimulatory requirements in CD28-deficient mice. *Science* **261**, 609–612 (1993).

23. Borriello, F. *et al.* B7-1 and B7-2 have overlapping, critical roles in immunoglobulin class switching and germinal center formation. *Immunity* **6**, 303–313 (1997).
24. Yoshinaga, S. K. *et al.* T-cell co-stimulation through B7RP-1 and ICOS. *Nature* **402**, 827–832 (1999).
25. Rudd, C. E. & Schneider, H. Unifying concepts in CD28, ICOS and CTLA4 co-receptor signalling. *Nature Reviews Immunology* **3**, 544–556 (2003).
26. Qureshi, O. S. *et al.* Trans-Endocytosis of CD80 and CD86: A Molecular Basis for the Cell-Extrinsic Function of CTLA-4. *Science* **332**, 600–603 (2011).
27. Khattri, R., Auger, J. A., Griffin, M. D., Sharpe, A. H. & Bluestone, J. A. Lymphoproliferative disorder in CTLA-4 knockout mice is characterized by CD28-regulated activation of Th2 responses. *J Immunol* **162**, 5784–5791 (1999).
28. Hutloff, A. *et al.* ICOS is an inducible T-cell co-stimulator structurally and functionally related to CD28. *Nature* **397**, 263–266 (1999).
29. Coyle, A. J. *et al.* The CD28-related molecule ICOS is required for effective T cell-dependent immune responses. *Immunity* **13**, 95–105 (2000).
30. Bauquet, A. T. *et al.* The costimulatory molecule ICOS regulates the expression of c-Maf and IL-21 in the development of follicular T helper cells and TH-17 cells. *Nature Publishing Group* **10**, 167–175 (2009).
31. Kim, J. I., Ho, I. C., Grusby, M. J. & Glimcher, L. H. The transcription factor c-Maf controls the production of interleukin-4 but not other Th2 cytokines. *Immunity* **10**, 745–751 (1999).
32. Ho, I. C., Lo, D. & Glimcher, L. H. c-maf promotes T helper cell type 2 (Th2) and attenuates Th1 differentiation by both interleukin 4-dependent and -independent mechanisms. *J Exp Med* **188**, 1859–1866 (1998).
33. Grimbacher, B. *et al.* Homozygous loss of ICOS is associated with adult-onset common variable immunodeficiency. *Nature Immunology* **4**, 261–268 (2003).
34. Dong, C., Temann, U. A. & Flavell, R. A. Cutting edge: critical role of inducible costimulator in germinal center reactions. *J Immunol* **166**, 3659–3662 (2001).
35. McAdam, A. J. *et al.* ICOS is critical for CD40-mediated antibody class switching. *Nature* **409**, 102–105 (2001).
36. Akiba, H. *et al.* The role of ICOS in the CXCR5+ follicular B helper T cell maintenance in vivo. *J Immunol* **175**, 2340–2348 (2005).
37. Bossaller, L. *et al.* ICOS deficiency is associated with a severe reduction of CXCR5+CD4 germinal center Th cells. *J Immunol* **177**, 4927–4932 (2006).
38. Dong, C. *et al.* ICOS co-stimulatory receptor is essential for T-cell activation and function. *Nature* **409**, 97–101 (2001).
39. Vinuesa, C. G. *et al.* A RING-type ubiquitin ligase family member required to repress follicular helper T cells and autoimmunity. *Nature* **435**, 452–458 (2005).
40. Pollok, K. *et al.* Inducible T cell antigen 4-1BB. Analysis of expression and function. *The Journal of Immunology* **150**, 771 (1993).
41. Wang, C., Lin, G. H. Y., McPherson, A. J. & Watts, T. H. Immune regulation by 4-1BB and 4-1BBL: complexities and challenges. *Immunological reviews* **229**, 192–215 (2009).
42. Croft, M. Control of immunity by the TNFR-related molecule OX40 (CD134). *Annual Review of Immunology* **28**, 57–78 (2010).
43. Weinberg, A. D. The role of OX40 (CD134) in T-cell memory generation. *Adv Exp Med Biol* **684**, 57–68 (2010).
44. Murata, K. *et al.* Constitutive OX40/OX40 ligand interaction induces autoimmune-like diseases. *J Immunol* **169**, 4628–4636 (2002).
45. Bansal-Pakala, P., Jember, A. G. & Croft, M. Signaling through OX40 (CD134) breaks peripheral T-cell tolerance. *Nat Med* **7**, 907–912 (2001).

46. Vanhaesebroeck, B. & Alessi, D. R. The PI3K-PDK1 connection: more than just a road to PKB. *Biochem. J.* **346 Pt 3**, 561–576 (2000).
47. Sun, S.-C. Non-canonical NF-κB signaling pathway. *Cell Res.* **21**, 71–85 (2010).
48. Seminario, M.-C. *et al.* PTEN permits acute increases in D3-phosphoinositide levels following TCR stimulation but inhibits distal signaling events by reducing the basal activity of Akt. *Eur. J. Immunol.* **34**, 3165–3175 (2004).
49. Buckler, J. L., Walsh, P. T., Porrett, P. M., Choi, Y. & Turka, L. A. Cutting edge: T cell requirement for CD28 costimulation is due to negative regulation of TCR signals by PTEN. *J Immunol* **177**, 4262–4266 (2006).
50. Hagenbeek, T. J. The Loss of PTEN Allows TCR Lineage Thymocytes to Bypass IL-7 and Pre-TCR-mediated Signaling. *Journal of Experimental Medicine* **200**, 883–894 (2004).
51. Suzuki, A. *et al.* T cell-specific loss of Pten leads to defects in central and peripheral tolerance. *Immunity* **14**, 523–534 (2001).
52. Verweij, C. L., Geerts, M. & Aarden, L. A. Activation of interleukin-2 gene transcription via the T-cell surface molecule CD28 is mediated through an NF-kB-like response element. *J. Biol. Chem.* **266**, 14179–14182 (1991).
53. Lai, J. H. *et al.* RelA is a potent transcriptional activator of the CD28 response element within the interleukin 2 promoter. *Molecular and Cellular Biology* **15**, 4260–4271 (1995).
54. Shapiro, V. S., Truitt, K. E., Imboden, J. B. & Weiss, A. CD28 mediates transcriptional upregulation of the interleukin-2 (IL-2) promoter through a composite element containing the CD28RE and NF-IL-2B AP-1 sites. *Molecular and Cellular Biology* **17**, 4051–4058 (1997).
55. Grumont, R. J. & Gerondakis, S. Rel induces interferon regulatory factor 4 (IRF-4) expression in lymphocytes: modulation of interferon-regulated gene expression by rel/nuclear factor kappaB. *J Exp Med* **191**, 1281–1292 (2000).
56. Vallabhapurapu, S. & Karin, M. Regulation and Function of NF-κB Transcription Factors in the Immune System. *Annual Review of Immunology* **27**, 693–733 (2009).
57. Liou, H. C., Nolan, G. P., Ghosh, S., Fujita, T. & Baltimore, D. The NF-kappa B p50 precursor, p105, contains an internal I kappa B-like inhibitor that preferentially inhibits p50. *The EMBO Journal* **11**, 3003–3009 (1992).
58. Dobrzanski, P., Ryseck, R. P. & Bravo, R. Specific inhibition of RelB/p52 transcriptional activity by the C-terminal domain of p100. *Oncogene* **10**, 1003–1007 (1995).
59. Sun, S.-C. & Harhaj, E.in *NF-κB/Rel Transcription Factor Family* (Liou, H.-C.) 26–40 (Springer US, 2006).
60. Chen, Z. J. Ubiquitin signalling in the NF-kappaB pathway. *Nat Cell Biol* **7**, 758–765 (2005).
61. Perkins, N. D. Integrating cell-signalling pathways with NF-κB and IKK function. *Nat Rev Mol Cell Biol* **8**, 49–62 (2007).
62. Tuosto, L. *et al.* Mitogen-activated kinase kinase kinase 1 regulates T cell receptor- and CD28-mediated signaling events which lead to NF-kappaB activation. *Eur. J. Immunol.* **30**, 2445–2454 (2000).
63. Lai, J. H. & Tan, T. H. CD28 signaling causes a sustained down-regulation of I kappa B alpha which can be prevented by the immunosuppressant rapamycin. *J. Biol. Chem.* **269**, 30077–30080 (1994).
64. Bryan, R. G. *et al.* Effect of CD28 signal transduction on c-Rel in human peripheral blood T cells. *Molecular and Cellular Biology* **14**, 7933–7942 (1994).

65. Gerondakis, S. & Siebenlist, U. Roles of the NF- B Pathway in Lymphocyte Development and Function. *Cold Spring Harbor Perspectives in Biology* **2**, 1–29 (2010).
66. Zhou, L., Chong, M. M. W. & Littman, D. R. Plasticity of CD4+ T Cell Lineage Differentiation. *Immunity* **30**, 646–655 (2009).
67. Nakayamada, S., Takahashi, H., Kanno, Y. & O'shea, J. J. Helper T cell diversity and plasticity. *Curr Opin Immunol* **24**, 297–302 (2012).
68. Murphy, K. M. & Stockinger, B. Effector T cell plasticity: flexibility in the face of changing circumstances. *Nature Publishing Group* **11**, 674–680 (2010).
69. Johnston, R. J. *et al.* Bcl6 and Blimp-1 Are Reciprocal and Antagonistic Regulators of T Follicular Helper Cell Differentiation. *Science* **325**, 1006–1010 (2009).
70. Nurieva, R. I. *et al.* Bcl6 Mediates the Development of T Follicular Helper Cells. *Science* **325**, 1001–1005 (2009).
71. Yu, D. *et al.* The Transcriptional Repressor Bcl-6 Directs T Follicular Helper Cell Lineage Commitment. *Immunity* **31**, 457–468 (2009).
72. Jabeen, R. & Kaplan, M. H. The symphony of the ninth: the development and function of Th9 cells. *Curr Opin Immunol* **24**, 303–307 (2012).
73. Mosmann, T. R., Cherwinski, H., Bond, M. W., Giedlin, M. A. & Coffman, R. L. Two Types of Murine Helper T Cell Clone. I. Definition According to Profiles of Lymphokine Activities and Secreted Proteins. *J. Immunol.* **175**, 5–14 (2005).
74. Lighvani, A. A. *et al.* T-bet is rapidly induced by interferon-gamma in lymphoid and myeloid cells. *Proc. Natl. Acad. Sci. U.S.A.* **98**, 15137–15142 (2001).
75. Afkarian, M. *et al.* T-bet is a STAT1-induced regulator of IL-12R expression in naïve CD4+ T cells. *Nature Immunology* **3**, 549–557 (2002).
76. Shimoda, K. *et al.* Lack of IL-4-induced Th2 response and IgE class switching in mice with disrupted Stat6 gene. *Nature* **380**, 630–633 (1996).
77. Takeda, K. *et al.* Essential role of Stat6 in IL-4 signalling. *Nature* **380**, 627–630 (1996).
78. Kaplan, M. H., Schindler, U., Smiley, S. T. & Grusby, M. J. Stat6 is required for mediating responses to IL-4 and for development of Th2 cells. *Immunity* **4**, 313–319 (1996).
79. Ouyang, W. *et al.* Inhibition of Th1 development mediated by GATA-3 through an IL-4-independent mechanism. *Immunity* **9**, 745–755 (1998).
80. Hegazy, A. N. *et al.* Interferons Direct Th2 Cell Reprogramming to Generate a Stable GATA-3+T-bet+ Cell Subset with Combined Th2 and Th1 Cell Functions. *Immunity* **32**, 116–128 (2010).
81. Krawczyk, C. M., Shen, H. & Pearce, E. J. Functional plasticity in memory T helper cell responses. *J Immunol* **178**, 4080–4088 (2007).
82. Chen, Z., Laurence, A. & O'shea, J. J. Signal transduction pathways and transcriptional regulation in the control of Th17 differentiation. *Seminars in immunology* **19**, 400–408 (2007).
83. Kanangat, S. *et al.* Disease in the scurfy (sf) mouse is associated with overexpression of cytokine genes. *Eur. J. Immunol.* **26**, 161–165 (1996).
84. Kim, J. M., Rasmussen, J. P. & Rudensky, A. Y. Regulatory T cells prevent catastrophic autoimmunity throughout the lifespan of mice. *Nature Publishing Group* **8**, 191–197 (2006).
85. Khattri, R., Cox, T., Yasayko, S.-A. & Ramsdell, F. An essential role for Scurfin in CD4+CD25+ T regulatory cells. *Nature Immunology* **4**, 337–342 (2003).
86. Bettelli, E. *et al.* Reciprocal developmental pathways for the generation of pathogenic effector TH17 and regulatory T cells. *Nature* **441**, 235–238 (2006).

87. Mucida, D. *et al.* Reciprocal TH17 and Regulatory T Cell Differentiation Mediated by Retinoic Acid. *Science* **317**, 256–260 (2007).
88. Zhou, L. *et al.* TGF-beta-induced Foxp3 inhibits T(H)17 cell differentiation by antagonizing RORgammat function. *Nature* **453**, 236–240 (2008).
89. Osorio, F. *et al.* DC activated via dectin-1 convert Treg into IL-17 producers. *Eur. J. Immunol.* **38**, 3274–3281 (2008).
90. Brüstle, A. *et al.* The development of inflammatory TH-17 cells requires interferon-regulatory factor 4. *Nature Publishing Group* **8**, 958–966 (2007).
91. Zheng, Y. *et al.* Regulatory T-cell suppressor program co-opts transcription factor IRF4 to control TH2 responses. *Nature* **458**, 351–356 (2009).
92. Linterman, M. A. *et al.* Foxp3+ follicular regulatory T cells control the germinal center response. *Nat Med* **17**, 975–982 (2011).
93. Chung, Y. *et al.* Follicular regulatory T cells expressing Foxp3 and Bcl-6 suppress germinal center reactions. *Nat Med* **17**, 983–988 (2011).
94. Crotty, S. Follicular Helper CD4 T Cells (T FH). *Annual Review of Immunology* **29**, 621–663 (2011).
95. Fazilleau, N., McHeyzer-Williams, L. J., Rosen, H. & McHeyzer-Williams, M. G. The function of follicular helper T cells is regulated by the strength of T cell antigen receptor binding. *Nature Publishing Group* **10**, 375–384 (2009).
96. Choi, Y. S. *et al.* ICOS receptor instructs T follicular helper cell versus effector cell differentiation via induction of the transcriptional repressor Bcl6. *Immunity* **34**, 932–946 (2011).
97. Ansel, K. M., McHeyzer-Williams, L. J., Ngo, V. N., McHeyzer-Williams, M. G. & Cyster, J. G. In vivo-activated CD4 T cells upregulate CXC chemokine receptor 5 and reprogram their response to lymphoid chemokines. *J Exp Med* **190**, 1123–1134 (1999).
98. Kim, C. H. *et al.* Subspecialization of CXCR5+ T cells: B helper activity is focused in a germinal center-localized subset of CXCR5+ T cells. *J Exp Med* **193**, 1373–1381 (2001).
99. Breitfeld, D. *et al.* Follicular B helper T cells express CXC chemokine receptor 5, localize to B cell follicles, and support immunoglobulin production. *J Exp Med* **192**, 1545–1552 (2000).
100. Baumjohann, D., Okada, T. & Ansel, K. M. Cutting Edge: Distinct Waves of BCL6 Expression during T Follicular Helper Cell Development. *The Journal of Immunology* **187**, 2089–2092 (2011).
101. Betz, B. C. *et al.* Batf coordinates multiple aspects of B and T cell function required for normal antibody responses. *Journal of Experimental Medicine* **207**, 933–942 (2010).
102. Ise, W. *et al.* The transcription factor BATF controls the global regulators of class-switch recombination in both B cells and T cells. *Nature Publishing Group* **12**, 536–543 (2011).
103. Kroenke, M. A. *et al.* Bcl6 and Maf Cooperate To Instruct Human Follicular Helper CD4 T Cell Differentiation. *The Journal of Immunology* **188**, 3734–3744 (2012).
104. Kwon, H. *et al.* Analysis of Interleukin-21-Induced Prdm1 Gene Regulation Reveals Functional Cooperation of STAT3 and IRF4 Transcription Factors. *Immunity* **31**, 941–952 (2009).
105. Bollig, N. *et al.* Transcription factor IRF4 determines germinal center formation through follicular T-helper cell differentiation. *Proceedings of the National Academy of Sciences* **109**, 8664–8669 (2012).

106. Johnston, R. J., Choi, Y. S., Diamond, J. A., Yang, J. A. & Crotty, S. STAT5 is a potent negative regulator of TFH cell differentiation. *Journal of Experimental Medicine* **209**, 243–250 (2012).
107. Glasmacher, E. *et al.* A genomic regulatory element that directs assembly and function of immune-specific AP-1-IRF complexes. *Science* **338**, 975–980 (2012).
108. Nakayamada, S. *et al.* Early Th1 Cell Differentiation Is Marked by a Tfh Cell-like Transition. *Immunity* **35**, 919–931 (2011).
109. Lüthje, K. *et al.* The development and fate of follicular helper T cells defined by an IL-21 reporter mouse. *Nature Publishing Group* **13**, 491–498 (2012).
110. Hu, Y.-L., Metz, D. P., Chung, J., Siu, G. & Zhang, M. B7RP-1 blockade ameliorates autoimmunity through regulation of follicular helper T cells. *The Journal of Immunology* **182**, 1421–1428 (2009).
111. Linterman, M. A. *et al.* Follicular helper T cells are required for systemic autoimmunity. *Journal of Experimental Medicine* **206**, 561–576 (2009).
112. Simpson, N. *et al.* Expansion of circulating T cells resembling follicular helper T cells is a fixed phenotype that identifies a subset of severe systemic lupus erythematosus. *Arthritis Rheum* **62**, 234–244 (2010).
113. Cappione, A., III *et al.* Germinal center exclusion of autoreactive B cells is defective in human systemic lupus erythematosus. *J. Clin. Invest.* **115**, 3205–3216 (2005).
114. Vinuesa, C. G., Sanz, I. & Cook, M. C. Dysregulation of germinal centres in autoimmune disease. *Nature Reviews Immunology* **9**, 845–857 (2009).
115. Radic, M. Z. & Weigert, M. Genetic and structural evidence for antigen selection of anti-DNA antibodies. *Annual Review of Immunology* **12**, 487–520 (1994).
116. Rosen, A. & Casciola-Rosen, L. Clearing the way to mechanisms of autoimmunity. *Nat Med* **7**, 664–665 (2001).
117. Lohr, J., Knoechel, B., Nagabhushanam, V. & Abbas, A. K. T-cell tolerance and autoimmunity to systemic and tissue-restricted self-antigens. *Immunological reviews* **204**, 116–127 (2005).
118. Linterman, M. A. *et al.* Roquin Differentiates the Specialized Functions of Duplicated T Cell Costimulatory Receptor Genes Cd28 and Icos. *Immunity* **30**, 228–241 (2009).
119. Yu, D. *et al.* Roquin represses autoimmunity by limiting inducible T-cell co-stimulator messenger RNA. *Nature* **450**, 299–303 (2007).
120. Bertossi, A. *et al.* Loss of Roquin induces early death and immune deregulation but not autoimmunity. *Journal of Experimental Medicine* **208**, 1749–1756 (2011).
121. Anderson, P. Post-transcriptional regulons coordinate the initiation and resolution of inflammation. *Nature Reviews Immunology* **10**, 24–35 (2010).
122. Hoefig, K. P. & Heissmeyer, V. MicroRNAs grow up in the immune system. *Curr Opin Immunol* **20**, 281–287 (2008).
123. Hao, S. & Baltimore, D. The stability of mRNA influences the temporal order of the induction of genes encoding inflammatory molecules. *Nature Publishing Group* **10**, 281–288 (2009).
124. Stoecklin, G. & Anderson, P. Posttranscriptional mechanisms regulating the inflammatory response. *Adv Immunol* **89**, 1–37 (2006).
125. Hollams, E. M., Giles, K. M., Thomson, A. M. & Leedman, P. J. MRNA stability and the control of gene expression: implications for human disease. *Neurochem. Res.* **27**, 957–980 (2002).
126. Ross, H. J., Sato, N., Ueyama, Y. & Koeffler, H. P. Cytokine messenger RNA stability is enhanced in tumor cells. *Blood* **77**, 1787–1795 (1991).

127. Hollis, G. F., Gazdar, A. F., Bertness, V. & Kirsch, I. R. Complex translocation disrupts c-myc regulation in a human plasma cell myeloma. *Molecular and Cellular Biology* **8**, 124–129 (1988).
128. Aghib, D. F. *et al.* A 3' truncation of MYC caused by chromosomal translocation in a human T-cell leukemia increases mRNA stability. *Oncogene* **5**, 707–711 (1990).
129. Sandberg, R., Neilson, J. R., Sarma, A., Sharp, P. A. & Burge, C. B. Proliferating Cells Express mRNAs with Shortened 3' Untranslated Regions and Fewer MicroRNA Target Sites. *Science* **320**, 1643–1647 (2008).
130. Bernstein, P. & Ross, J. Poly(A), poly(A) binding protein and the regulation of mRNA stability. *Trends in Biochemical Sciences* **14**, 373–377 (1989).
131. Bernstein, P., Peltz, S. W. & Ross, J. The poly(A)-poly(A)-binding protein complex is a major determinant of mRNA stability in vitro. *Molecular and Cellular Biology* **9**, 659–670 (1989).
132. Parker, R. & Song, H. The enzymes and control of eukaryotic mRNA turnover. *Nat Struct Mol Biol* **11**, 121–127 (2004).
133. Tharun, S. *et al.* Yeast Sm-like proteins function in mRNA decapping and decay. *Nature* **404**, 515–518 (2000).
134. Fenger-Grøn, M., Fillman, C., Norrild, B. & Lykke-Andersen, J. Multiple Processing Body Factors and the ARE Binding Protein TTP Activate mRNA Decapping. *Molecular Cell* **20**, 905–915 (2005).
135. Weston, A. Xp54 and related (DDX6-like) RNA helicases: roles in messenger RNP assembly, translation regulation and RNA degradation. *Nucleic Acids Research* **34**, 3082–3094 (2006).
136. Anderson, P. Post-transcriptional control of cytokine production. *Nature Publishing Group* **9**, 353–359 (2008).
137. Taylor, G. A. *et al.* A pathogenetic role for TNF alpha in the syndrome of cachexia, arthritis, and autoimmunity resulting from tristetraprolin (TTP) deficiency. *Immunity* **4**, 445–454 (1996).
138. Brennan, C. M. & Steitz, J. A. HuR and mRNA stability. *Cell. Mol. Life Sci.* **58**, 266–277 (2001).
139. Kim, H. H. *et al.* HuR recruits let-7/RISC to repress c-Myc expression. *Genes & Development* **23**, 1743–1748 (2009).
140. Jones, M. R. *et al.* Zcchc11-dependent uridylation of microRNA directs cytokine expression. *Nat Cell Biol* **11**, 1157–1163 (2009).
141. Thai, T. H. *et al.* Regulation of the Germinal Center Response by MicroRNA-155. *Science* **316**, 604–608 (2007).
142. Zhang, B., Pan, X., Cobb, G. P. & Anderson, T. A. microRNAs as oncogenes and tumor suppressors. *Developmental Biology* **302**, 1–12 (2007).
143. Xiao, C. *et al.* Lymphoproliferative disease and autoimmunity in mice with increased miR-17-92 expression in lymphocytes. *Nature Publishing Group* **9**, 405–414 (2008).
144. Watts, J. M. *et al.* Architecture and secondary structure of an entire HIV-1 RNA genome. *Nature* **460**, 711–716 (2009).
145. Parker, R. & Sheth, U. P Bodies and the Control of mRNA Translation and Degradation. *Molecular Cell* **25**, 635–646 (2007).
146. Chu, C.-Y. & Rana, T. M. Translation repression in human cells by microRNA-induced gene silencing requires RCK/p54. *Plos Biol* **4**, 1122–1136 (2006).
147. Anderson, P. & Kedersha, N. Visibly stressed: the role of eIF2, TIA-1, and stress granules in protein translation. *Cell Stress Chaperones* **7**, 213–221 (2002).
148. Kedersha, N. *et al.* Stress granules and processing bodies are dynamically linked sites of mRNP remodeling. *The Journal of Cell Biology* **169**, 871–884 (2005).

149. Glasmacher, E. *et al.* Roquin binds inducible costimulator mRNA and effectors of mRNA decay to induce microRNA-independent post-transcriptional repression. *Nature Publishing Group* **11**, 725–733 (2010).
150. Glasmacher, E. Roquin binds to ICOS mRNA for P body-dependent and miRNA-independent posttranscriptional gene silencing. *Ludwig-Maximilians-Universität München* –Dissertation an der Fakultät für Biologie (2010).
151. Siess, D. C. A Human Gene Coding for a Membrane-associated Nucleic Acid-binding Protein. *Journal of Biological Chemistry* **275**, 33655–33662 (2000).
152. Lee, P. P. *et al.* A critical role for Dnmt1 and DNA methylation in T cell development, function, and survival. *Immunity* **15**, 763–774 (2001).
153. Wilkinson, K. A., Merino, E. J. & Weeks, K. M. Selective 2′-hydroxyl acylation analyzed by primer extension (SHAPE): quantitative RNA structure analysis at single nucleotide resolution. *Nat Protoc* **1**, 1610–1616 (2006).
154. Su, H., Trombly, M. I., Chen, J. & Wang, X. Essential and overlapping functions for mammalian Argonautes in microRNA silencing. *Genes & Development* **23**, 304–317 (2009).
155. Athanasopoulos, V. *et al.* The ROQUIN family of proteins localizes to stress granules via the ROQ domain and binds target mRNAs. *FEBS Journal* **277**, 2109–2127 (2010).
156. MacNicol, M. C. & MacNicol, A. M. Developmental timing of mRNA translation-integration of distinct regulatory elements. *Mol. Reprod. Dev.* **77**, 662–669 (2010).
157. Chang, P. P. *et al.* Breakdown in Repression of IFN- mRNA Leads to Accumulation of Self-Reactive Effector CD8+ T Cells. *The Journal of Immunology* **189**, 701–710 (2012).
158. Chen, L. Co-inhibitory molecules of the B7–CD28 family in the control of T-cell immunity. *Nature Reviews Immunology* **4**, 336–347 (2004).
159. Lee, S. K. *et al.* Interferon-γ Excess Leads to Pathogenic Accumulation of Follicular Helper T Cells and Germinal Centers. *Immunity* **37**, 880–892 (2012).
160. Sawada, S., Scarborough, J. D., Killeen, N. & Littman, D. R. A lineage-specific transcriptional silencer regulates CD4 gene expression during T lymphocyte development. *Cell* **77**, 917–929 (1994).
161. Schneider, K., Potter, K. G. & Ware, C. F. Lymphotoxin and LIGHT signaling pathways and target genes. *Immunological reviews* **202**, 49–66 (2004).
162. Spolski, R. & Leonard, W. J. IL-21 and T follicular helper cells. *International Immunology* **22**, 7–12 (2009).
163. Lu, K. T. *et al.* Functional and Epigenetic Studies Reveal Multistep Differentiation and Plasticity of In Vitro-Generated and In Vivo-Derived Follicular T Helper Cells. *Immunity* **35**, 622–632 (2011).
164. Mestas, J. Endothelial cell co-stimulation through OX40 augments and prolongs T cell cytokine synthesis by stabilization of cytokine mRNA. *International Immunology* **17**, 737–747 (2005).
165. Huber, M. *et al.* IRF4 is essential for IL-21-mediated induction, amplification, and stabilization of the Th17 phenotype. *Proceedings of the National Academy of Sciences* **105**, 20846–20851 (2008).
166. Murray, S. E. *et al.* NF-κB–inducing kinase plays an essential T cell–intrinsic role in graft-versus-host disease and lethal autoimmunity in mice. *J. Clin. Invest.* **121**, 4775–4786 (2011).
167. Rolf, J. *et al.* Phosphoinositide 3-Kinase Activity in T Cells Regulates the Magnitude of the Germinal Center Reaction. *The Journal of Immunology* **185**, 4042–4052 (2010).

168. Lunde, B. M., Moore, C. & Varani, G. RNA-binding proteins: modular design for efficient function. *Nat Rev Mol Cell Biol* **8**, 479–490 (2007).
169. Laroia, G., Sarkar, B. & Schneider, R. J. Ubiquitin-dependent mechanism regulates rapid turnover of AU-rich cytokine mRNAs. *Proc. Natl. Acad. Sci. U.S.A.* **99**, 1842–1846 (2002).
170. Cano, F. *et al.* The RNA-binding E3 ubiquitin ligase MEX-3C links ubiquitination with MHC-I mRNA degradation. *The EMBO Journal* **31**, 3596–3606 (2012).
171. Nowak, M. A., Boerlijst, M. C., Cooke, J. & Smith, J. M. Evolution of genetic redundancy. *Nature* **388**, 167–171 (1997).
172. Chen, Q. *et al.* IRF-4-Binding Protein Inhibits Interleukin-17 and Interleukin-21 Production by Controlling the Activity of IRF-4 Transcription Factor. *Immunity* **29**, 899–911 (2008).
173. Fanzo, J. C. *et al.* Loss of IRF-4–binding protein leads to the spontaneous development of systemic autoimmunity. *J. Clin. Invest.* **116**, 703–714 (2006).
174. Gaspal, F. M. *et al.* Abrogation of CD30 and OX40 signals prevents autoimmune disease in FoxP3-deficient mice. *Journal of Experimental Medicine* **208**, 1579–1584 (2011).
175. Brocker, T. *et al.* CD4 T cell traffic control: in vivo evidence that ligation of OX40 on CD4 T cells by OX40-ligand expressed on dendritic cells leads to the accumulation of CD4 T cells in B follicles. *Eur. J. Immunol.* **29**, 1610–1616 (1999).
176. Gigoux, M. *et al.* Inducible costimulator promotes helper T-cell differentiation through phosphoinositide 3-kinase. *Proceedings of the National Academy of Sciences* **106**, 20371–20376 (2009).
177. So, T., Choi, H. & Croft, M. OX40 Complexes with Phosphoinositide 3-Kinase and Protein Kinase B (PKB) To Augment TCR-Dependent PKB Signaling. *The Journal of Immunology* **186**, 3547–3555 (2011).
178. Mueller, S. N. & Germain, R. N. Stromal cell contributions to the homeostasis and functionality of the immune system. *Nature Publishing Group* **9**, 618–629 (2009).
179. Simpson, T. R., Quezada, S. A. & Allison, J. P. Regulation of CD4 T cell activation and effector function by inducible costimulator (ICOS). *Curr Opin Immunol* **22**, 326–332 (2010).
180. Steiniger, B. & van der Meide, P. H. High-dose interferon-gamma alters the distribution of B lymphocytes and macrophages in rat spleen and lymph nodes. *Immunology* **78**, 461–467 (1993).

11 Publications

Articles based on this thesis

Vigo Heissmeyer and **Katharina U. Vogel**. Molecular control of follicular helper T cell differentiation by Roquin family proteins. *Immunological Reviews*, 253(1):273–89 (2013)

Vogel K.U.*, Edelmann S.L.*, Jeltsch K.M., Bertossi A., Heger K., Heinz G.A., Zöller J., Warth S.C., Hoefig K.P., Lohs C., Neff F., Kremmer E., Schick J., Schmidt-Supprian M. and Heissmeyer V. Combined loss of Roquin paralogs -1 and -2 derepresses Icos and Ox40 target mRNAs and imposes Tfh differentiation on CD4 (+) T cells. *Immunity,* 38(4):655–68 (2013)
*equal contribution

Glasmacher E., Hoefig K.P.*, **Vogel K.U.***, Rath N., Du L., Wolf C., Kremmer E., Wang X. and Heissmeyer V. Roquin binds inducible costimulator mRNA and effectors of mRNA decay to induce microRNA-independent post-transcriptional repression. *Nature Immunology*, 11(8):725–33 (2010)
*equal contribution

Posters presented based on this thesis

Gene Expression and Signaling in the Immune System, 2012, CSHL, N.Y., USA

Spring School on Immunology, 2012, Ettal, Germany

Signaling in the immune system, 2011, Siena, Italy

Autumn School – Current Concepts in Immunology, 2010, Bad Schandau, Germany

40th Annual meeting of the DGfI, 2010, Leipzig, Germany

Bayreuther Strukturtage, 2010, Thurnau, Germany

Oral presentations based on this thesis

Combined loss of Roquin paralogs -1 and -2 derepresses their mRNA targets Ox40 and Icos and imposes Tfh differentiation on CD4 T cells.
Munich Minisymposia in Immunology 2012, Munich, Germany

Combined loss of Rc3h1 and Rc3h2 derepresses their mRNA targets Ox-40 and Icos and imposes Tfh differentiation on CD4 T cells.
T cell Meeting 2012, Marburg, Germany

Redundant and unique functions of Roquin and Mnab proteins.
T cell Meeting 2011, Marburg, Germany

Roquin and Mnab proteins: What role do they play in the prevention of autoimmunity.
SFB571 Meeting 2009, Herrsching, Germany

12 Contributions and acknowledgements

I would like to thank all people who were involved in the development and support of this research project.

First of all I would like to thank Prof. Dr. Vigo Heissmeyer for the committed supervision of this research project. I am deeply thankful for the unlimited support, the enormous motivation and ingenious input into this project, leading to a high quality publications.

Furthermore I would like to thank Prof. Dr. Dirk Eick and PD Dr. Bettina Bölter for the evaluation of this thesis work. Also many thanks to Prof. Dr. Dirk Eick for the support in my Thesis Advisory Committee.

Special thanks to Dr. Marc Schmidt-Supprian for the great support of this project as member of my Thesis Advisory Committee. In addition I cordially thank Dr. Marc Schmidt-Supprian and Dr. Arianna Bertossi for the Roquin-1 knockout mouse and Klaus Heger for the generation of the CAR-transgenic mouse.

I would like to especially thank Dr. Elke Glasmacher for introducing me into the lab work and the perfect cooperation on the Roquin project, which I deeply enjoyed.

I deeply thank Dr. Stephanie L. Edelmann for her help in the project. She provided outstanding help in the characterization of *Rc3h1/2*-deficient mice (Figure 29, Figure 30 and Figure 32) and accomplished almost all adoptive transfers of Th1-cultured T cells (Figure 35 and Figure 36).

Moreover, I am very grateful for the help of Gitta A. Heinz, Sebastian Warth, Dr. Kai P. Höfig, Christine Wolf and Claudia Lohs at the development and final completion of this thesis. Gitta A. Heinz performed the EMSA experiments on Ctla4 and Ox40 binding (Figure 19 and Figure 42 A). Sebastian Warth conducted the *in vitro* differentiation experiments in Figure 38, after the cells had been isolated and sorted. Dr. Kai P. Höfig evaluated potential targets of Roquin-1/2 by qPCR (Figure 18). Christine Wolf technically supported this work and demonstrated interaction of Roquin-1 and Roquin-2 with Edc4 (Figure 31). Claudia Lohs

greatly helped in the development of Western blots in Figure 20 C and Figure 40 A–C and performed the qPCR analysis in Figure 41. Nina Martin conducted the Western blot and Coomassie gel (Figure 20 A–B) under my supervision.

In addition, I would like to thank all staff of the animal facility, especially Michael Hagemann, Franziska Liebel and Martina Möschter for their excellent cooperativeness and Albert Geishauser for injecting mice on short notice.

Many thanks also to Prof. Dr. Mathias Heikenwälder and Jessica Zöller for the generation and staining of splenic cryo-sections in Figure 33, Figure 34, Figure 45 and Figure 47.

Moreover I appreciate the valuable cooperation with Prof. Dr. Wolfgang Wurst who provided the Roquin-2 knockout mouse and Dr. Joel Schick who validated the knockout by Southern blotting (Figure 22).

Special thanks also to Prof. Dr. Birgitta Wöhrl and Dr. Maximilian Hartl for the help with the SHAPE assay and the accomplishment of the primer extension and sequencing reactions as well as the analysis of the SHAPE data (Figure 13 and Figure 14).

I would like to thank Dr. Elisabeth Kremmer for the generation of valuable antibodies and Dr. Arie Geerlof for the purification of Roquin-2 (aa 1–438) protein.

Furthermore I thank Dr. Helmut Blum for the conduction of the Affymetrix microarrays and Dr. Dirk Repsilber for the statistical evaluation.

Many thanks to Christoph Vahl for always providing help and a running sorter device when needed.

Finally I would like to thank Prof. Dr. Vigo Heissmeyer, Dr. Kai Höfig, Katharina M. Jeltsch, Dr. Stephanie Edelmann, Sebastian Warth, Gitta A. Heinz, Felix Deschler, Nina Martin and Alexander Vogel for critical proof-reading of my thesis.